DISCLAIMER:

This document does not meet the
current format guidelines of
the Graduate School at
The University of Texas at Austin.

It has been published for
informational use only.

The Thesis Committee for William Hamilton Woodruff Jr.
Certifies that this is the approved version of the following thesis:

Late Cenozoic growth and exhumation of the northern Lunggar extensional basin, west-central Tibetan plateau

APPROVED BY
SUPERVISING COMMITTEE:

Supervisor:

Brian K. Horton

Daniel F. Stockli

Richard A. Ketcham

Late Cenozoic growth and exhumation of the northern Lunggar extensional basin, west-central Tibetan plateau

by

William Hamilton Woodruff Jr, B.S.

Thesis

Presented to the Faculty of the Graduate School of

The University of Texas at Austin

in Partial Fulfillment

of the Requirements

for the Degree of

Master of Science in Geological Sciences

The University of Texas at Austin

December 2011

Acknowledgements

This work would not have been possible without the guidance of my supervisor, Dr. Brian Horton, and my committee members, Dr. Daniel Stockli and Dr. Richard Ketcham. Dr. Paul Kapp provided invaluable field and laboratory assistance, as well as insight. Dr. Ding Lin, Dr. Michael Taylor, Kurt Sundell, Andrew McCallister, Richard Styron, and Dr. Roman Kislitsyn all provided extremely valuable advice and assistance, as did members of Dr. Horton's research group, especially Joel Saylor and Ben Siks. I also would not have been able to complete this work without the support of my family: Dr. William Woodruff, Sharon Woodruff, Holly Parker, and Dr. C.M. Woodruff.

Abstract

Late Cenozoic growth and exhumation of the northern Lunggar extensional basin, west-central Tibetan plateau

William Hamilton Woodruff Jr., M.S. Geo.Sci.

The University of Texas at Austin, 2011

Supervisor: Brian K. Horton

Despite major shortening during India-Asia convergence, the dominant late Cenozoic geological features across the southern to central Tibetan plateau are north-trending rifts and associated strike-slip faults. Fault orientations and slip directions suggest broadly distributed east-west extension, but the dominant modes of extensional deformation and basin formation are unclear. The Lunggar extensional basin in west-central Tibet is bounded by a <40° low-angle normal fault (detachment), contains active high-angle normal faults, and displays higher topography toward the basin center with outward axial drainage toward the northern and southern basin terminations. Structural and stratigraphic features of the Lunggar extensional system are variably consistent with a high-angle half-graben geometry or a low-angle fault-related supradetachment basin, possibly suggesting a temporal or spatial change in deformational style. This study aims to constrain the depositional and exhumational history of the Lunggar extensional basin

and bounding east-dipping fault system by assessing the sedimentologic, structural, and thermochronological record of upper Cenozoic basin fill.

Clastic sedimentary facies filling the Lunggar extensional basin include alluvial-fan debris-flow conglomerates and fluviolacustrine sandstones and siltstones. Sandstone petrographic point count data, conglomerate clast compositions, and detrital zircon U/Pb age spectra suggest systematic unroofing of the western footwall (including Upper Jurassic-Cretaceous and Miocene granitic crystalline rocks that intruded Permian to Cretaceous strata), which strongly influenced sediment transport and basin sedimentation. Paleoflow measurements are effectively opposite to the current flow regime, suggesting that the modern topographic high in the central basin modified the original basin configuration. As a proxy for cooling histories of previously eroded footwall rocks, 4 sandstones and 11 leucogranite boulder clasts from proximal hanging-wall strata were sampled for low-temperature thermochronometry. Apatite and zircon (U-Th)/He results support conglomerate clast compositional trends in suggesting rapid footwall exhumation and a pattern of subsequent hanging-wall exhumation in which the youngest exposed range-front deposits are focused along the central segment of the basin-bounding detachment fault. Collectively, the sedimentologic, structural, and thermochronological results support a model of rift evolution predicting upper crustal thinning, supradetachment basin subsidence, and subsequent isostatic rebound that initiated along the more-evolved central segments of Tibetan extensional systems.

Table of Contents

1. Introduction

Although the Tibetan plateau (Figure 1) was formed by India-Asia convergence from late Mesozoic to present, the dominant expressions of late Cenozoic deformation across the plateau are recent to active normal faults and kinematically linked conjugate strike-slip faults (e.g., Molnar and Tapponnier, 1978; Yin and Harrison, 2000; Yin, 2000, 2010; Taylor et al., 2003, 2012; Horton, 2012). The north-south orientation of most fault-bounded basins suggest that Tibet extends in an east-west direction (e.g., Armijo et al., 1986; Yin et al., 1999; Ni and York, 1978), as confirmed by GPS studies indicating eastward motion at a rate of up to 21-26 mm/yr, greater than half of the 36-38 mm/yr north-south India-Asia convergence rate (Wang et al., 2001; P.Z. Zhang et al., 2004). Mechanisms of extension are debated, and include (1) gravitational collapse after the plateau reached a maximum threshold elevation (England and Houseman, 1989; Molnar et al., 1993), (2) partial melting and eastward flow in the mid-lower crust (e.g., Royden et al., 1997; Clark and Royden, 2000), (3) lateral tectonic extrusion along major strike-slip faults (e.g., Tapponnier et al., 1982, 2001), (4) tensile stresses induced by India collision and underthrusting (e.g., Armijo et al., 1986; Kapp and Guynn, 2004), and (5) lithospheric extension linked to eastward slab retreat along the Asia-Pacific margin (e.g., Northrup et al., 1995; Yin, 2000). The morphology and evolutionary history of extensional basins across the Tibetan plateau provide insights into the potential underlying causes of extension (e.g., Armijo et al., 1986; Harrison et al., 1995; J.L.D. Kapp et al., 2005) as well as mechanical properties of Tibetan crust and lithosphere (Bird,

1991; Masek et al., 1994; Yin, 2000). Nevertheless, integrated basin-scale field investigations of Tibetan extensional basins are relatively limited (e.g., Garzione et al., 2003; Kempf et al., 2009; Saylor et al., 2010; Adhikari and Wagreich, 2011).

The evolution of extensional basins is closely related to the mode of extension of continental crust, which is influenced by the overall stress regime, strain rate, thermal structure, rheology, and preexisting structures in the crust and lithosphere (Lister and Davis, 1989; Ruppel, 1995). Regions dominated by pure shear are commonly expected to produce symmetrical extensional systems with conventional high-angle normal faults bounding "traditional" rift basins (e.g., Buck, 1988, 1991). In some cases, an asymmetry is revealed by a series of tilt-block half-graben basins bounded by the principal normal faults of the extensional system (Leeder and Gawthorpe, 1987). In contrast, extensional systems governed by simple shear with gently dipping shear zones or detachments commonly result in highly extended hanging-wall "supradetachment" basins bounded by low-angle normal faults (Wernicke, 1981, 1985). Multiple characteristics of the depositional systems within a given basin are affected by extensional style, including the depositional environments, total duration of basin filling, dominant sediment source (i.e., hanging wall versus footwall), and sediment transport pathways (i.e., axial versus transverse) (Friedman and Burbank, 1995).

The Lunggar extensional basin in the west-central Tibetan plateau (Figure 1) displays structural, sedimentary, and topographic elements that could be attributed to processes associated with either (a) a conventional rift or half-graben basin along a major bounding fault or (b) a supradetachment basin above a low-angle normal fault. The

Lunggar basin (Kapp et al., 2008) is one of two recognized Tibetan extensional basins bounded at least in part by a low-angle or detachment fault, the other being the Yadong Gulu rift in southeastern Tibet (Armijo et al., 1986; Harrison et al., 1995; J.L.D. Kapp et al., 2005). In addition to its association with a detachment fault, the Lunggar extensional system features an intrabasinal topographic high in its central segment, resulting in external drainage northward and southward toward the basin terminations.

The purpose of this study is to investigate the sedimentary record of the Lunggar extensional basin, with the aim of evaluating the timing and mode of extension as well as possible changes in extensional style and basin configuration through time. To address these issues, we utilize the stratigraphy and sedimentology of basin fill, paleocurrent patterns, detrital compositions of sandstone and conglomerate, detrital zircon U/Pb geochronology, and detrital apatite and zircon (U-Th)/He thermochronology. From these results, we present an integrated interpretation of the evolution of the Lunggar extensional basin that is compatible with and expands upon previous structural and thermochronological investigations of Tibetan rifts (e.g., Taylor et al., 2003, 2012; J.L.D. Kapp et al., 2005; Kapp et al., 2008).

2. Geologic Background

The Tibetan plateau is the world's largest and highest orogenic plateau, covering ~3 million km^2 at an average elevation of ~5000 m (Royden et al., 2008). The plateau is composed of several terranes accreted to the southern edge of Eurasia since the early

Paleozoic, with the youngest, the Lhasa terrane (Figure 1), docking with the previously accreted Qiangtang terrane along the Bangong suture between Late Jurassic and mid-Cretaceous time (Yin and Harrison, 2000). There is disagreement about the Cretaceous tectonic regime and degree of uplift in the Lhasa terrane of southern Tibet prior to the India-Asia collision. Contrasting models include one or more of the following elements: (a) extensive thrusting and shortening resulting in high elevation and a possible "proto-plateau" (England and Searle, 1986; Murphy et al., 1997; P. Kapp et al., 2005; Leier et al., 2007), (b) back-arc extension with low elevation and marine sedimentation (K.J. Zhang et al., 2004), and (c) an Andean-style volcanic arc (e.g., Searle et al., 1987; P. Kapp et al., 2005). Whichever model or combination of models are correct, the principally east-west structural grain of the Lhasa terrane was largely inherited from subduction and accretion processes preceding the India-Asia collision (England and Searle, 1986; Dewey et al., 1988). North-south shortening of the Lhasa terrane due to the India-Asia collision commenced in the early Eocene (~55-50 Ma), as evidenced by plate circuit reconstructions and paleomagnetic data showing a slowdown in the India-Asia convergence rate at that time (e.g., Molnar and Tapponnier, 1975; Patriat and Achache, 1984; Dupont-Nivet et al., 2010).

The presence of active, north-south trending extensional basins has long been recognized on the Tibetan plateau (Tapponnier and Molnar, 1977; Molnar and Tapponnier, 1978; Ni and York, 1978). These features are perpendicular to the antecedent east-west structural grain of the plateau, and it has been argued that their initiation was coincident with the Tibetan plateau reaching its present, and maximum

attainable, elevation (Molnar and Tapponnier, 1978; England and Houseman, 1989). Timing for the initiation of extension on the plateau is estimated at ~10-15 Ma, based on cross-cutting of dateable igneous features by extensional faults (Coleman and Hodges, 1995; Blisniuk et al., 2001). The surface of the modern Tibetan plateau is characterized by widely distributed extensional basins (Yin, 2000; Kapp and Guynn, 2004) featuring internal drainage, with high evaporation resulting in widespread saline lakes. With the exception of the plateau-traversing Yarlong river, external drainage of the plateau is mainly limited to the eastern plateau margin.

3. Structural and Stratigraphic Configuration

3.1. Structural Geology

Tibetan rift systems (Figure 1) typically form internally drained 10-15 km wide half-graben or full-graben basins bounded by high angle normal faults and 30-40 km wide rift-flank uplifts (Armijo et al., 1986, Taylor et al., 2003, Pan et al., 2004, Kapp et al., 2008). The Lunggar extensional basin in west-central Tibet (Figure 2) differs from typical Tibetan extensional basins in that it features a low-angle (<40°) range-bounding normal fault and an intrabasinal topographic high inducing external drainage away from the central part of the basin (Kapp et al., 2008). The detachment juxtaposes a 6-6.5-km-high footwall (the Lunggar range) composed of Jurassic-Cretaceous and Miocene granitoids, mylonitic orthogneiss, and Permian–Cretaceous cover strata against a 4-4.5-km-high hanging wall containing Neogene basin fill unconformably overlying

Cretaceous strata (Kapp et al., 2008). The surface trace of the detachment, exposed along the central segment of the Lunggar range, appears to be inactive, as glacial moraines and alluvial-fan sediments unconformably overlap it. In the northern part of the Lunggar system, the detachment fault is no longer the major structure defining the range front; rather, the detachment is exposed in the footwall of a younger, high angle normal fault (Figure 2). The current locus of active normal faulting is situated within in the basin ~2-4 km east of the range front, where >1-10 m fault scarps cut synextensional sediments. This basinward shift in active faulting may be attributed to progressive formation of normal faults soling into a master detachment in the shallow crust (e.g., Wernicke, 1985; Horton and Schmitt, 1998; J.L.D. Kapp et al., 2005; Kapp et al., 2008). Along the eastern basin margin, minor west-dipping faults juxtapose the underlying Cretaceous (including carbonate and probable volcanic and intrusive rocks) against Cenozoic basin fill (Figure 2). Locally along the eastern basin margin, small normal fault pairs produce small-scale graben geometries.

3.2. Growth Structures

Stratal geometries observed in stratigraphic sections within conglomerate units along the western margin of the Lunggar extension basin reveal changes that indicate sedimentation synchronous with slip along the main basin-bounding detachment. Proximal conglomerate strata to the north of the basin center (Figure 2, stratigraphic sections N1 & N2) feature relatively uniform westward dips throughout their measured intervals (20-25° in section N1, and 30-35° in section N2). In the basin center (Figure 2,

section C), conglomerate strata feature uniform 35-40° westward dip in lower ~200m of measured section; in the upper ~500m there is a progressive, approximately 30° shallowing of dips to nearly flat-lying at the top of the measured interval (Figure 3).

These changes in stratal geometry with stratigraphic level are consistent with initial deposition of flat-lying strata, followed by continued sedimentation during slip along a simple listric normal fault, or formation of a half-graben in the upper structural levels of a ramp-flat listric fault system (e.g. Ellis and McClay, 1988; Gibbs, 1987). Other possible explanations for the observed stratal geometries include (1) an along-strike change from a relatively steeper, planar basin-bounding fault to a shallower-angle listric fault or (2) a progressive shallowing of the fault though time. The Lunggar detachment appears to be currently inactive at the surface, so obtaining age estimates of the growth strata deposits may allow for constraining the timing of cessation of slip on the main basin-bounding fault and the beginning of basinward migration of active normal faulting.

3.3. Basin Stratigraphy

The oldest deposits of the Lunggar basin (Figure 2) consist of conglomerates exposed along the Lunggar Shan range front defining the western margin of the Lunggar basin, and in modern incised drainages to the east of the modern north-flowing river along the basin axis. Stratigraphic sections (Figure 4) were measured at four representative outcrops of the basin-fill succession, and named according to their relative

map position within the Lunggar basin as “C” (central basin, range-front section), “N1” and “N2” (northern range-front sections 1 and 2), and “E” (eastern section).

The exposed stratigraphic thickness at each locality ranges from about 300 to 700 m (Figure 4). However, lithostratigraphic correlations along the western basin margin indicate that the two northern sections N1 (~650 m) and N2 (~600 m) represent equivalent levels of the basin that are both stratigraphically below the coarse-grained growth-stratal interval exposed in the central section C (~700 m). Therefore, the total thickness of exposed basin fill approaches ~1300 m.

The absence of syndepositional igneous rocks or diagnostic fossil assemblages precludes accurate age assignments for exposed fill of the Lunggar basin. Regional mapping efforts have regarded basin fill as generally late Miocene to Quaternary in age (Pan et al., 2004).

4. Depositional Systems

Sedimentological analyses performed in the context of the four measured stratigraphic sections and at selected local exposures throughout the Lunggar basin (Figures 2 and 4) provide the basis for evaluation of depositional systems. We identified a total of 11 sedimentary lithofacies (6 conglomerate, 3 sandstone, 2 mudstone) representative of variable depositional processes (Table 1). On the basis of their stratigraphic occurrence, these lithofacies are then grouped into five separate lithofacies associations representative of different depositional processes (Table 2).

4.1. Alluvial Fan Conglomerates

Facies Associations 1 and 2 are best expressed in the range-front alluvial-fan conglomerates along the western basin margin, the sites of measured sections C, N1, and N2 (Figure 2). These deposits principally consist of disorganized, very poorly sorted, cobble to boulder conglomerates (Figure 5A, 5B) attributable to debris flow and sheet-flow deposition (e.g., Whipple and Dunne, 1992; Horton and Schmitt, 1996; Hampton and Horton, 2007), with a basal interval of breccia in section N1 possibly representing dry-rock avalanche deposits (e.g., Yarnold, 1993). The basal unconformable contact is only evident in section N2, where conglomerates rest on a carbonate mapped regionally as a Permian and/or Cretaceous unit along the northern segment of the Lunggar Shan (Figure 2). The range-front alluvial-fan conglomerates are dominantly gray in color and clast-supported, with matrix-supported intervals most prevalent in exposures at the basin center (section C). The conglomerate matrix consists of principally silt- to medium sand-sized material. The matrix is grey in sections N1 and N2, but is oxidized to a reddish-grey in section C and a deep brick red in the lower most exposed levels to the east (section E). Crude bedding, typically several meters thick (possibly up to 10 m thick), is defined in Facies Association 1 by changes in modal clast size and/or occurrence of thin sandstone beds. Bedding is better organized in Facies Association 2, with the dominantly conglomeratic intervals of sections C and N2 broken up by lenticular sandstone beds <1 m thick (Figure 5C, 5D).

Clast lithologies in the northern outcrops (sections N1 and N2) include carbonate, sandstone, quartzite, marble, phyllite, and granite, whereas the basin-center (section C)

conglomerates are composed nearly entirely of crystalline basement lithologies: biotite leucogranite, amphibole-rich granitoids, and amphibolite (quantitative conglomerate clast compositinoal data are presented below). Clast lithologies in the lowermost eastern outcrops (section E) also consist of carbonate, sandstone, and granite, with the granite clasts displaying very strong weathering (effectively to grus in some cases). Paleocurrent measurements from clast imbrication in western exposures of Facies Associations 1 and 2 (intermediate levels of section N2) show southeast-directed paleoflow (Figure 4), consistent with a principal sediment source in the uplifted footwall that forms the modern Lunggar range.

4.2. Fluvial Sandstones and Conglomerates

Facies Association 3 consists of interbedded conglomerates and sandstones in the lower levels of the northernmost section (N2) and the lower and upper levels of the eastern section (E). These fluvial deposits are finer grained, better organized, and exhibit thinner and better-defined beds than the alluvial-fan deposits of Facies Associations 1 and 2. Most conglomerate beds of Facies Association 3 have pebble and cobble clasts within a moderately well-sorted sandstone matrix, and generally display some degree of normal grading within beds 1-5 m thick (Figure 5E). The < 1 m-thick sandstone beds generally have moderately developed sedimentary structures, typically trough-cross stratification (Figure 5E). In one section (N2), the mixed conglomerates and sandstones of Facies Association 3 are transitional with coarser deposits of Facies Association 2 and finer deposits of Facies Associations 4 and 5. We attribute gravel and sand deposition of

Facies Association 3 to braided fluvial systems downstream of basin-margin alluvial fans (e.g., Steel and Aasheim, 1978; Miall, 1996; Smith, 2000).

Clast lithologies are comparable to those reported above for Facies Associations 2 and 3. Measurements of clast imbrication and trough axes along the western basin margin (lower levels of section N2) show paleoflow to the southeast, consistent with Facies Assocations 1 and 2. In contrast, along the eastern basin margin (section E), imbricated beds containing oblate carbonate and sandstone clasts indicate paleoflow to the south-southwest, toward the original depocenter of the basin.

4.3. Lacustrine Mudstones and Sandstones

Lacustrine strata of Facies Associations 4 and 5 (Figure 5F, 5G, 5H) are preserved in lower levels of the northernmost section (N) along the western basin margin and in intermediate levels of the eastern section (E). Unconfomably overlying the lower conglomerate (Facies Associations 1-3) in section E is a ~200 m, upward-fining succession of lacustrine mudstone, siltstone, and minor sandstone, in turn capped by a section of cross-stratified fluvial sandstone and conglomerate (Facies Association 3). The lacustrine facies in section E consist of a basal unit of yellow, fine-grained sandstone with intermittent lenticular beds (10-30 cm) of indurated, rippled medium-grained sandstone. Fossil gastropods and organic debris was found near the basal contact of the yellow lacustrine unit. This unit grades smoothly upsection to white fine-grained sandstone and siltstone, which contains bivalve fossils in its upper portion.

We attribute deposits of Facies Associations 4 and 5 to suspension settling within an open lacustrine setting, with potential influence by delta or fan-delta systems along lake margins (e.g., Link and Osborne, 1978; Hamblin, 1992; Ridgway and DeCelles, 1993; Horton and Schmitt, 1996). Locally, this interval potentially contains overbank fluvial deposits that recorded floodplain suspension settling and/or crevasse-splay deposition (e.g., Slingerland and Smith, 2004).

The slope-forming character of the lacustrine unit, along with extensive post-depositional faulting, slope failure, and overall poor exposure preclude the measurement of detailed stratigraphic sections in this interval. Both the lower, yellow portion of the lacustrine unit and the underlying lower conglomerate pinch out ~8 km north of section E, where the upper lacustrine white siltstone directly overlies strongly tilted beds of Aptian-Albian carbonate (Figure 2).

5. Provenance

5.1. Paleocurrents

Sediment dispersal patterns were analyzed within the context of the measured stratigraphic sections of the Lunggar basin (Figure 4). Field measurements of imbricated clasts within pebble to cobble conglomerates and trough axes within cross-stratified sandstones and conglomerates provide estimates of sediment dispersal patterns during basin filling. These paleoflow patterns show marked contrasts with the modern fluvial drainage systems.

Along the western basin margin, the coarsest basin fill consisting of principally debris-flow conglomerates exhibits clast imbrication and trough axes yielding a mean paleoflow direction of 140°, >90° from the modern, north-northeast-flowing axial river (Figure 6). The distal eastern part of the basin shows roughly southward flow, with a mean paleocurrent direction of 211°, effectively opposite the modern axial river (Figure 6). In addition, the sedimentologic evidence presented above shows the basin once experienced moderate to significant levels of lacustrine sedimentation. Collectively, the sharp changes in sediment dispersal patterns and absence of modern lake systems highlight a major late Cenozoic reorganization of drainage patterns within the Lunggar extensional system.

5.2. Sandstone Modal Compositions

Sandstone framework grain compositions were assessed for 15 thin sections prepared from samples of the Lunggar basin, including sandstones from conglomeratic alluvial-fan units as well as younger lacustrine and fluvial units. Point counts of 450-500 framework sand grains (>0.0625 mm) per thin section were conducted according to the Gazzi-Dickison method (Gazzi, 1966; Dickinson, 1970, 1985; Dickinson and Suczek, 1979; Dickinson et al., 1983; Ingersoll et al., 1984). Framework grain categories defined for this study (Table 3) reflect the range of quartz (Q), feldspar (F), and lithic fragments (L).

Point-count results for all 15 samples are presented in three standard ternary diagrams (Figure 7). Each diagram reflects different ratios of framework grains

recalculated on the basis of the grain classifications defined in this study (Table 4): (A) the common Q-F-L sandstone classification scheme using proportions of total quartz-feldspar-lithic fragments (Folk, 1980); (B) the Q-F-L provenance categories for different tectonic settings, also based on proportions of total quartz-feldspar-lithic fragments (Dickinson et al., 1983); (3) the Ls-Lm-Li comparison reflecting provenance from sedimentary-metamorphic-igneous lithic fragments (Dickinson and Suczek, 1979).

Sandstones of the Lunggar basin are texturally and mineralogically immature, featuring subangular to angular framework grains with only mild to moderate alteration (e.g., grain dissolution or replacement). Lithic fragments are abundant in the Lunggar samples, forming at least a plurality of Q-F-L constituents in 10 of 15 samples. Quartz and feldspar grains make up lesser percentages, with feldspar composition being highly variable. The mean composition for all samples is $Q_{27}F_{19}L_{54}$.

Significant contrasts in sandstone composition are observed according to geographic location and position within the overall basin stratigraphy. Lunggar sandstone samples from the conglomerate-dominated exposures along western basin margin (sections C, N1, and N2) show substantially higher proportions of feldspar and metamorphic lithic fragments than eastern regions (section E). The western range-front samples are moderately to well-sorted, medium-grained sandstones classified compositionally as lithic arkose to litharenite, with mean compositions of $Q_{28}F_{34}L_{38}$ and $Ls_{40}Lm_{52}Lv_{8}$ (Figure 7A). In contrast, sandstones from the conglomerate section near the eastern margin of the basin (E) are well-sorted, fine- to medium-grained feldspathic litharenite to litharenite (Table 4, Figure 7) exhibiting relatively lower feldspar and

higher lithic content (mean Q-F-L: $Q_{15}F_8L_{77}$) and a greater proportion of sedimentary lithic fragments ($Ls_{85}Lm_{15}Li_0$).

These trends are interpreted as the product of contrasting compositions of exposed rocks along the western and eastern basin margins. The Lunggar Shan, which forms the western footwall, is distinguished by widespread crystalline rocks, including Jurassic-Cretaceous and Miocene granitoids that intrude a Permian-Cretaceous panel of sedimentary rocks (Figure 2). In contrast, Cretaceous sedimentary rocks dominate eastern regions (Figure 2), consistent with increased sedimentary lithic fragments and reduced feldspar and metamorphic lithic fragments releative to the western basin. These results are consistent with paleocurrent data (Figure 6) in implicating sediment sources in both the west and east for their respective basin margins.

Additional compositional variations may be related to contrasting exhumational levels in the source regions. Although the western range-front samples from sections C and N2 have similar mean Q-F-L compositions ($Q_{28}F_{38}L_{34}$ and $Q_{29}F_{23}L_{49}$, respectively), their lithic compositions differ significantly ($Ls_{23}Lm_{68}Li_9$ and $Ls_{82}Lm_{13}Li_5$, respectively). In addition, sandstones from section C are distinguished by significant percentages of accessory minerals, most notably amphibole (≤ 25%), chlorite (≤ 5%), and epidote (≤ 5%). Because the western range-front deposits are all derived from the west, the compositional discrepancies among these sections are considered to be the product of different exhumational levels within the footwall. Specifically, we infer a greater contribution of structurally lower igneous intrusive rocks for section C relative to section N2. Similarly, the high amounts of sedimentary lithic fragments in sandstone samples

from the western range-front section N2 and the eastern sections E, both of which are dominated by detrital carbonate grains and carbonate cementation, suggests increased sediment input from the erosion of Permian-Cretaceous carbonate rocks exposed in upper structural levels of the western footwall and in widespread regions east of the Lunggar basin (Figure 2).

5.3. Conglomerate Clast Compositions

Conglomerate clast compositional data were acquired at 29 locations within the four measured sections: 6 in section N2, 13 in section N1, 7 in section C, and 3 in section E. Grids measuring ~1 m^2 were marked on the outcrop surface, and ~100 clasts were counted within each grid. Relative proportions of clast lithologies, using a simplified classification scheme (Figure 8), reveal important spatial and stratigraphic trends. Dark- to medium-gray carbonate makes up large percentages of the clast counts in sections N1, N2, and E. With the exception of four clast counts within section N1 composed entirely of quartzite, limestone clasts makes up large proportions of the conglomerates low in the sections, with a general decrease upsection. Clasts of clean, light tan to white quartz sandstones make up variable percentages of sections N1, N2, and E, with no discernable overall trend in their occurrence. Metasedimentary clasts, including quartzite, marble, and dark grey to black slate are common in sections N1 and N2, but do not appear in section E. Sedimentary and metasedimentary rocks are absent in section C, closest to the basin center. Crystalline rocks in all sections are dominated by granitoids, usually coarse-grained, light-colored quartz/K-feldspar/plagioclase/biotite granites; however the western

growth strata locality (section C) has a large amount of amphibole-rich granite, as well as plagioclase/amphibole amphibolite. In the sections that contain sedimentary and metasedimentary rocks, the proportion of igneous and meta-igneous rocks increases upsection.

The broad upsection increase in clasts of crystalline rocks at the expense of carbonate clasts, as observed in sections N1, N2, and E, suggests an unroofing trend with progressively increased contributions from lower structural levels (e.g., Colombo, 1994; Horton and Schmitt, 1998). Continual footwall uplift along the main rift-bounding detachment, as well as other synthetic and antithetic faults related to the detachment system, led to erosion of the overlying sedimentary carapace, eventually exposing basement igneous and metamorphic rocks during deposition of the upper parts of sections N1, N2, and E. The lack of sedimentary and metasedimentary conglomerate clasts in growth strata of section C suggests that this phase of basin accumulation represents a continuation of this trend.

5.4. Detrital Zircon U/Pb Geochronology

U/Pb analyses were performed on detrital zircons from medium-grained sandstone samples collected from measured stratigraphic sections and additional localities during the course of mapping and regional reconnaissance (Figures 2 and 6). The 2-5 kg sandstone samples were crushed, and zircon grains separated using standard heavy liquid techniques. Separated zircons were selected randomly from all size and shapes, avoiding only a small proportion of metamict grains and those with significant

cracks or inclusions. Seven sandstone samples were analyzed using the multicollector laser ablation inductively coupled mass spectrometer (LA-ICP-MS) at the University of Arizona LaserChron center using procedures described by Gehrels (2000) and Gehrels et al. (2008). Approximately 100 individual zircon grains were analyzed from each sample. In-run analyses of a 564 ± 4 Ma (2σ error) zircon standard were conducted approximately every five measurements in order to correct for inter- and intra- element fractionation. The uncertainty resulting from the calibration correction is generally 1-2% (2 σ error) for both $^{206}Pb/^{207}Pb$ and $^{206}Pb/^{238}U$ ages. The analytical data are reported in Appendix 1. Analyses exhibiting >20% uncertainty, >30% discordance (by comparison of $^{206}Pb/^{238}U$ and $^{206}Pb/^{207}Pb$ ages) or >5% reverse discordance are omitted from further consideration. Probability density plots of detrital zircon ages are presented for the seven analyzed samples (Figure 9). Crystallization ages for additional bedrock samples around the broader study region (Figures 2 and 6; Kapp et al., 2008; P. Kapp, personal communication) are included for comparison with the detrital samples (Figure 9). Only zircon ages <300 Ma are depicted, as there were no significant older populations (Figure 9; Appendix 1).

The combined probability density functions and histogram plots for all detrital zircon samples of the Lunggar Rift show prominent peaks at 150-155 Ma (Figure 9), with no other large peaks in common across all samples. Zircons from both the base (4 m) and top (635 m) of section C show a significant peak at ~100 Ma, and a minor peak occurs at ~49 Ma in the fluvial unit and at 380 m in section N2. The 22 bedrock crystallization ages fall into two main populations: a set of 7 ages between 140-155 Ma that

approximately match the main detrital signal, and a set of 12 ages between 9-15 Ma that is not significantly represented in the detrital record.

These results indicate major contributions from the intrusive and extrusive igneous units of Upper Jurassic-Lower Cretaceous age, consistent with regional sources in this part of the Lhasa terrane (Volkmer et al., 2007). Although it is tempting to assign these age signatures to direct contribution from uplifted crystalline rocks, we suggest that a significant component may be recycled from widespread Cretaceous clastic deposits throughout the region which may have been ultimately derived from such Mesozoic igneous sources. The existence of an early Cenozoic age peak, albeit limited in scale, suggests some detrital contributions from reported Paleocene-Eocene volcanic rocks of the Lhasa terrane. The occurrence of this age peak in eastern basin fill (sample WW082209-05) is consistent with derivation from Linzizong volcanic rocks, or their equivalents, extensively and exclusively exposed in the central Lhasa terrane east of the Lunggar basin (Volkmer, 2010; Wang et al., 2010).

6. Detrital (U-Th)/He Thermochronology

Examination of the thermochronologic record contained in clastic basin fill may assist in the understanding of the exhumation histories of adjacent fault blocks, particularly the early uplift histories subsequently removed by erosion. The uplifted footwall range, the Lunggar Shan, bounding the Lunggar extensional basin stands at elevations of up to ~6000-6500 m, with much of the upper range under perennial snow

and ice cover (Figures 2 and 6). The proximal range-front deposits of the western Lunggar basin are thus attractive targets for sampling as proxies for the exhumational record of the adjacent footwall.

In the course of measuring stratigraphic sections, crystalline basement (granitoid) clasts from boulder conglomerates were sampled at regular intervals with the intention of separating apatite and zircon grains for (U-Th)/He thermochronometric analysis. To ensure maximum consistency in cooling history, all samples represent a single uniform lithology common throughout the study area: the quartz/K-spar/plagioclase/±biotite leucogranite. Where possible, these granitic boulders were collected near the sandstone horizons sampled for detrital zircon analyses, with the intention of using the same thermochronometric techniques to enable comparison of results of the sandstone samples with those of the granitic boulders. Because of its higher proportion of crystalline basement clasts, and more continuous exposure, the greatest number of samples were taken from range-front section C, along the central segment of the Lunggar extensional system .

The conglomerate clasts were crushed and apatite and zircon grains were separated using standard heavy liquid techniques. Both apatite and zircon separates were prepared and analyzed at the Isotope Geochemistry Laboratory at the University of Kansas. Apatite separates were analyzed using methods described by Stockli et al. (2000), and zircons using methods described by Reiners et al. (2004). Thermochronometric analyses were performed on samples from the three range-front sections (N1, N2, and C); apatite crystals separated from clasts within section E were of

insufficient quality (i.e., contained inclusions, irregularly shaped, insufficient size) for analysis.

Nine apatite (U-Th)/He ages were acquired from three conglomerate clasts sampled from sections N1 and N2 (Figure 11). These ages show a younging trend from 27.4 Ma average age at 250 m, to 10.4 Ma at 650 m in section N1, and 9.4 Ma at 555 m in section N2. (U-Th)/He ages from the tops of sections N1 and N2 are considered correlatable on the basis of stratigraphic correlations (Figure 4), proximity (<3 km, Figure 2), and topographic position (~5320 m in section N1, ~5240 m in section N2). Zircons recovered from clasts sampled from the N1 and N2 sections were not analyzed for this study.

Eight samples of conglomerate clasts and sandstones were taken in the course of measuring section C. Apatite and zircon (U-Th)/He ages for these samples are shown in Figure 12 and Appendix 2. Zircon (U-Th)/He average ages from both conglomerate clasts and sandstone samples are within experimental error, and define an upward-younging trend. Seven of ten apatite (U-Th)/He ages also define an upward-younging trend. We recognize scatter in some apatite (U-Th)/He ages, for example the three grains from section C that deviate significantly from the aforementioned trend (Figure 11B, Appendix DR3), as well as the sample at 230m in section N1 (Figure 11A, Appendix DR3). We regard this scatter as a potential product of (a) inclusions undetected in the course of grain selection (Ehlers and Farley, 2003), or (b) He implantation from nearby U-Th-rich mineral phases (Spiegel et al., 2009); both processes would have the effect of increasing the apparent apatite (U-Th)/He ages. Nevertheless, even if only the youngest individual

ages are considered, the upward younging trends remain intact, and the differences in rate of change of age vs. stratigraphic position are preserved, albeit lessened.

The thermochronologic data from proximal basin fill show trends in age versus stratigraphic level that are consistent with progressive cooling due to erosional unroofing of footwall bedrock and deposition into proximal fill of the adjacent Lunggar extension basin. For this reason, the age profiles expressed by the detrital thermochronological data show an upsection younging (Figures 11-12) that can be considered as an "inversion" of the conventional vertical age:elevation profiles for adjacent bedrock (Figure 10). The age profiles for basin fill further indicate that the apatite and zircon (U-Th)/He thermochronometers (apatite and zircon) were not thermally reset by sedimentary burial. Finally, the detrital apatite (U-Th)/He ages provide a critical upper (older) bound on the age of the Lunggar basin fill. The ~ 5-2.5 Ma cooling ages for granite boulder clasts require a younger age of deposition, consistent with Pliocene to Pleistocene accumulation of the upper stratigraphic levels of the basin.

7. Discussion

Although previous studies have demonstrated the broad extent of Cenozoic extension across the Tibetan plateau (e.g., Molnar and Tapponnier, 1978; Armijo et al., 1986; Yin et al., 1999; Yin, 2000), significant uncertainties persist over the style and architecture of deformation and basin filling. At issue are the structural geometries, kinematics, potential linkages among different structures, and the long-term evolution of

upper-crustal structures in terms of their activation, deactivation, and role in basin formation. For many extensional basins of Tibet, these issues are compounded by the fact that Cenozoic basin fill is largely buried, with limited exposures and no subsurface data. New data for the Lunggar basin of central Tibet highlight several key points summarized below

7.1. Deposystems and Basin Geometry

The time-space evolution of depositional systems and sedimentation pathways show a complex shift from internal to external drainage. Facies distributions and sediment dispersal patterns within the Lunggar basin suggest that the basin center was, at one time, the depocenter for the extensional system. On the northwest margin of the basin, flat-lying beds of the upper lacustrine siltstone unit pinch out against Mesozoic carbonate bedrock in an apparent onlap relationship. The lacustrine facies exposed in eastern regions thicken to the southwest toward the basin center to eventually comprise the full Lunggar lacustrine succession (Figure 2). However, at the basin center itself, only the lower yellow lacustine facies are observed along the intrabasin topographic high, suggesting that the upper portion of the lacustrine deposits has been eroded. Paleocurrent indicators within western-margin debris flow deposits (section N2) and eastern-basin fluvial deposits (section E) show that the flow regime within the basin during deposition of the conglomeratic units was toward the basin center in the south (Figure 4), effectively opposite of the modern flow regime (Figure 6). These features and relationships support an interpretation that the center of the Lunggar basin has rebounded.

Stratal geometries of the proximal debris flow conglomerates along the western basin margin reveal a change in depositional style over time. The stratigraphically lower northern units feature relatively uniform westward dips of 20-25° in the section N1 strata, and 30-35° in section N2. By contrast, the stratigraphically higher conglomerate interval at the rift center (section C) exhibits a change from uniform 35-40° westward dip in its lower ~200 m to a progressive, ~30° shallowing of stratal dip through its upper ~500 m. We interpret the formation of these growth strata as being either the product sedimentation synchronous with displacement along a fault with an irregular geometry in the subsurface (i.e., listric or ramp-flat geometry) and/or a temporal change in fault geometry (i.e., planar to listric).

Further map relationships and modern fault scarps in the Lunggar basin (Figure 2) demonstrate a basinward advance of deformation in which the main detachment fault apparently decelerated or ceased motion while younger, steeper faults within the basin became active. Fault deactivation and activation suggests complex deformation compatible with basinward advance of faulting in other normal fault systems (e.g., Dart et al., 1995; Horton and Schmitt, 1998).

7.2. Sediment Provenance

Sandstone Q-F-L data and conglomerate clast compositions reveal progressive unroofing and increasing contributions from footwall lithologies during basin accumulation. Sandstones from the lower levels of the basin (lacustrine, fluvial, and debris flow deposits of sections E, N1, and N2; Figure 4) feature large proportions of

carbonate lithic fragments, consistent with erosion of the Permian to Cretaceous sedimentary cover sequence, the remnants of which are exposed in the northern footwall and in the hanging wall along the eastern basin margin (Figure 2). Upsection increases in the quartz and feldspar fractions in these rocks indicate exposure and erosion of structurally lower crystalline rocks in the footwall. Sandstone samples from debris flow deposits along the central basin segment (section C) are of a completely different character; they display higher feldspar fractions, smaller lithic fractions dominated by metamorphic rock fragments, and hematite rather than carbonate cementation. These characteristics suggest further erosional exhumation of crystalline footwall rocks. The sandstone Q-F-L data are reinforced by trends in conglomerate clast compostion. Specifically, the northern debris flow units (sections N1 and N2) and eastern fluvial conglomerates (section E) feature upsection increases in granite clasts, consistent with an unroofing sequence. The uppermost basin fill, consisting of central-basin proximal debris flow conglomerate (section C), is composed entirely of granitiods and metamorphic rocks, suggesting a continuation of unroofing with complete erosional stripping of the Permian–Cretaceous sedimentary cover in some parts of the footwall.

Detrital zircon U/Pb geochronologic data consistently show major ~140-160 Ma peaks across all samples, suggesting proximal crystalline source rocks of similar age. Of the 22 analyzed bedrock samples in and around the study area (Kapp et al., 2008; P. Kapp, personal communication), seven are in the 144-154 Ma age range. These samples are distributed across the footwall and hanging wall of the rift (Figure 3), suggesting mixed hanging wall and footwall sources. Minor Paleocene-Eocene age peaks seen the

base of the fluvial unit, and at 380 m in section N2 may indicate input from the early Cenozoic Linzizong volcanic rocks, exposed extensively in the central Tibetan plateau to the east of the study area.

Thirteen bedrock crystallization ages in the central Lunggar footwall have ages ranging from ~9-22 Ma (Figure 3); however, these bedrock ages are not significantly represented in any detrital zircon samples analyzed for this study. All but one of the <25 Ma bedrock crystallization ages are situated south of the intrabasin drainage divide, possibly suggesting that the divide precluded significant contribution of <25 Ma zircons to the northern Lunggar basin. However, given the evidence from facies distribution patterns and paleocurrent data for central basin rebound, we suggest that the <25 Ma rocks were exhumed more recently such that young zircon populations were not incorporated into the exposed record of basin accumulation.

7.3. Basin Chronology

Thermochronologic data reinforce the interpretation, gleaned from detrital compositions, that the northern proximal debris flow deposits (section N1 and N2) are lower in the basin-wide stratigraphic column than those exposed in the rift center (section C). Mean apatite (U-Th)/He ages from the tops of sections N1 and N1 are older (~10 Ma) than the basal mean apatite age from section C (4.8 Ma). On the basis of these age relationships and detrital compositions, we interpret the base of section C to be approximately correlatable with the tops of sections N1 and N2 (Figures 8 & 11).

A lack of significant post-Eocene volcanism across most of the Tibetan plateau (P. Kapp et al., 2005; Miller et al., 2000) presents difficulties in assessing the onset of fault-related subsidence in Tibetan extensional basins. Datable horizons (e.g., ash beds) within the Lunggar rift sedimentary record are not in evidence, and fossils are rare. In the absence of direct dating of basin fill, we utilize the apatite (U-Th)/He ages of detrital material, both sandstone and granitic boulder clasts, to broadly constrain the initiation of extension and sediment accommodation in the Lunggar basin. These results provide a maximum (older) age constraints of ~10 Ma for lower stratigraphic levels (specifically, the uppermost section N1 and N2 mean ages) and ~5 Ma for upper stratigraphic levels (mean age from the lowermost section C). Although these age boundaries are younger than the estimated middle to early late Miocene ages for the initiation of extension in southernmost Tibetan plateau (Coleman and Hodges, 1995; Edwards and Harrison, 1997; Blisniuk et al., 2001; Garzione et al., 2003), they are consistent with an age of 8 ± 1 Ma in the Nyainquentanghla region (Harrison et al., 1995), which is situated at a comparable position as the Lunggar basin (Figure 1). This trend, along with reported younger ages of initial rifting farther north in the Qiangtang terrane (Figure 1; Yin et al., 1999) suggests a broad northward advance of initial extension.

7.4. Exhumational Record

The shape of a plotted profile of thermochronologic age data versus sampling elevation/depth can give insight into the style of uplift in orogenic regions (Harrison and Zeitler, 2005; Ehlers and Farley, 2003; Stockli, 2005). A constant slope may be

interpreted as a constant uplift rate, whereas a changing slope with pronounced inflection points may be the result of periods of tectonic quiescence punctuated by episodic rapid exhumation events (Harrison and Zeitler, 2005; Ehlers and Farley, 2003; Stockli, 2000; Stockli, 2002). The thermochronological data acquired during the course of this study was obtained from detrital deposits, so there are potential complications in interpreting plots of (U-Th)/He ages versus stratigraphic positions. These complications include the possibility of changing sedimentation rates, and/or that conglomerate clasts or sandstone zircon grains may be deposited out of sequence with respect to the exhumation history of the uplift. Despite these caveats, section C detrital (U-Th)/He ages largely follow linear trends, with similar slopes for both the apatite and zircon samples. These relatively linear trends seen in the conglomerate clast zircon, sandstone zircon, and conglomerate clast apatite conform to an anticipated age versus stratigraphic position profile for a deposit proximal to an uplift undergoing exhumation at a constant rate, which did not change greatly between the zircon and apatite closure temperatures (Figure 10). Additionally, the conformity between the conglomerate clast and sandstone zircon ages reinforces the assumption that the thermal histories of conglomerate clasts are representative of the thermal history of the drainage catchment as a whole.

Apatite (U-Th)/He age profiles differ significantly between the northern proximal debris flow deposits (sections N1 and N2) and those in the basin center (section C). In the lower stratigraphic levels (section N2), there exists a 17 difference in mean apatite cooling ages over a 420 m stratigraphic interval. The upper proximal strata (section C) display a smaller 2.3 Myr age difference over a greater, 622 m stratigraphic interval. We

interpret the shallow cooling age versus stratigraphic position profile seen in the northern deposits as evidence for an exhumed and eroded apatite (U-Th)/He partial retention zone (PRZ). A PRZ is the product of progressive He loss below the ~60°C apatite (U-Th)/He closure temperature, and is typically expressed as a rapid decrease in apatite (U-Th)/He ages over a relatively short vertical interval. The presence of an apatite PRZ may be interpreted as reflecting a period of tectonic quiescence. Alternatively, the age profile in the northern deposits may be the product of slow exhumation through the apatite (U-Th)/He closure temperature. By contrast, the relatively steep cooling age versus stratigraphic position profile in section C is indicative of rapid exhumation of rocks through the apatite (U-Th)/He closure temperature. Based on these observations, we posit that the proximal debris flow deposits in the Lunggar basin record negligible to slow footwall exhumation followed by rapid, recent exhumation and uplift.

7.5. Basin Reconstruction

Distinctive features of the modern Lunggar rift include the intrabasin topographic high, external drainage from the basin center, systematice footwall unroofing, and progressive basinward advance of extensional deformation. We consider several possible hypotheses consistent with the principal observations.

One possible explanation for the intrabasin topographic high and external axial drainage toward the northern and southern rift terminations seen in the Lunggar basin is that the modern configuration is the product of two separate, north-striking normal fault-bounded basin systems propagating with continued extension until their fault tips

overlapped and began to interact. This hypothesis would predict a topographic high between two kinematically linked sub-basins (Anders and Schlische, 1994; Gawthorpe and Leeder, 2000). However, this hypothesis suggests the intrabasinal topographic high was an enduring feature of the system; facies distributions and the flow reversal argue against this fault linkage interpretation.

Another hypothesis for the configuration of the Lunggar basin is that the intrabasinal topographic high and external drainage pattern are the product of a large flux of footwall-derived sediment concentrated at the basin center. In this case, evidence for extensive alluvial fan formation across the width of the central basin would be expected. However, no evidence for aggradational alluvial-fan sedimentation exists in the rift center. Rather, lacustrine facies are exposed and currently undergoing incision along the intrabasinal high, with debris-flow alluvial fan deposits confined to the proximity of the range front topographic break.

Kapp et al. (2008) proposed an alternative model for Tibetan extensional basin evolution wherein basins experience rebound in their central portions due to fault slip, with resultant thinning of the elastic upper crust, and influx of ductile middle crustal material beneath the basin center. This isostatic rebound is accompanied by tilting of the main basin-bounding fault to shallower angles consistent with a typical detachment fault configuration (Davis and Lister, 1988). In this scenario, the locus of active faulting shifts systematically basinward as older faults are abandoned and younger faults sole into the detachment at shallow crustal levels (e.g., Horton and Schmitt, 1998; J.L.D. Kapp et al., 2005).

These various competing hypotheses make different predictions in terms of sediment dispersal patterns, facies occurrence, basin structure, and footwall exhumational history. In this paper we present structural, stratigraphic, geochronologic, and thermochronologic evidence that support the interpretation of the Lunggar rift as an intermediate step in a continuum of Tibetan basin evolution with continued extension on the plateau (Kapp et al., 2008). Such a model predicts that internally drained, high-angle normal fault-bounded "traditional" extensional basins evolve into surpadetachment basins associated with developing metamorphic core complexes.

8. Conclusions

1) A low-angle (<40°), east-dipping detachment fault in the west-central Tibetan plateau controlled late Cenozoic uplift of crystalline footwall rocks and subsidence then exhumation of a north-trending hanging-wall basin now exposed at ~5-5.5 km elevation. Within the >500-1000 m succession of the Lunggar extensional basin, stratigraphic variations in sedimentary facies and sediment dispersal patterns indicate a transformation from an internally drained, fluvial and lacustrine configuration to an externally drained fluvial system. Paleocurrent indicators in coarse-grained fill of the northern basin show paleoflow to the south-southwest, toward the basin center. Coeval lacustrine deposits thicken toward the basin center, suggesting the central portion of the basin was the site of the original lower-elevation depocenter. In contrast, the basin center is now defined by an intrabasinal topographic high, with a modern, north-northeast-

flowing axial river effectively opposite to that of the original paleoflow regime.

2) Provenance data from detrital compositions, U/Pb age spectra, and paleocurrent measurements indicate major erosional exhumation of uplifted footwall rocks. Sandstone petrographic data show predominantly lithic fragments, with significant carbonate detritus derived from a Permian to Cretaceous cover section. Sandstone Q-F-L trends within Lunggar basin fill show upsection increases in the quartz and feldspar fraction, consistent with progressive exhumation of granitic bodies. These data are supported by stratigraphic trends in conglomerate clast compositions, which show increasing upsection proportions of granitic clasts within alluvial-fan conglomerates of the western basin margin (sections N1, N2, and C) and fluvial conglomerates of the eastern margin (section E).

Detrital zircon U/Pb data show a remarkably unimodal distribution, with all seven sandstone samples showing major age peaks at ~140-160 Ma. Widespread exposures of Mesozoic intrusive and extrusive igneous rocks suggest sediment sources from both the western footwall and the eastern hanging wall, with limited lower Cenozoic ages representative of farther eastern sources of the Lhasa terrane (e.g., Linzizong volcanic rocks). Paleocurrent patterns suggest an internally directed flow pattern toward the basin center with footwall sediment sources dominating Lunggar basin fill. However, the ~9–22 Ma population of footwall granitic rocks (based on results from 22 samples) is not represented in any samples from exposed fill of the northern Lunggar basin, suggesting that these rocks were situated at deeper footwall structural levels and were fully exhumed after the main phase of basin accumulation.

3) The presence of hanging-wall growth strata along the western margin of the Lunggar extensional basin (section C) argues for sedimentation synchronous with displacement along the main basin-bounding fault, the relatively low angle (<40°) east-dipping Lunggar fault. Approximately 30° of syndepositional tilting of proximal hanging-wall strata is recorded in the upper ~500 m of a 705 m section of conglomeratic basin fill, with the lower ~200 m having relatively uniform 35-40° westward dip. This upsection change from uniform stratal dip to growth stratal geometries may be the product of an irregular fault geometry at depth (i.e., listric or ramp-flat geometry), or a temporal change in geometry from a planar to listric configuration.

4) Determining the precise onset of the Lunggar extensional basin is limited by a shortage of Cenozoic igneous or fossil materials. However, apatite (U-Th)/He ages from the >500–1000 m-thick succession of coarse-grained hanging-wall strata adjacent to the east-dipping Lunggar normal fault help constrain maximum depositional ages. For lower stratigraphic levels (northern section), non-reset mean (U-Th)/He ages of apatite grains, both from sandstones and from granitoid boulders in conglomerate beds, indicate exhumational cooling (through the ~60°C isotherm) over a broad timeframe ranging from roughly 27 to 10 Ma, thereby providing a rough bound on maximum depositional age. The upper stratigraphic levels (central section) yield much tighter age constraints in which apatite (U-Th)/He ages of granite boulders yield ~ 5-2.5 Ma cooling ages. This upsection change in detrital (U-Th)/He ages is consistent with erosional unroofing of a partial retention zone (PRZ) during rapid Plio-Pleistocene uplift of the footwall and coeval subsidence of the hanging-wall basin. A genetic linkage between fault activation

and Lunggar basin initiation suggests that rapid footwall exhumation was synchronous with basin accumulation, commencing at roughly 5–2.5 Ma.

5) Detrital (U-Th)/He thermochronological data from basin-fill sandstones and granitic boulders suggest rapid recent exhumation of footwall crystalline rocks along the western flank of the Lunggar basin. Granite boulder and sandstone zircon (U-Th)/He ages within the central range-front conglomerate (section C) show remarkable congruity, with linear relationships between age and stratigraphic level (~1.5 Myr younging trend over ~625 m), indicative of relatively uniform footwall exhumation (Figure 11). Apatite (U-Th)/He ages from the same clasts, while more limited in number, are consistent with this trend (~2.5 Myr over ~625 m). The stratigraphically higher proximal deposits thus suggest continuous exhumation consistent with rapid uplift.

Clasts from lower stratigraphic levels (northern range-front deposits) record older apatite (U-Th)/He ages and a significant age difference over the sampled stratigraphic interval (~17 Myr over ~400 m of section). The central range-front growth strata display a much smaller apatite (U-Th)/He age difference over a greater stratigraphic interval. We interpret this difference in rate of apatite (U-Th)/He age with stratigraphic position as recording the exhumation of an apatite partial retention zone (PRZ) in the northern deposits. These data suggest that the footwall block endured a period of tectonic quiescence, resulting in the formation of the PRZ, followed by rapid, recent uplift. Our interpretation of recent uplift is supported by published data from direct sampling of footwall lithologies showing cooling ages of <2 ma in the rift center (Kapp et al., 2008)

6) The results of this study suggest that the Lunggar rift experienced important changes in basin geometry over the course of its history. Facies distributions, paleocurrent data, and stratal geometries support an interpretation that the Lunggar rift was initially fed material from the eastern hangingwall, and then dominated by a major footwall sediment source. Reversal of sediment dispersal within the basin resulted in a transformation from closed (internal) drainage to external drainage, a point underscored by the presence of the topographic high undergoing incision and recycling of lacustrine facies in the center of the modern basin. A basinward migration of active normal faulting further modified the geometry of the Lunggar basin. These criteria suggest a supradetachment basin characterized by significant isostatic rebound (Kapp et al., 2008). Alternative hypotheses for the Lunggar basin's configuration including (1) propagating, interacting fault tips of separate normal fault systems, or (2) a concentrated point source of sediment are not supported by the data.

9. Figures

9.1. Figure Captions

Figure 1: Regional tectonic map of the Tibetan Plateau, showing basin-bounding normal faults (blue), strike-slip faults (red), and Mesozoic to early Cenozoic suture zones (dashed lines) (modified from Kapp and Gyunn, 2004)

Figure 2: Geologic map of the northern Lunggar basin study area (modified from Kapp et al., 2008).

Figure 3: Panoramic photo mosaic (upper) and line drawing (lower) of growth strata exposed along the western basin margin (section C), highlighting the progressive shallowing of stratal dip and the locations of samples for apatite and zircon (U-Th)/He analyses, and detrital zircon U/Pb analyses.

Figure 4: Stratigraphic sections measured within debris flow conglomerates. Section labels refer to map locations (Figure 2): C—central section; N1 and N2—northern 1 and 2 sections; E—eastern sections.

Figure 5: Photographs of sedimentary lithofacies of the Lunggar basin. (A) Clast-supported and (B) matrix-supported debris-flow boulder conglomerate representing

proximal alluvial fan deposition of Facies Association 1 (FA1). (C) Normally graded, upward fining packages (arrows) of (D) imbricated pebble to cobble conglomerate representing medial alluvial fan deposition (FA2). (E) Interbedded cross-stratified sandstone and pebble conglomerate representing braided fluvial deposition (FA3). (F) Angular unconformity (arrow) between FA1 cobble to boulder conglomerate and overlying sandstone, mudstone, and local pebble conglomerate of the overbank fluvial to marginal lacustrine interval (FA4). (F) Slope-forming mudstone and sandstone deposits of the lacustrine facies associations (FA4 and FA5). (G) Resistant siltstone and very fine-grained sandstone of the open lacustrine facies association (FA5) with internal bedding contacts accentuated by organic material.

Figure 6: Landsat map of the Lunggar basin and adjacent western footwall range formed by the Lunggar Shan (blue color represents snow), showing U/Pb basement samples (Kapp et al., 2008; P. Kapp, personal communication), modern axial river drainage patterns (aqua lines) and the intrabasinal topographic high (dashed purple line).

Figure 7: Modal petrographic data for framework grains in sandstones from the Lunggar basin. (A) Q-F-L ternary diagram showing sandstone classification of Folk (1980). Arrow highlights upsection increase in Q and F in samples from section N2 (FA1), section E (FA2), FA3, FA4, and FA5. (B) Q-F-L and (C) Ls-Lm-Lv ternary diagrams showing tectonic provenance fields of Dickinson (1983, 1985). Grey arrow in (A) shows upsection trend toward increased Q and F. Units sampled include proximal alluvial fan deposits

(sections N2 & C, 9 samples), medial alluvial fan deposits (section E, 2 samples), marginal lacustrine to overbank fluvial deposits (2 samples), and braided fluvial deposits (2 samples).

Figure 8: Conglomerate clast composition data from Lunggar extensional basin debris flow deposits (>100 counts per station) using a simplified lithological classification. Data are plotted by stratigraphic level within sections C, N1, N2, and E. Inset shows stratigraphic correlations from Figure 4.

Figure 9: Combined probability density functions (black lines) and histogram plots (red bars) depicting detrital zircon U/Pb ages, arranged in stratigraphic order with youngest basin fill at the top. Included at the base a plot of 22 basement crystallization ages (Kapp et al., 2008; P. Kapp, personal communication).

Figure 10: Highly schematic 2-D diagram of the expected (U-Th)/He age profiles for a normal fault system with an adjacent extensional basin. The expected age versus elevation relationships within the footwall (right) are shown with respect to apatite and zircon closure depths (assuming a constant geothermal gradient). Erosional unroofing of footwall bedrock results in the inversion of the age profile (age versus stratigraphic level) within the detrital record of the adjacent hanging-wall basin.

Figure 11: (A) Apatite (U/Th)/He ages for granitic boulder clasts, including individual ages (open diamonds) and mean ages (closed diamonds), plotted against stratigraphic level for the northern Lunggar range-front conglomerates (sections N1 and N2). (B) Apatite and zircon (U-Th)/He ages for granitic boulder clasts and zircon (U-Th)/He ages for sandstone zircon , including individual (open diamonds) and mean (closed diamonds), plotted against stratigraphic level for the central Lunggar range-front conglomerate (section C). Younging trends in which the (U-Th)/He ages decrease upsection are expressed in both the apatite and zircon results, with particularly uniform trends revealed by the zircon ages.

Figure 12. Schematic cross sections depicting evolution of the Lunggar extensional basin in relationship to the bounding normal fault. (A) Initial displacement along main bounding fault, internal drainage with alluvial-fan deposition on both basin margins, sediment sources on both margins. (B) Shallowing of main fault due to isostatic rebound, deposition of proximal growth strata, internally drained lacustrine system along basin axis, dominant footwall sediment source. (C) Continued shallowing of main fault, basinward migration of normal faulting (i.e., hanging-wall fragmentation), external axial drainage.

9.2. Figures

Figure 1

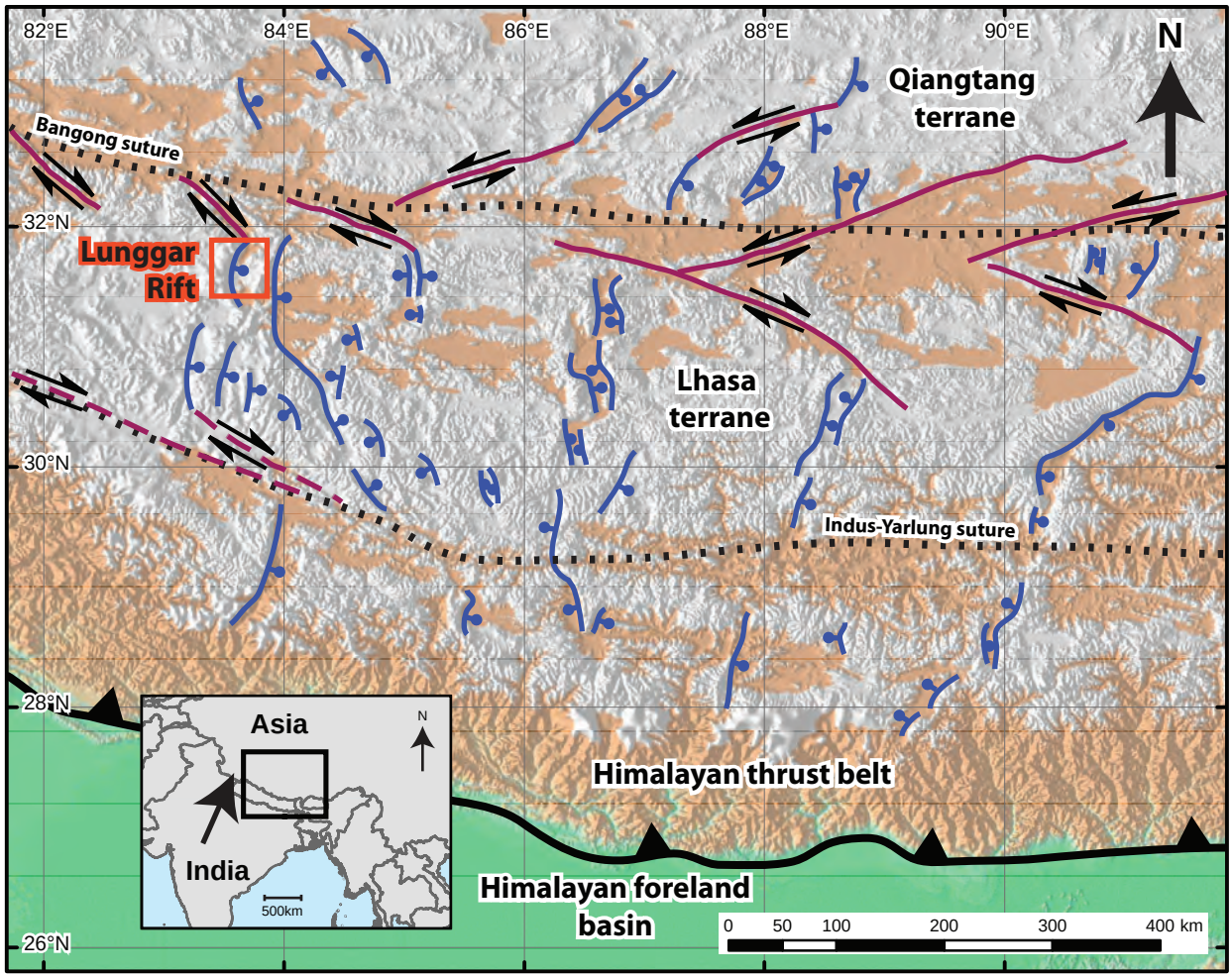
82°E
84°E
86°E
88°E
90°E
N
Qiangtang terrane
Bangong suture
32°N
Lunggar Rift
Lhasa terrane
30°N
Indus-Yarlung suture
28°N
Asia
N
India
500km
Himalayan thrust belt
Himalayan foreland basin
0 50 100 200 300 400 km
26°N

Figure 2

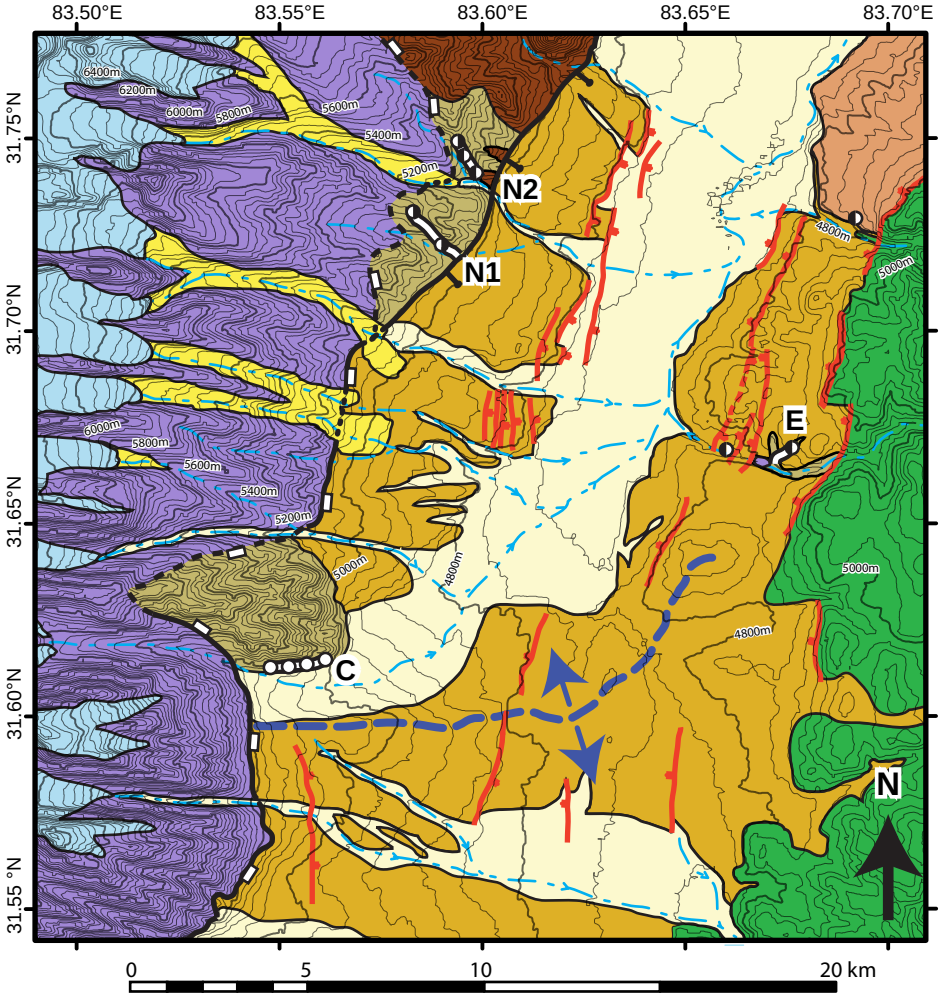

Explanation

- Quaternary fluvial & alluvial deposits
- Quaternary glacial deposits
- Cenozoic braided fluvial deposits
- Cenozoic lacustrine depostis
- Cenozoic debris flow deposits
- Aptian - Albian carbonate
- Permian - Cretaceous strata
- Granitoid, orthogneiss, mylonite
- Snow & ice

- Apatite (U-Th)/He clast age
- Detrital zircon U/Pb sandstone sample
- Apatite & zircon (U-Th)/He clast age & Detrital zircon U/Pb sandstone sample

- Active normal fault
- Inactive normal fault
- Drainage divide
- Low-angle normal fault (detachment)
- Stream
- Measured stratigraphic section (C, N1, N2, E)

Figure 3

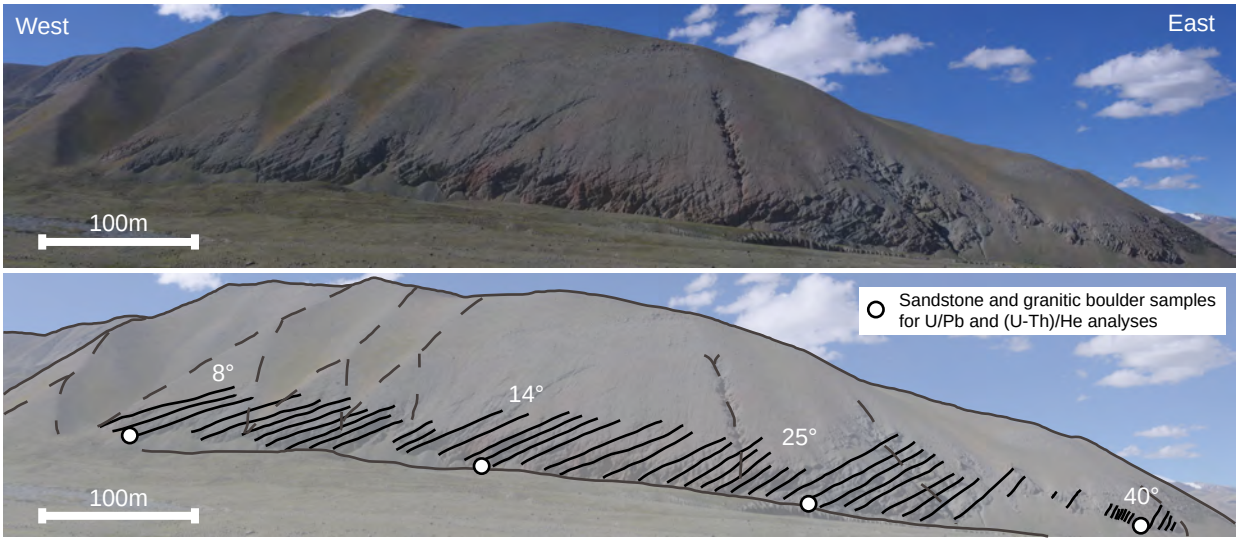
West
East
100m
Sandstone and granitic boulder samples for U/Pb and (U-Th)/He analyses
8°
14°
25°
40°
100m

Figure 4

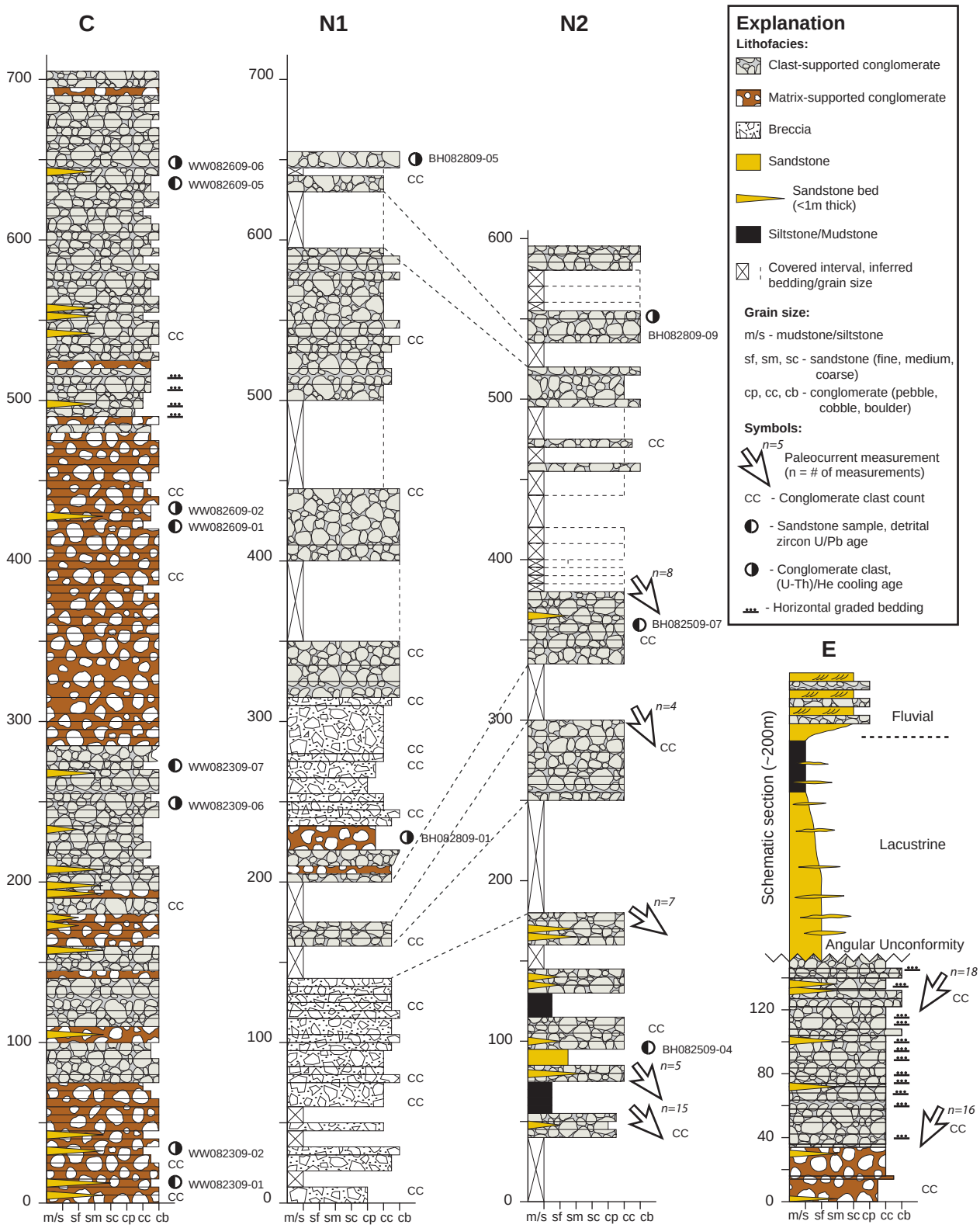
C
N1
N2
E
Explanation
Lithofacies:
Clast-supported conglomerate
Matrix-supported conglomerate
Breccia
Sandstone
Sandstone bed (<1m thick)
Siltstone/Mudstone
Covered interval, inferred bedding/grain size
Grain size:
m/s - mudstone/siltstone
sf, sm, sc - sandstone (fine, medium, coarse)
cp, cc, cb - conglomerate (pebble, cobble, boulder)
Symbols:
n=5
Paleocurrent measurement (n = # of measurements)
CC - Conglomerate clast count
- Sandstone sample, detrital zircon U/Pb age
- Conglomerate clast, (U-Th)/He cooling age
- Horizontal graded bedding
WW082609-06
WW082609-05
WW082609-02
WW082609-01
WW082309-07
WW082309-06
WW082309-02
WW082309-01
BH082809-05
BH082809-01
BH082809-09
BH082509-07
BH082509-04
n=8
n=4
n=7
n=5
n=15
n=18
n=16
CC
Fluvial
Lacustrine
Angular Unconformity
Schematic section (~200m)
m/s sf sm sc cp cc cb
0
100
200
300
400
500
600
700
80
120
40

Figure 5

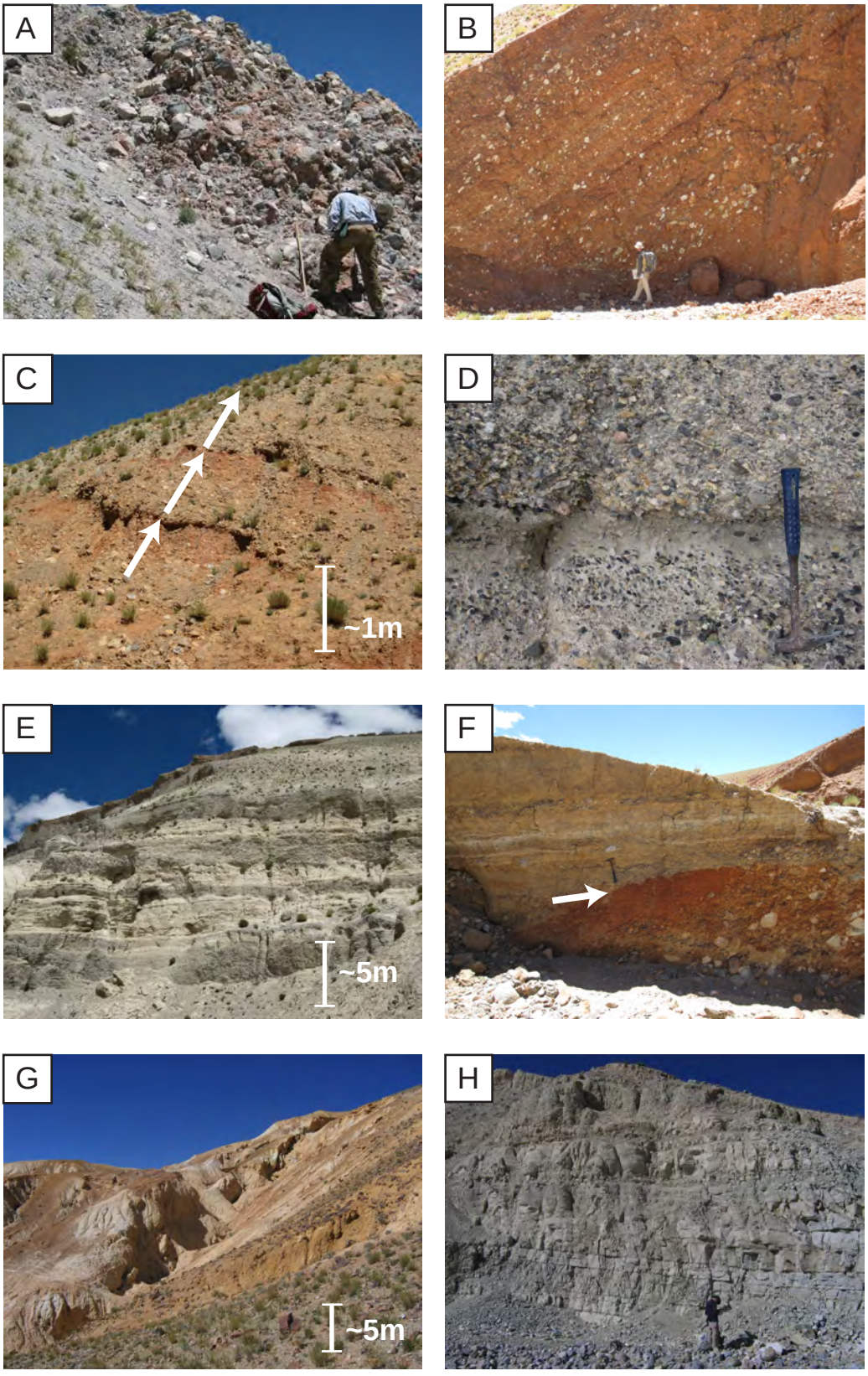

Figure 6

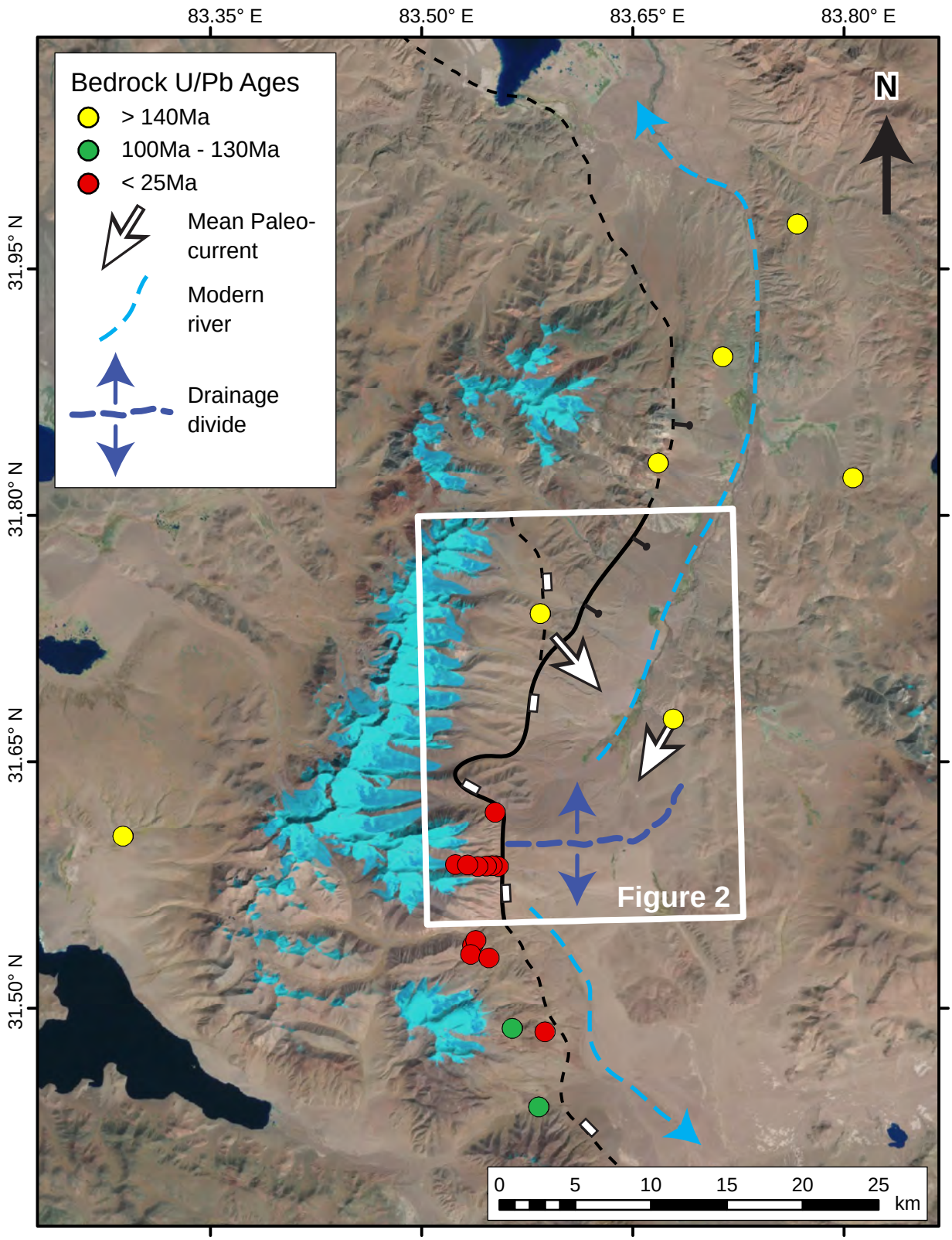
83.35° E
83.50° E
83.65° E
83.80° E
31.95° N
31.80° N
31.65° N
31.50° N
Bedrock U/Pb Ages
> 140Ma
100Ma - 130Ma
< 25Ma
Mean Paleo-current
Modern river
Drainage divide
N
Figure 2
0
5
10
15
20
25
km

Figure 7

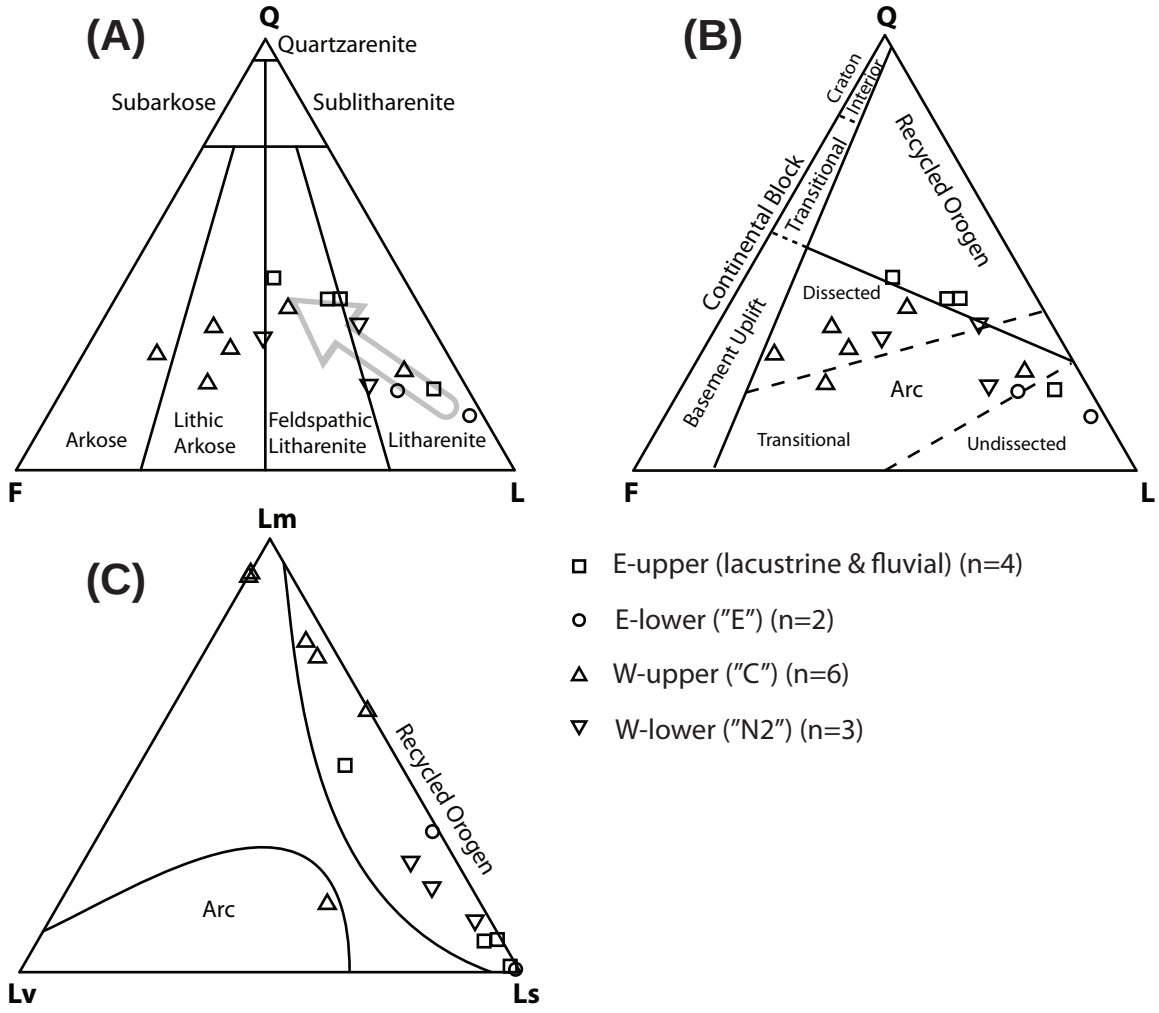
(A)
Q
Quartzarenite
Subarkose
Sublitharenite
Arkose
Lithic Arkose
Feldspathic Litharenite
Litharenite
F
L
(B)
Q
Craton Interior
Transitional
Recycled Orogen
Continental Block
Basement Uplift
Dissected
Arc
Transitional
Undissected
F
L
(C)
Lm
Recycled Orogen
Arc
Lv
Ls
E-upper (lacustrine & fluvial) (n=4)
E-lower ("E") (n=2)
W-upper ("C") (n=6)
W-lower ("N2") (n=3)

Figure 8

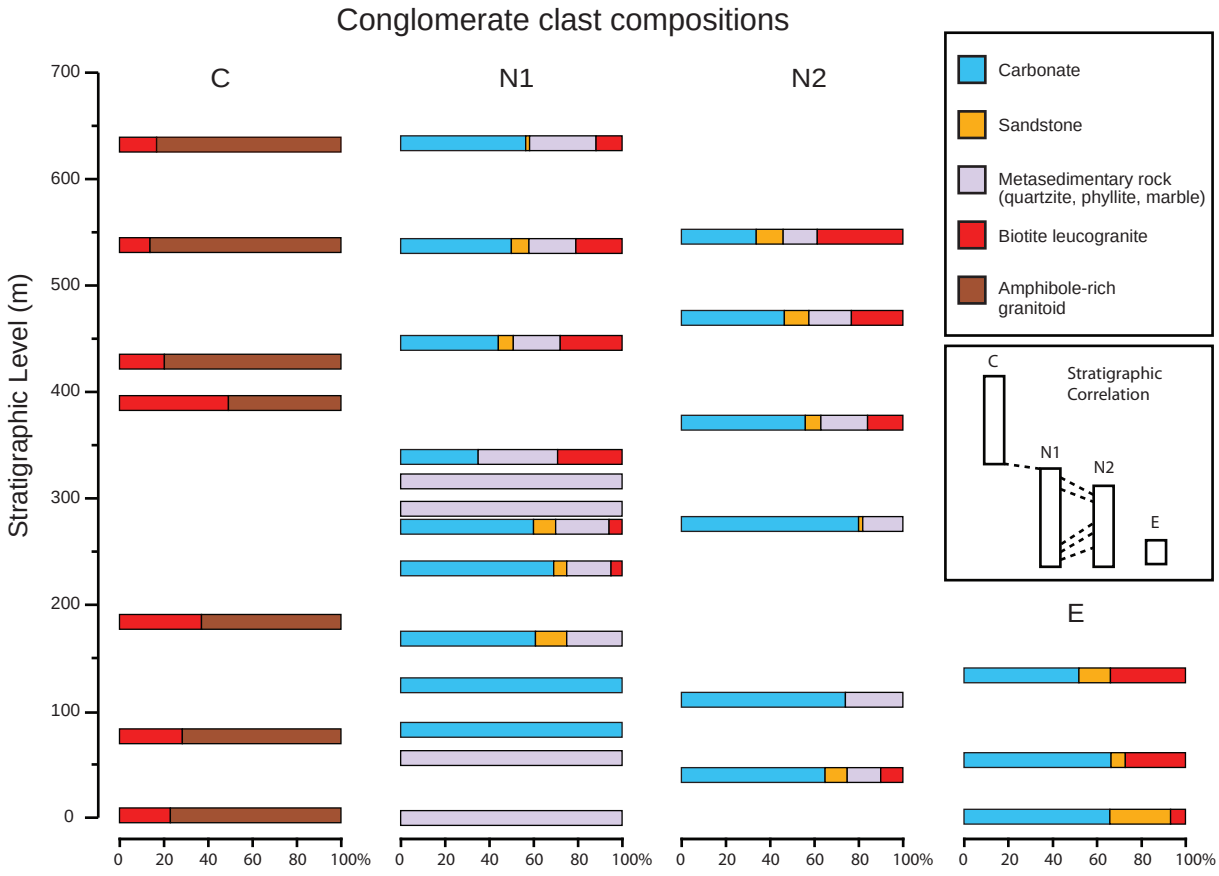
Conglomerate clast compositions
C
N1
N2
E
Stratigraphic Level (m)
700
600
500
400
300
200
100
0
0 20 40 60 80 100%
Carbonate
Sandstone
Metasedimentary rock (quartzite, phyllite, marble)
Biotite leucogranite
Amphibole-rich granitoid
Stratigraphic Correlation
C
N1
N2
E

Figure 9

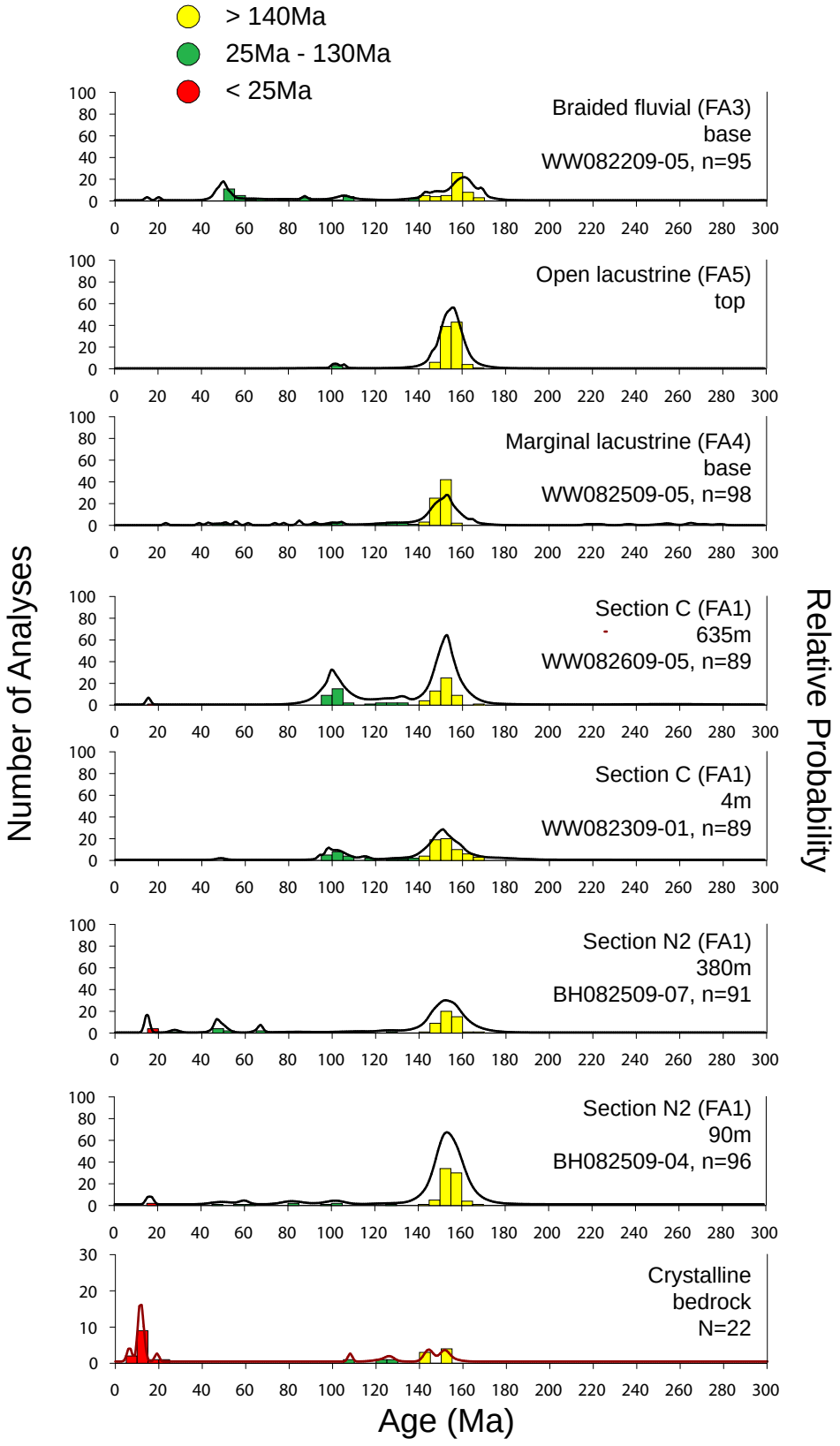
> 140Ma
25Ma - 130Ma
< 25Ma
Braided fluvial (FA3)
base
WW082209-05, n=95
Open lacustrine (FA5)
top
Marginal lacustrine (FA4)
base
WW082509-05, n=98
Section C (FA1)
635m
WW082609-05, n=89
Section C (FA1)
4m
WW082309-01, n=89
Section N2 (FA1)
380m
BH082509-07, n=91
Section N2 (FA1)
90m
BH082509-04, n=96
Crystalline
bedrock
N=22
Number of Analyses
Relative Probability
Age (Ma)

Figure 10

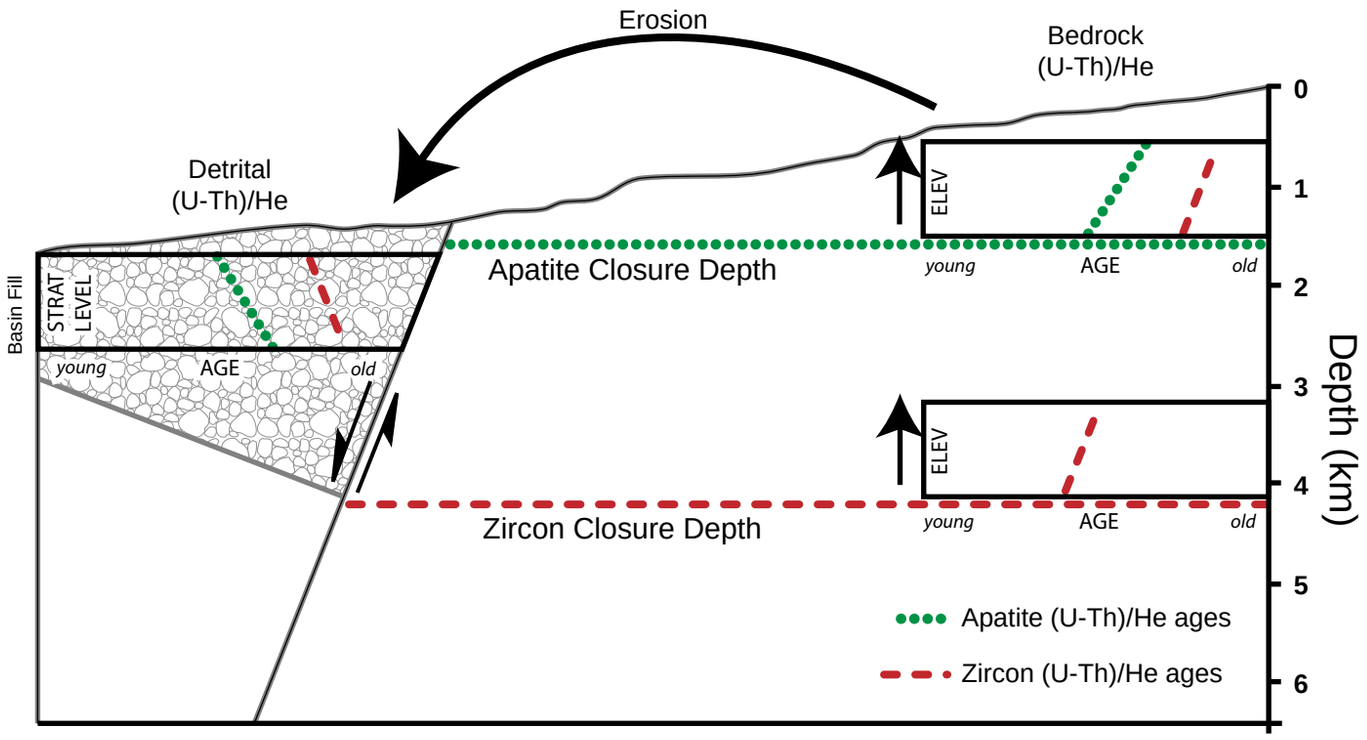
Erosion
Bedrock
(U-Th)/He
Detrital
(U-Th)/He
Basin Fill
STRAT
LEVEL
young
AGE
old
ELEV
young
AGE
old
Apatite Closure Depth
ELEV
young
AGE
old
Zircon Closure Depth
Apatite (U-Th)/He ages
Zircon (U-Th)/He ages
0
1
2
3
4
5
6
Depth (km)

Figure 11

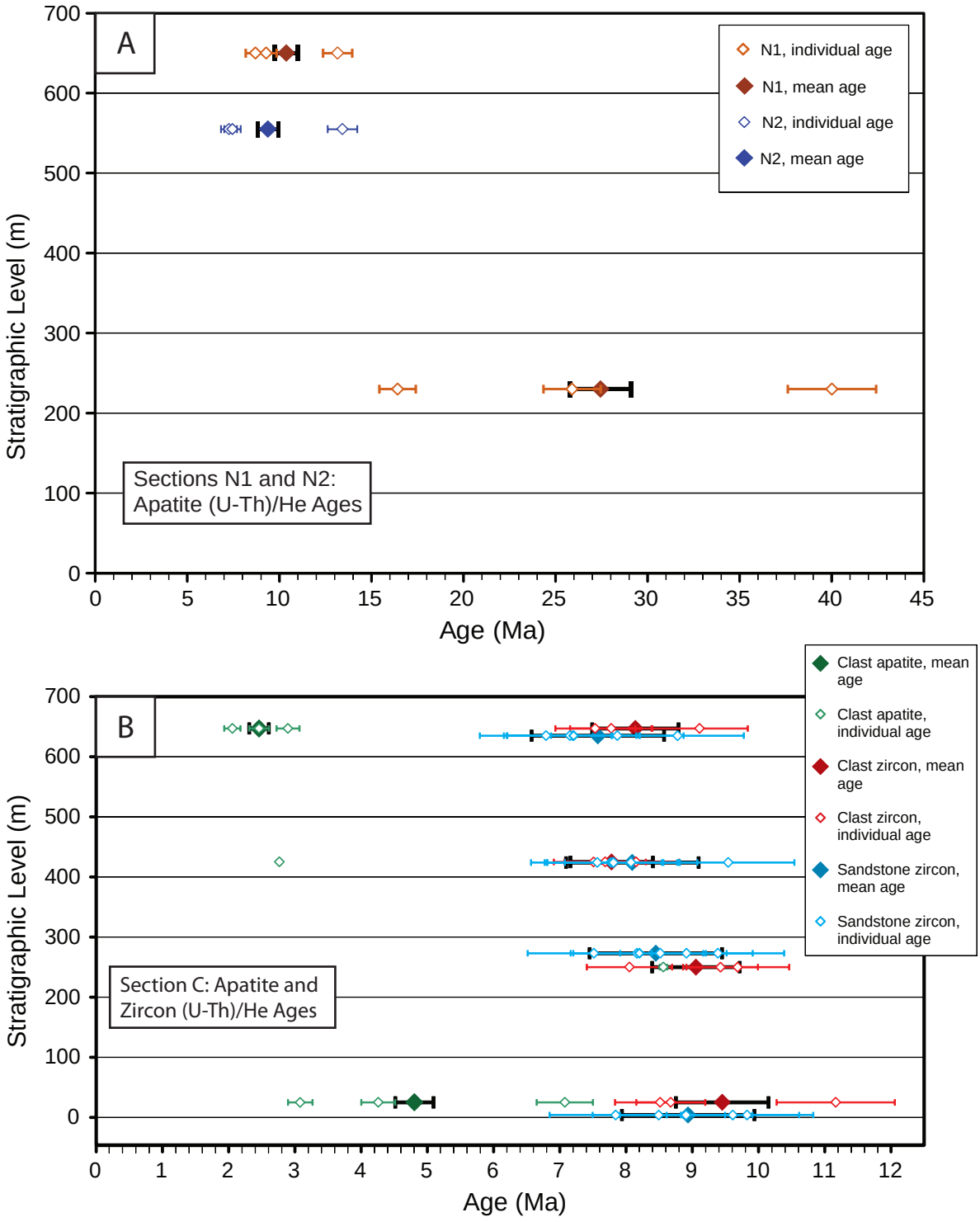
A
N1, individual age
N1, mean age
N2, individual age
N2, mean age
Sections N1 and N2:
Apatite (U-Th)/He Ages
Stratigraphic Level (m)
Age (Ma)
B
Clast apatite, mean age
Clast apatite, individual age
Clast zircon, mean age
Clast zircon, individual age
Sandstone zircon, mean age
Sandstone zircon, individual age
Section C: Apatite and
Zircon (U-Th)/He Ages
Stratigraphic Level (m)
Age (Ma)

Figure 12

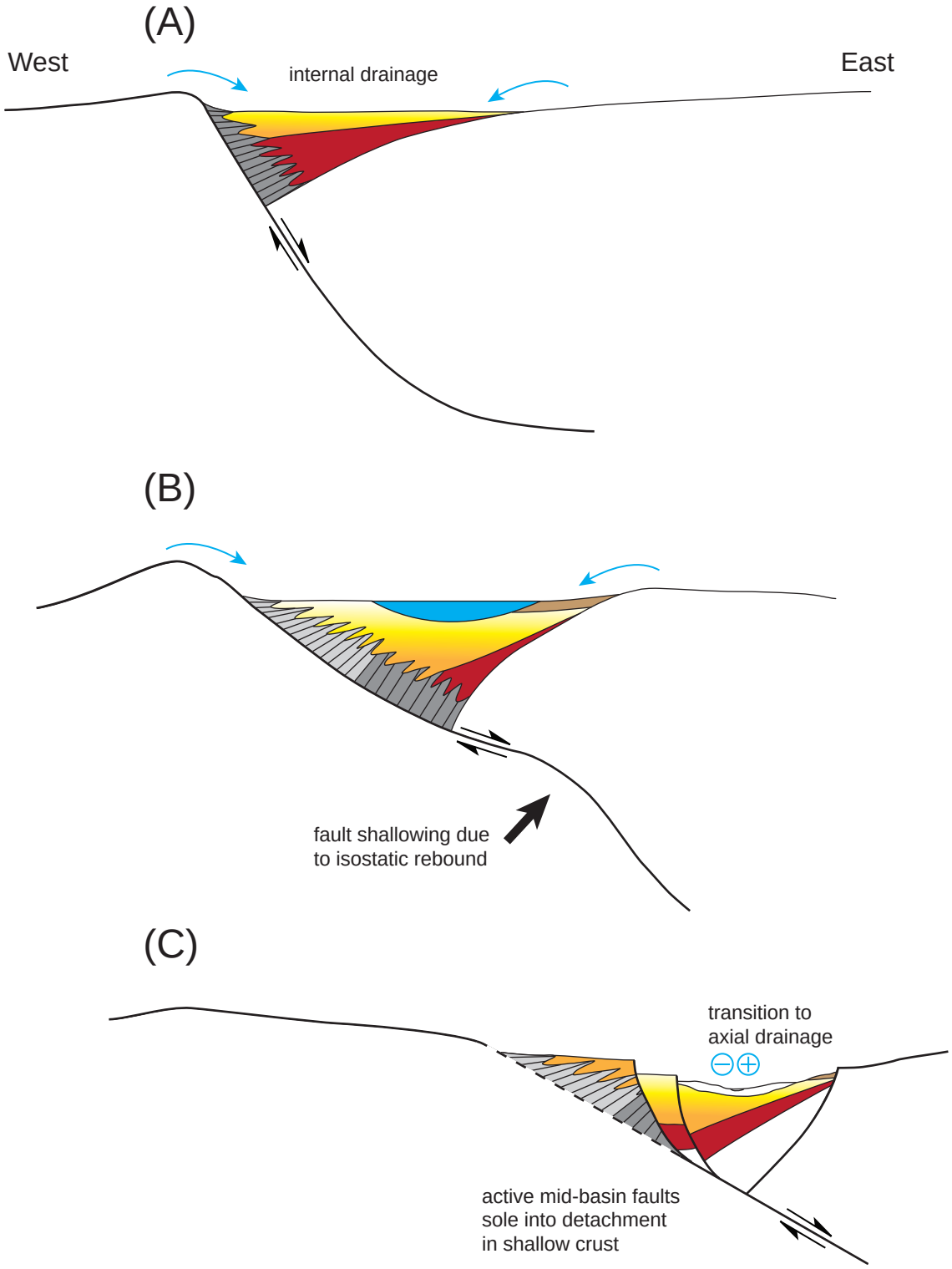
(A)
West
internal drainage
East
(B)
fault shallowing due
to isostatic rebound
(C)
transition to
axial drainage
active mid-basin faults
sole into detachment
in shallow crust

11. Tables

Table 1: Lunggar basin facies & descriptions

Facies Code	Description	Interpretation
Gcb	Clast supported, massive (structureless), cobble to boulder breccia, 1.0-10.0 m	Debris flow, dry-rock avalanche
Gcm	Clast-supported, massive (structureless), cobble to boulder conglomerate, local poor normal grading, 1.0-10.0 m	Clast-rich debris flow
Gmm	Matrix-supported, massive (structureless), cobble to boulder conglomerate, local poor normal grading, 1.0-10.0 m	Matrix-rich debris flow
Gh	Normally graded, sandy pebble to cobble conglomerate, poor horizontal stratification, 0.5-2.0 m	Hyperconcentrated flow
Gi	Clast-supported, imbricated, normally graded, pebble to cobble conglomerate, 0.1-1.0 m	Traction bedload, fluvial gravel bar
Gt	Trough cross-stratified sandy pebble conglomerate, 0.5-2.0 m	3D dune migration
St	Trough cross-stratified, medium- to coarse- grained sandstone, 0.1-2.0 m	3D dune migration
Sr	Ripple cross-stratified fine- to medium-grained sandstone, 0.1-0.5 m	2D to 3D ripple migration
Ss	Medium- to very coarse (local granule to pebble) sandstone filling broad, shallow scours, 0.1-0.5 m	Scour fill
Fl	Siltstone to very fine-grained sandstone, massive (structureless) with faint laminations and/or ripples	Waning flood flow in overbank fluvial setting
Fm	Massive (structureless) mudstone to siltstone, with organic material on bedding planes, 0.1-1.0 m	Suspension fallout in lacustrine setting

Table 2: Lunggar basin lithofacies associations (FA) with descriptions, interpretations, and geographic occurrence

Facies Association	Lithofacies	Description	Interpretation	Occurrence
1: Disorganized cobble to boulder conglomerate (local breccia) with minor interbedded sandstone	Gcb, Gcm, Gmm, St	Massive, clast-rich cobble to boulder conglomerate with few sedimentary structures (rare clast imbrication). Poorly expressed bedding (defined by changes in clast size), weak normal grading. Local occurrences of thin, lenticular, massive (structureless) to trough cross-stratified, medium- to coarse-grained sandstone.	Proximal alluvial fan with debris flow conglomerate and sheetflow sandstone	Western basin margin (along range front) and locally along eastern basin margin
2: Organized pebble to cobble conglomerate, with interbedded sandstone	Gh, Gi, St, Ss	Imbricated, commonly normally graded, matrix-supported conglomerate. Sheets of trough cross-stratified and scour-fill medium-grained sandstone.	Medial alluvial fan with sheetflood and local channel deposits	Along western and eastern basin margins
3: Interbedded trough cross-stratified sandstone and pebble conglomerate	Gi, Gt, St	Beige, trough cross-stratified, medium-grained sandstones (0.5-1.0 m). Clast-supported, normally graded pebble conglomerate (1.0-5.0 m)	Braided fluvial system with mixed sand and gravel	Northeastern basin margin, uppermost levels
4: Mixed siltstone with medium- to fine-grained sandstone	Fl, Sr, St	Yellow, massive (structureless) siltstone (0.5-1.0 m). Lenticular, ripple to trough cross-stratified channel sandstones (0.1 m). Sparse gastropod fossils and organic debris.	Marginal lacustrine environment (with local overbank fluvial deposition)	Along eastern and western basin margins, and the intrabasinal topographic high
5: Mixed siltstone and mudstone, with minor very fine-grained sandstone	Fm	White, massive (structureless) mudstone to siltstone (0.1-1.0 m). Beds defined by dark brown organic-rich horizons and/or faintly rippled very fine-grained sandstone. Sparse bivalve fossils.	Open lacustrine environment	Eastern basin margin, north of intrabasinal topographic high

Table 3: Sandstone point counting parameters

Symbol	Grain	Calculated Parameters
Qm	monocrystalline quartz	
Qmu	monocrystalline quartz, unstrained	Q-F-L:
Qms	monocrystalline quartz, strained	Q = Qm + Qp
Qp	polycrystalline quartz	F = Fu + Fk
Fu	feldspar (undifferentiated)	L = Lm + Lv + Ls
Fk	potassium feldspar	
Lie	volcanic lithic fragments	
Lii	intrusive igneous lithic fragments	Lm-Lv-Ls:
Lm	metamorphic lithic fragments	Lm = Lm
Lch	chert lithic fragments	Li = Lie + Lii
Lsc	carbonate lithic fragments	Ls = Lch + Lss + Lsc + Lsm
Lss	sandstone lithic fragments	
Lsm	mudstone/claystone lithic fragments	
Ama	accessory mineral: amphibole	
Amb	accessory mineral: biotite	
Amc	accessory mineral: chlorite	
Ame	accessory mineral: epidote	
Amm	accessory mineral: muscovite	
Amo	accessory mineral: other	
Ox	opaque oxides	
Cc	cement: carbonate	
Ch	cement: hematite	

Table 4: Q-F-L and Ls-Lm-Lv relative percentages

Sample	Level (m)	Section/unit	Q-F-L %			Ls-Lm-Lv%		
			Q	F	L	Ls	Lm	Lv
WW082209-06	~100	fluvial	39.7	15.2	45.2	92.0	7.3	0.7
WW082209-05	base	fluvial	18.7	6.8	74.5	97.6	1.2	1.2
WW082409-02	~100	lacustrine	44.5	26.1	29.3	89.5	7.0	3.5
WW082509-05	base	lacustrine	39.6	17.8	42.6	41.4	47.6	11.0
WW082609-05	635	C	23.4	10.4	66.2	0.0	91.7	8.3
WW082609-03	540	C	20.5	51.5	28.0	23.1	73.1	3.8
WW082609-01	424	C	33.6	43.7	22.7	39.3	60.7	0.0
WW082309-07	273	C	38.0	26.5	35.5	19.0	76.7	4.3
WW082309-03	103	C	28.6	42.9	28.6	0.0	92.5	7.5
WW082309-01	4	C	27.3	58.3	14.4	53.6	16.1	30.4
WW082509-02	105	E	18.3	14.3	67.4	99.1	0.5	0.5
WW082109-03	0	E	12.5	2.7	84.8	66.5	32.3	1.2
BH082509-07	380	N2	30.1	35.5	34.4	85.6	11.2	3.2
BH082509-06	180	N2	33.3	14.6	52.1	73.1	18.9	8.0
BH082509-04	90	N2	19.1	19.7	61.2	65.9	24.8	9.3

12. Appendices

Appendix 1: Detrital Zircon U/Pb Data

						Isotope ratios					Apparent ages (Ma)							
Analysis	U	206Pb	U/Th	206Pb*	±	207Pb*	±	206Pb*	±	error	206Pb*	±	207Pb*	±	206Pb*	±	**Best age**	**±**
	(ppm)	204Pb		207Pb*	(%)	235U*	(%)	238U	(%)	corr.	238U*	(Ma)	235U	(Ma)	207Pb*	(Ma)	**(Ma)**	**(Ma)**
WW082209-05: Fluvial unit (base), 31°43.360'N 83°41.526'E																		
1	426	11559	1.4	20.6747	5.3	0.1461	5.6	0.0219	1.8	0.31	139.7	2.4	138.5	7.3	117.3	125.8	**139.7**	**2.4**
2	993	31708	6.8	22.0837	6.0	0.0824	6.2	0.0132	1.7	0.28	84.6	1.4	80.4	4.8	-40.4	144.7	**84.6**	**1.4**
3	196	7855	1.2	19.9694	20.8	0.1646	21.5	0.0238	5.6	0.26	151.9	8.4	154.7	30.9	198.6	486.8	**151.9**	**8.4**
4	855	35601	24.0	20.0728	4.0	0.1513	4.3	0.0220	1.5	0.35	140.4	2.1	143.0	5.7	186.5	92.8	**140.4**	**2.1**
5	422	14214	1.0	19.7873	6.7	0.1763	6.8	0.0253	1.1	0.16	161.1	1.7	164.9	10.3	219.8	155.4	**161.1**	**1.7**
6	85	20493	1.8	13.3885	3.3	1.7211	9.1	0.1671	8.5	0.93	996.2	78.7	1016.4	58.8	1060.2	66.1	**1060.2**	**66.1**
7	102	4378	1.4	16.0207	22.2	0.1896	22.8	0.0220	5.5	0.24	140.5	7.6	176.3	37.0	688.5	478.5	**140.5**	**7.6**
8	325	2963	0.8	21.9537	34.7	0.0489	35.2	0.0078	6.0	0.17	50.0	3.0	48.5	16.7	-26.1	863.8	**50.0**	**3.0**
9	287	18881	1.0	21.8506	7.7	0.1510	8.1	0.0239	2.7	0.34	152.5	4.1	142.8	10.9	-14.7	185.7	**152.5**	**4.1**
10	244	60760	1.6	13.8523	1.5	1.7336	3.0	0.1742	2.5	0.86	1035.0	24.1	1021.1	19.0	991.3	31.1	**991.3**	**31.1**
11	237	10863	1.1	19.9247	8.0	0.1693	8.3	0.0245	2.5	0.30	155.8	3.9	158.8	12.3	203.7	184.8	**155.8**	**3.9**
12	364	10781	1.1	20.8021	6.1	0.1573	9.4	0.0237	7.1	0.76	151.2	10.6	148.3	12.9	102.8	144.8	**151.2**	**10.6**
13	243	8695	1.3	23.0545	13.6	0.1425	14.0	0.0238	3.6	0.25	151.8	5.3	135.2	17.7	-146.0	337.4	**151.8**	**5.3**
14	151	1245	0.9	26.2853	51.3	0.0392	52.2	0.0075	9.5	0.18	48.0	4.5	39.0	20.0	-482.1	1445.4	**48.0**	**4.5**
15	159	6320	1.3	23.2307	33.3	0.1320	33.4	0.0222	2.1	0.06	141.8	2.9	125.9	39.5	-164.9	848.9	**141.8**	**2.9**
16	302	16219	1.4	21.7605	10.8	0.1539	11.0	0.0243	1.8	0.17	154.7	2.8	145.3	14.9	-4.7	261.6	**154.7**	**2.8**
17	417	6224	1.2	30.5127	35.0	0.0334	35.6	0.0074	6.6	0.18	47.5	3.1	33.4	11.7	-895.2	1039.7	**47.5**	**3.1**
18	841	14714	1.4	20.8081	10.0	0.0518	10.3	0.0078	2.8	0.27	50.2	1.4	51.3	5.2	102.1	235.9	**50.2**	**1.4**
19	1402	257999	6.7	13.9850	0.4	1.2715	3.1	0.1290	3.1	0.99	782.0	22.6	833.1	17.6	971.9	9.0	**782.0**	**22.6**
20	494	1250	1.1	24.8127	67.2	0.0142	67.4	0.0026	5.6	0.08	16.5	0.9	14.3	9.6	-331.6	1942.4	**16.5**	**0.9**
21	1873	1539	0.5	21.0829	18.6	0.0217	18.8	0.0033	2.9	0.16	21.3	0.6	21.8	4.0	71.0	444.7	**21.3**	**0.6**
22	133	6053	2.1	20.6054	22.6	0.1078	23.2	0.0161	5.4	0.23	103.0	5.5	103.9	22.9	125.2	537.1	**103.0**	**5.5**
23	508	4707	8.2	22.1356	21.0	0.0450	21.3	0.0072	3.6	0.17	46.4	1.7	44.6	9.3	-46.1	514.4	**46.4**	**1.7**
24	395	9904	1.2	20.2848	9.6	0.1734	10.0	0.0255	2.7	0.27	162.4	4.3	162.4	15.0	162.0	225.0	**162.4**	**4.3**
25	349	7511	0.8	23.7380	16.2	0.0918	16.3	0.0158	2.3	0.14	101.1	2.3	89.2	14.0	-218.9	409.1	**101.1**	**2.3**
26	269	7649	1.0	22.3376	14.0	0.1266	14.4	0.0205	3.2	0.22	130.9	4.1	121.0	16.4	-68.3	344.1	**130.9**	**4.1**
27	329	11577	1.3	21.1094	16.0	0.1548	16.8	0.0237	5.2	0.31	151.0	7.7	146.1	22.8	68.1	382.1	**151.0**	**7.7**
28	171	6970	1.0	21.8983	25.9	0.1580	26.4	0.0251	5.1	0.19	159.8	8.1	148.9	36.6	-20.0	635.7	**159.8**	**8.1**

29	803	5301	1.8	19.4422	13.8	0.0575	13.9	0.0081	1.8	0.13	52.0	0.9	56.8	7.7	260.4	318.3	**52.0**	**0.9**
30	261	8603	1.2	19.5678	13.7	0.1518	14.0	0.0215	3.1	0.22	137.4	4.2	143.5	18.8	245.5	315.8	**137.4**	**4.2**
31	426	16257	1.2	20.4915	6.3	0.1520	6.6	0.0226	1.8	0.27	144.0	2.6	143.6	8.8	138.3	148.4	**144.0**	**2.6**
32	321	4522	0.5	20.1701	14.6	0.0799	16.0	0.0117	6.5	0.41	74.9	4.8	78.0	12.0	175.2	343.0	**74.9**	**4.8**
33	312	8547	1.2	20.5022	12.3	0.1580	12.5	0.0235	2.0	0.16	149.7	2.9	149.0	17.3	137.1	290.4	**149.7**	**2.9**
34	162	1668	1.3	26.5194	14.3	0.1289	15.0	0.0248	4.6	0.31	157.9	7.1	123.1	17.4	-505.7	382.3	**157.9**	**7.1**
35	156	6379	1.2	22.8974	27.7	0.1303	28.0	0.0216	4.1	0.15	138.1	5.6	124.4	32.8	-129.1	696.8	**138.1**	**5.6**
36	111	2861	1.4	21.2172	37.8	0.0859	38.5	0.0132	7.4	0.19	84.6	6.2	83.6	30.9	55.9	931.4	**84.6**	**6.2**
37	319	10592	1.6	20.8278	9.1	0.1420	9.3	0.0215	2.1	0.22	136.8	2.8	134.8	11.8	99.9	215.1	**136.8**	**2.8**
38	246	3864	1.1	28.7574	52.5	0.0360	52.8	0.0075	5.4	0.10	48.2	2.6	35.9	18.6	-726.7	1558.7	**48.2**	**2.6**
39	163	13271	1.6	17.7839	4.0	0.5745	4.7	0.0741	2.5	0.53	460.8	11.0	460.9	17.3	461.5	87.7	**460.8**	**11.0**
40	189	1667	0.9	24.9360	21.3	0.0557	25.1	0.0101	13.4	0.53	64.6	8.6	55.0	13.5	-344.3	554.5	**64.6**	**8.6**
41	223	3195	0.8	21.8209	23.7	0.0476	24.5	0.0075	6.4	0.26	48.3	3.1	47.2	11.3	-11.4	579.0	**48.3**	**3.1**
42	1482	65480	3.0	20.3477	1.5	0.1614	2.2	0.0238	1.6	0.73	151.7	2.4	151.9	3.1	154.8	34.9	**151.7**	**2.4**
43	64	1330	1.5	22.9263	75.3	0.0888	76.5	0.0148	13.3	0.17	94.5	12.5	86.4	63.4	-132.2	2197.3	**94.5**	**12.5**
44	536	13951	1.0	21.8942	7.0	0.1347	7.1	0.0214	1.1	0.15	136.4	1.4	128.3	8.5	-19.5	169.5	**136.4**	**1.4**
45	561	11315	2.2	20.4431	5.4	0.1618	5.9	0.0240	2.5	0.42	152.8	3.7	152.3	8.4	143.8	126.8	**152.8**	**3.7**
46	447	82328	3.1	14.5237	1.4	1.1083	7.2	0.1167	7.1	0.98	711.8	47.6	757.4	38.5	894.4	29.2	**711.8**	**47.6**
47	102	3437	1.2	17.9221	23.5	0.1598	24.6	0.0208	7.2	0.29	132.5	9.4	150.5	34.4	444.3	529.4	**132.5**	**9.4**
48	214	2947	1.2	20.6575	35.8	0.0523	38.0	0.0078	12.7	0.33	50.4	6.4	51.8	19.2	119.3	869.5	**50.4**	**6.4**
49	466	12869	0.7	20.9825	5.4	0.1536	6.3	0.0234	3.2	0.51	149.0	4.7	145.1	8.5	82.3	128.0	**149.0**	**4.7**
50	295	19578	0.9	20.4730	7.6	0.1586	8.0	0.0236	2.6	0.32	150.1	3.8	149.5	11.1	140.4	177.5	**150.1**	**3.8**
51	154	3597	1.4	20.1909	16.8	0.1590	17.8	0.0233	5.9	0.33	148.4	8.7	149.8	24.8	172.8	394.3	**148.4**	**8.7**
52	206	6177	1.4	20.9528	13.2	0.1581	13.8	0.0240	4.1	0.29	153.0	6.1	149.0	19.1	85.7	313.4	**153.0**	**6.1**
53	234	8914	1.4	22.1158	10.0	0.1488	10.8	0.0239	4.0	0.37	152.0	6.0	140.8	14.2	-43.9	243.9	**152.0**	**6.0**
54	152	2396	1.2	18.8638	17.4	0.1779	17.9	0.0243	4.3	0.24	155.0	6.5	166.3	27.5	329.3	398.0	**155.0**	**6.5**
55	173	7562	1.1	24.0258	19.8	0.1376	20.0	0.0240	2.7	0.13	152.7	4.0	130.9	24.5	-249.3	504.8	**152.7**	**4.0**
56	178	3311	0.9	18.2594	38.5	0.0574	39.1	0.0076	6.6	0.17	48.8	3.2	56.7	21.5	402.7	893.5	**48.8**	**3.2**
57	128	1408	0.9	14.6386	44.2	0.0760	46.7	0.0081	14.9	0.32	51.8	7.7	74.4	33.5	878.1	962.3	**51.8**	**7.7**
58	85	20223	2.2	14.1506	5.0	1.5357	6.2	0.1576	3.6	0.58	943.5	31.2	944.8	37.8	947.8	102.8	**947.8**	**102.8**
59	602	11198	1.5	21.5551	7.7	0.1011	8.7	0.0158	4.2	0.48	101.1	4.2	97.8	8.1	18.1	184.6	**101.1**	**4.2**
60	192	6657	1.2	20.7968	10.0	0.1613	10.4	0.0243	2.8	0.27	155.0	4.3	151.9	14.7	103.4	237.6	**155.0**	**4.3**
61	253	7144	1.0	22.8528	16.3	0.1476	16.5	0.0245	2.4	0.15	155.8	3.7	139.8	21.5	-124.2	404.8	**155.8**	**3.7**

62	270	9327	1.0	20.6538	13.5	0.1603	13.9	0.0240	3.2	0.23	153.0	4.9	151.0	19.5	119.7	318.9	**153.0**	**4.9**
63	387	6725	0.7	23.2473	30.9	0.0450	31.2	0.0076	3.9	0.12	48.7	1.9	44.7	13.6	-166.7	785.9	**48.7**	**1.9**
64	124	1684	0.9	98.5588	233.2	0.0126	233.6	0.0090	14.3	0.06	57.6	8.2	12.7	29.4	0.0	0.0	**57.6**	**8.2**
65	312	13393	1.0	21.9934	8.2	0.1529	8.7	0.0244	2.9	0.34	155.3	4.5	144.4	11.7	-30.5	199.2	**155.3**	**4.5**
66	246	18029	0.9	21.9301	10.7	0.1526	10.9	0.0243	2.0	0.18	154.6	3.0	144.2	14.6	-23.5	259.1	**154.6**	**3.0**
67	1117	65779	77.9	16.1942	0.6	0.7800	2.1	0.0916	2.0	0.95	565.1	10.8	585.5	9.4	665.5	13.7	**565.1**	**10.8**
68	80	2255	0.9	22.7887	31.5	0.1447	32.9	0.0239	9.6	0.29	152.4	14.5	137.2	42.3	-117.3	792.4	**152.4**	**14.5**
69	231	4504	1.0	21.8892	8.7	0.0977	9.8	0.0155	4.5	0.46	99.2	4.5	94.7	8.8	-19.0	209.7	**99.2**	**4.5**
70	248	5056	0.9	27.6322	28.1	0.0378	30.7	0.0076	12.3	0.40	48.6	6.0	37.7	11.4	-616.5	780.2	**48.6**	**6.0**
71	197	21216	1.0	21.8480	20.3	0.1512	20.6	0.0240	3.5	0.17	152.7	5.3	143.0	27.5	-14.4	495.6	**152.7**	**5.3**
72	454	16582	4.6	15.2282	3.2	0.4234	4.1	0.0468	2.5	0.62	294.6	7.2	358.5	12.3	795.8	66.9	**294.6**	**7.2**
73	164	10718	1.6	20.1559	15.9	0.1653	16.7	0.0242	5.3	0.32	153.9	8.0	155.3	24.1	176.9	371.8	**153.9**	**8.0**
74	369	6518	0.9	21.8922	13.2	0.1488	13.7	0.0236	3.4	0.25	150.5	5.1	140.8	18.0	-19.3	321.1	**150.5**	**5.1**
75	416	16767	1.2	20.4549	4.3	0.1643	5.2	0.0244	2.9	0.56	155.3	4.4	154.5	7.4	142.4	100.3	**155.3**	**4.4**
76	281	12742	1.2	19.0944	11.7	0.1744	12.5	0.0242	4.5	0.36	153.8	6.8	163.2	18.9	301.7	266.7	**153.8**	**6.8**
77	391	10880	1.2	20.7749	6.6	0.1576	7.3	0.0237	3.1	0.43	151.3	4.7	148.6	10.2	105.9	157.1	**151.3**	**4.7**
78	571	4479	0.6	21.7512	6.5	0.1501	6.9	0.0237	2.2	0.33	150.9	3.3	142.0	9.1	-3.7	156.9	**150.9**	**3.3**
79	175	1974	1.7	18.4248	20.3	0.0743	21.4	0.0099	6.9	0.32	63.7	4.4	72.8	15.0	382.4	460.3	**63.7**	**4.4**
80	286	133868	1.7	9.1908	0.5	4.5034	3.3	0.3002	3.3	0.99	1692.2	48.6	1731.6	27.5	1779.5	10.0	**1779.5**	**10.0**
81	380	15767	0.9	20.3166	9.4	0.1683	9.8	0.0248	3.0	0.31	157.9	4.7	157.9	14.4	158.4	219.6	**157.9**	**4.7**
82	516	5535	1.4	23.4031	14.5	0.0438	15.6	0.0074	5.7	0.36	47.8	2.7	43.6	6.7	-183.3	364.7	**47.8**	**2.7**
83	307	9811	1.0	21.2211	6.8	0.1573	7.0	0.0242	1.8	0.26	154.2	2.8	148.3	9.7	55.4	162.1	**154.2**	**2.8**
84	465	13930	0.7	21.2733	11.6	0.1131	13.1	0.0175	6.0	0.46	111.5	6.6	108.8	13.5	49.6	277.8	**111.5**	**6.6**
85	143	726	0.7	13.9500	34.5	0.1292	37.6	0.0131	14.9	0.40	83.7	12.4	123.4	43.7	977.0	724.5	**83.7**	**12.4**
86	285	8504	1.6	20.4324	10.6	0.1068	11.6	0.0158	4.7	0.41	101.2	4.7	103.0	11.4	145.0	249.3	**101.2**	**4.7**
87	288	10488	1.1	20.5126	12.5	0.1636	13.7	0.0243	5.7	0.42	155.0	8.7	153.8	19.6	135.8	294.1	**155.0**	**8.7**
88	689	16959	0.9	21.2148	14.2	0.0497	14.6	0.0076	3.3	0.22	49.1	1.6	49.2	7.0	56.2	340.0	**49.1**	**1.6**
89	974	80783	1.2	19.8407	1.3	0.1757	1.8	0.0253	1.2	0.69	160.9	1.9	164.3	2.7	213.6	29.2	**160.9**	**1.9**
90	253	13945	1.0	22.0018	11.9	0.1523	12.2	0.0243	3.0	0.25	154.8	4.7	143.9	16.4	-31.4	288.5	**154.8**	**4.7**
91	1096	12806	1.4	21.4436	7.2	0.0492	7.5	0.0077	1.8	0.24	49.1	0.9	48.8	3.6	30.5	173.9	**49.1**	**0.9**
92	241	9540	1.0	21.4876	17.2	0.1546	18.0	0.0241	5.4	0.30	153.5	8.1	146.0	24.5	25.6	415.4	**153.5**	**8.1**
93	262	7136	1.0	21.7854	21.3	0.1449	21.6	0.0229	3.5	0.16	145.9	5.1	137.4	27.7	-7.5	518.5	**145.9**	**5.1**
94	731	15773	0.7	20.2022	4.2	0.1595	4.7	0.0234	2.2	0.47	148.9	3.3	150.2	6.6	171.5	97.0	**148.9**	**3.3**

95	136	2788	1.0	6.1050	435.7	0.2229	435.9	0.0099	13.6	0.03	63.3	8.6	204.4	1100.6	2495.3	550.3	**2495.3**	**550.3**
						Isotope ratios					Apparent ages (Ma)							
Analysis	U	206Pb	U/Th	206Pb*	±	207Pb*	±	206Pb*	±	error	206Pb*	±	207Pb*	±	206Pb*	±	**Best age**	±
	(ppm)	204Pb		207Pb*	(%)	235U*	(%)	238U	(%)	corr.	238U*	(Ma)	235U	(Ma)	207Pb*	(Ma)	**(Ma)**	**(Ma)**
WW082509-05: Lacustrine unit (base), 31°39.934'N 83°39.828'E																		
1	583	129608	13.6	16.4463	4.2	0.8918	5.3	0.1064	3.2	0.60	651.6	19.8	647.3	25.4	632.3	91.3	**651.6**	**19.8**
2	193	17236	1.1	20.2223	14.4	0.1614	15.3	0.0237	5.0	0.33	150.8	7.5	151.9	21.6	169.2	338.6	**150.8**	**7.5**
3	1544	53257	0.7	19.8302	2.2	0.1587	2.7	0.0228	1.6	0.59	145.4	2.3	149.5	3.8	214.8	51.2	**145.4**	**2.3**
4	1799	15146	0.8	19.4609	4.8	0.1617	14.5	0.0228	13.7	0.94	145.4	19.6	152.2	20.5	258.1	110.1	**145.4**	**19.6**
5	468	26534	0.5	20.0516	6.4	0.1672	7.6	0.0243	4.2	0.55	154.9	6.4	157.0	11.0	189.0	147.9	**154.9**	**6.4**
6	211	11370	1.3	19.2541	23.3	0.1068	24.4	0.0149	7.1	0.29	95.4	6.7	103.0	23.9	282.7	540.2	**95.4**	**6.7**
7	520	5821	1.2	20.6164	5.3	0.1609	5.8	0.0241	2.3	0.40	153.3	3.5	151.5	8.1	123.9	124.6	**153.3**	**3.5**
8	732	49488	1.1	21.0116	2.6	0.1582	4.4	0.0241	3.5	0.80	153.5	5.3	149.1	6.0	79.0	61.8	**153.5**	**5.3**
9	849	14163	0.6	19.6044	5.9	0.1645	7.1	0.0234	4.1	0.57	149.0	6.0	154.6	10.2	241.2	135.1	**149.0**	**6.0**
10	790	24456	0.7	20.9516	5.6	0.1032	6.3	0.0157	2.9	0.46	100.3	2.9	99.7	6.0	85.9	133.4	**100.3**	**2.9**
11	703	6380	1.8	18.1962	7.5	0.1852	8.5	0.0244	4.0	0.47	155.7	6.2	172.5	13.5	410.4	167.9	**155.7**	**6.2**
12	233	12154	0.9	23.8712	29.3	0.0813	30.6	0.0141	9.0	0.29	90.1	8.1	79.4	23.4	-233.0	751.7	**90.1**	**8.1**
13	275	11361	1.1	23.0227	12.2	0.1448	15.5	0.0242	9.6	0.62	154.0	14.7	137.3	19.9	-142.6	302.3	**154.0**	**14.7**
14	1505	55307	0.8	19.7048	4.6	0.1600	5.9	0.0229	3.7	0.62	145.7	5.3	150.7	8.2	229.4	105.7	**145.7**	**5.3**
15	430	20920	1.1	19.5249	10.0	0.1711	10.8	0.0242	4.0	0.37	154.3	6.2	160.4	16.0	250.6	231.4	**154.3**	**6.2**
16	346	18918	0.9	22.1805	8.3	0.1502	8.8	0.0242	2.9	0.34	154.0	4.5	142.1	11.6	-51.1	201.3	**154.0**	**4.5**
17	355	21607	0.8	20.9336	12.2	0.1558	13.5	0.0236	5.7	0.42	150.7	8.4	147.0	18.4	87.9	290.7	**150.7**	**8.4**
18	361	16505	0.7	21.1831	5.4	0.1566	6.1	0.0241	2.9	0.47	153.3	4.4	147.8	8.4	59.8	128.4	**153.3**	**4.4**
19	679	72625	1.0	20.6710	5.5	0.1641	6.2	0.0246	3.0	0.48	156.7	4.6	154.3	8.9	117.8	128.6	**156.7**	**4.6**
20	665	8148	1.3	23.3943	28.4	0.0231	29.3	0.0039	7.5	0.25	25.2	1.9	23.2	6.7	-182.4	720.6	**25.2**	**1.9**
21	497	26321	1.1	20.4844	7.4	0.1600	8.4	0.0238	3.8	0.46	151.4	5.7	150.7	11.7	139.1	174.9	**151.4**	**5.7**
22	540	35941	0.7	20.4417	6.5	0.1567	6.8	0.0232	1.8	0.26	148.1	2.6	147.9	9.3	144.0	153.6	**148.1**	**2.6**
23	1525	56381	0.9	20.2690	2.4	0.1633	4.2	0.0240	3.5	0.83	152.9	5.3	153.6	6.0	163.8	55.0	**152.9**	**5.3**
24	1781	86961	1.2	21.1363	2.4	0.1030	4.0	0.0158	3.2	0.79	101.0	3.2	99.5	3.8	65.0	58.3	**101.0**	**3.2**
25	360	2882	1.2	19.5512	15.9	0.1688	16.5	0.0239	4.5	0.27	152.4	6.7	158.3	24.2	247.5	368.0	**152.4**	**6.7**

26	262	11871	1.1	21.4508	14.6	0.1544	14.9	0.0240	3.0	0.20	153.0	4.5	145.8	20.3	29.7	351.9	**153.0**	**4.5**
27	250	12485	0.9	18.6907	11.4	0.1678	11.6	0.0227	2.2	0.19	145.0	3.2	157.5	17.0	350.2	258.4	**145.0**	**3.2**
28	1367	17134	1.0	20.1684	2.1	0.1632	3.0	0.0239	2.1	0.72	152.1	3.2	153.5	4.2	175.4	48.0	**152.1**	**3.2**
29	220	20757	1.0	19.1862	12.3	0.1680	12.6	0.0234	2.6	0.21	149.0	3.9	157.7	18.4	290.7	282.2	**149.0**	**3.9**
30	212	8147	1.0	20.7632	16.2	0.1549	16.4	0.0233	2.8	0.17	148.7	4.2	146.3	22.4	107.3	384.3	**148.7**	**4.2**
31	301	14562	0.9	22.0682	9.1	0.1466	10.9	0.0235	6.0	0.55	149.5	8.8	138.9	14.1	-38.7	220.8	**149.5**	**8.8**
32	747	38924	0.8	20.0457	5.2	0.1625	6.5	0.0236	3.9	0.60	150.5	5.8	152.9	9.3	189.7	122.0	**150.5**	**5.8**
33	937	61863	1.0	20.5837	2.6	0.1566	5.5	0.0234	4.8	0.88	148.9	7.1	147.7	7.5	127.7	61.3	**148.9**	**7.1**
34	934	21781	1.3	21.9199	12.3	0.0463	13.8	0.0074	6.3	0.46	47.2	3.0	45.9	6.2	-22.4	299.1	**47.2**	**3.0**
35	436	4440	1.0	20.4926	5.3	0.1594	6.4	0.0237	3.5	0.56	151.0	5.3	150.2	8.9	138.1	124.3	**151.0**	**5.3**
36	454	861169	1.3	6.0226	0.6	10.2724	2.2	0.4487	2.1	0.96	2389.5	41.2	2459.6	19.9	2518.1	10.2	**2518.1**	**10.2**
37	79	2976	0.7	12.4176	53.5	0.2045	56.3	0.0184	17.3	0.31	117.6	20.2	188.9	97.3	1210.0	1142.0	**117.6**	**20.2**
38	872	49097	0.9	20.0521	4.6	0.1601	5.5	0.0233	3.0	0.55	148.4	4.4	150.8	7.6	188.9	106.1	**148.4**	**4.4**
39	601	29396	1.0	20.2535	8.1	0.1747	9.1	0.0257	4.1	0.45	163.4	6.7	163.5	13.7	165.6	189.5	**163.4**	**6.7**
40	688	16521	1.3	20.4731	4.2	0.1541	4.6	0.0229	1.7	0.38	145.9	2.5	145.5	6.2	140.4	98.7	**145.9**	**2.5**
41	910	12175	0.6	20.5405	10.6	0.0529	11.9	0.0079	5.4	0.46	50.6	2.7	52.4	6.1	132.6	249.5	**50.6**	**2.7**
42	105	6938	0.7	20.3671	48.1	0.1397	48.7	0.0206	7.6	0.16	131.7	9.9	132.8	60.7	152.6	1190.4	**131.7**	**9.9**
43	228	21759	1.6	17.3172	9.7	0.1839	10.4	0.0231	3.8	0.36	147.2	5.5	171.4	16.5	520.1	213.9	**147.2**	**5.5**
44	443	2612	1.2	18.9929	9.7	0.1741	9.8	0.0240	1.0	0.11	152.8	1.6	163.0	14.7	313.8	221.5	**152.8**	**1.6**
45	1022	21581	0.5	19.2334	5.5	0.1421	20.2	0.0198	19.5	0.96	126.5	24.4	134.9	25.6	285.1	127.0	**126.5**	**24.4**
46	471	18192	0.9	19.9851	9.8	0.1628	10.4	0.0236	3.7	0.35	150.3	5.4	153.1	14.8	196.7	227.4	**150.3**	**5.4**
47	271	20491	0.9	21.6943	20.7	0.1523	21.3	0.0240	5.0	0.24	152.6	7.6	143.9	28.6	2.6	503.6	**152.6**	**7.6**
48	1037	36375	0.8	20.6565	5.1	0.1546	6.2	0.0232	3.5	0.57	147.6	5.1	146.0	8.4	119.4	120.3	**147.6**	**5.1**
49	366	1762	0.9	20.5536	12.5	0.1624	12.7	0.0242	2.5	0.20	154.2	3.8	152.8	18.0	131.1	294.0	**154.2**	**3.8**
50	214	18429	0.8	19.1503	14.3	0.1457	15.5	0.0202	6.1	0.39	129.1	7.7	138.1	20.0	295.0	326.8	**129.1**	**7.7**
51	397	74086	1.0	21.0281	7.1	0.1598	8.9	0.0244	5.4	0.61	155.2	8.3	150.5	12.5	77.2	168.2	**155.2**	**8.3**
52	664	53621	0.9	19.7108	5.3	0.1666	7.0	0.0238	4.6	0.65	151.7	6.8	156.4	10.1	228.7	121.8	**151.7**	**6.8**
53	452	22560	1.2	19.5046	7.6	0.1718	9.2	0.0243	5.3	0.57	154.8	8.1	161.0	13.7	253.0	174.0	**154.8**	**8.1**
54	325	16930	1.1	19.4663	11.2	0.1701	12.0	0.0240	4.2	0.35	152.9	6.3	159.5	17.7	257.5	258.6	**152.9**	**6.3**
55	231	21116	0.9	23.8533	17.0	0.1418	17.6	0.0245	4.5	0.25	156.2	6.9	134.6	22.2	-231.1	432.0	**156.2**	**6.9**
56	252	15708	1.1	21.2835	18.4	0.1530	18.8	0.0236	3.9	0.21	150.4	5.8	144.5	25.3	48.5	442.3	**150.4**	**5.8**
57	505	17561	1.0	21.2908	10.8	0.1533	12.4	0.0237	6.2	0.50	150.9	9.2	144.9	16.8	47.6	258.7	**150.9**	**9.2**
58	398	1297	1.0	18.3850	12.6	0.1797	13.3	0.0240	4.3	0.32	152.6	6.5	167.8	20.6	387.3	284.9	**152.6**	**6.5**

59	674	7969	0.6	19.5224	10.1	0.1672	12.1	0.0237	6.7	0.55	150.8	10.0	156.9	17.7	250.9	233.9	**150.8**	**10.0**
60	575	20516	0.8	20.1232	4.4	0.1653	7.7	0.0241	6.4	0.82	153.7	9.6	155.3	11.1	180.7	102.7	**153.7**	**9.6**
61	320	22639	1.1	20.3265	10.5	0.1448	11.9	0.0213	5.6	0.47	136.1	7.5	137.3	15.2	157.2	245.7	**136.1**	**7.5**
62	1033	30762	0.7	20.3485	1.4	0.1564	3.0	0.0231	2.7	0.89	147.1	4.0	147.5	4.2	154.7	31.8	**147.1**	**4.0**
63	124	3931	0.5	19.1387	41.8	0.1493	42.4	0.0207	7.2	0.17	132.2	9.5	141.3	55.9	296.4	992.9	**132.2**	**9.5**
64	1129	4060	0.4	19.8530	4.9	0.1626	6.0	0.0234	3.5	0.58	149.2	5.1	152.9	8.5	212.1	113.3	**149.2**	**5.1**
65	323	14934	1.1	20.4184	9.1	0.1610	9.4	0.0238	2.5	0.26	151.9	3.7	151.5	13.3	146.7	214.0	**151.9**	**3.7**
66	2331	185069	0.9	20.0493	1.3	0.1673	2.7	0.0243	2.4	0.88	154.9	3.7	157.1	4.0	189.2	30.7	**154.9**	**3.7**
67	282	20308	0.9	20.3881	12.2	0.1581	13.1	0.0234	4.9	0.37	148.9	7.2	149.0	18.2	150.1	286.2	**148.9**	**7.2**
68	248	11327	1.2	19.1386	12.2	0.1621	13.5	0.0225	5.9	0.43	143.4	8.3	152.5	19.2	296.4	278.8	**143.4**	**8.3**
69	424	22561	0.7	21.4147	9.2	0.1441	9.7	0.0224	3.0	0.31	142.7	4.3	136.7	12.4	33.8	220.4	**142.7**	**4.3**
70	799	75426	0.7	20.7461	4.6	0.1555	6.6	0.0234	4.8	0.72	149.1	7.0	146.8	9.0	109.2	108.2	**149.1**	**7.0**
71	236	15318	1.1	21.7711	14.1	0.1486	15.1	0.0235	5.6	0.37	149.5	8.2	140.7	19.9	-5.9	340.9	**149.5**	**8.2**
72	2433	34726	0.7	20.1615	1.4	0.1546	2.9	0.0226	2.5	0.88	144.1	3.6	146.0	3.9	176.2	32.3	**144.1**	**3.6**
73	475	51387	1.2	21.3239	8.5	0.1545	9.1	0.0239	3.4	0.37	152.2	5.1	145.9	12.4	43.9	202.5	**152.2**	**5.1**
74	805	39261	0.8	20.1682	5.4	0.1749	7.1	0.0256	4.6	0.65	162.8	7.4	163.6	10.7	175.5	125.6	**162.8**	**7.4**
75	361	28866	1.3	20.8943	7.5	0.1572	8.0	0.0238	3.0	0.37	151.8	4.4	148.3	11.1	92.4	177.0	**151.8**	**4.4**
76	346	22342	0.9	21.8902	11.5	0.1486	11.9	0.0236	3.0	0.25	150.3	4.5	140.6	15.6	-19.1	278.7	**150.3**	**4.5**
77	622	44852	0.9	19.9452	5.2	0.1614	6.3	0.0233	3.5	0.56	148.8	5.2	151.9	8.9	201.4	121.2	**148.8**	**5.2**
78	425	62094	0.8	18.9867	10.5	0.1672	13.1	0.0230	7.7	0.59	146.7	11.2	157.0	19.0	314.5	240.4	**146.7**	**11.2**
79	672	39820	0.8	20.0797	4.5	0.1622	5.1	0.0236	2.4	0.48	150.5	3.6	152.6	7.2	185.7	104.5	**150.5**	**3.6**
80	196	8845	1.2	27.5184	60.9	0.0994	61.2	0.0198	6.1	0.10	126.6	7.6	96.2	56.2	-605.3	1810.2	**126.6**	**7.6**
81	429	28316	0.7	20.5201	7.7	0.1591	8.0	0.0237	2.5	0.31	150.9	3.7	149.9	11.2	135.0	180.0	**150.9**	**3.7**
82	978	42614	0.8	19.9555	3.9	0.1678	5.8	0.0243	4.3	0.75	154.7	6.6	157.5	8.4	200.2	89.5	**154.7**	**6.6**
83	893	3485	0.9	19.5558	9.7	0.1668	9.9	0.0237	2.1	0.21	150.7	3.1	156.7	14.4	247.0	222.9	**150.7**	**3.1**
84	915	65857	1.1	19.6249	3.3	0.1639	4.2	0.0233	2.6	0.62	148.7	3.8	154.1	6.0	238.8	76.4	**148.7**	**3.8**
85	840	19419	0.8	20.5166	3.1	0.1544	5.1	0.0230	4.0	0.79	146.4	5.8	145.8	6.9	135.4	73.3	**146.4**	**5.8**
86	715	69091	0.8	19.9596	5.2	0.1783	6.8	0.0258	4.5	0.65	164.3	7.2	166.6	10.5	199.7	120.4	**164.3**	**7.2**
87	265	10547	0.9	21.9200	13.0	0.1206	15.6	0.0192	8.6	0.55	122.5	10.5	115.6	17.1	-22.4	316.5	**122.5**	**10.5**
88	622	21637	0.8	19.3661	6.4	0.1168	8.8	0.0164	6.0	0.69	104.9	6.3	112.2	9.3	269.3	145.9	**104.9**	**6.3**
89	359	21197	1.2	20.0716	12.1	0.1647	12.5	0.0240	2.8	0.23	152.7	4.3	154.8	17.9	186.7	283.2	**152.7**	**4.3**
90	222	2226	0.9	16.4628	18.7	0.1603	19.4	0.0191	5.0	0.26	122.2	6.0	151.0	27.2	630.2	407.0	**122.2**	**6.0**
91	200	21666	1.2	18.9412	24.3	0.1809	24.4	0.0249	1.9	0.08	158.3	3.0	168.9	37.9	320.0	559.0	**158.3**	**3.0**

92	479	36381	1.2	20.8292	7.1	0.1555	7.8	0.0235	3.3	0.42	149.7	4.9	146.7	10.6	99.7	167.2	**149.7**	**4.9**
93	325	132318	5.9	13.4951	1.7	1.4989	11.3	0.1467	11.2	0.99	882.5	92.2	929.9	69.0	1044.2	33.6	**1044.2**	**33.6**
94	738	85884	0.9	19.6497	5.1	0.1670	7.0	0.0238	4.8	0.68	151.7	7.2	156.8	10.2	235.9	118.6	**151.7**	**7.2**
95	223	9619	0.8	22.8448	19.3	0.1449	20.6	0.0240	7.4	0.36	152.9	11.2	137.4	26.5	-123.4	479.1	**152.9**	**11.2**
96	489	45654	1.0	20.2007	6.1	0.1609	6.4	0.0236	2.1	0.33	150.2	3.1	151.5	9.0	171.7	141.9	**150.2**	**3.1**
97	529	31957	1.1	19.9254	7.5	0.1612	7.9	0.0233	2.4	0.31	148.4	3.6	151.7	11.1	203.6	173.9	**148.4**	**3.6**
98	445	28313	1.3	21.1003	6.5	0.1542	7.5	0.0236	3.8	0.51	150.4	5.7	145.6	10.2	69.0	153.8	**150.4**	**5.7**
						Isotope ratios					Apparent ages (Ma)							
Analysis	U	206Pb	U/Th	206Pb*	±	207Pb*	±	206Pb*	±	error	206Pb*	±	207Pb*	±	206Pb*	±	**Best age**	**±**
	(ppm)	204Pb		207Pb*	(%)	235U*	(%)	238U	(%)	corr.	238U*	(Ma)	235U	(Ma)	207Pb*	(Ma)	**(Ma)**	**(Ma)**
WW082609-05: Section C (635m), 31°36.727'N 83°32.864'E																		
1	546	48162	0.8	19.7313	2.8	0.1704	5.5	0.0244	4.7	0.86	155.3	7.2	159.7	8.1	226.3	65.0	**155.3**	**7.2**
2	465	24081	1.0	20.3792	9.2	0.1648	9.9	0.0244	3.6	0.37	155.2	5.5	154.9	14.2	151.1	215.7	**155.2**	**5.5**
3	173	4699	1.5	18.9872	28.5	0.1127	30.6	0.0155	11.1	0.36	99.3	10.9	108.4	31.5	314.5	661.0	**99.3**	**10.9**
4	900	129770	1.0	20.1841	4.7	0.1626	5.8	0.0238	3.4	0.59	151.6	5.1	152.9	8.2	173.6	109.3	**151.6**	**5.1**
5	312	23216	0.9	22.3166	9.6	0.1464	10.9	0.0237	5.1	0.47	151.0	7.6	138.7	14.1	-66.0	234.8	**151.0**	**7.6**
6	413	31971	0.8	20.4482	14.3	0.1572	15.4	0.0233	5.7	0.37	148.5	8.3	148.2	21.3	143.2	337.6	**148.5**	**8.3**
7	195	5389	1.0	20.2635	50.2	0.1084	50.4	0.0159	4.6	0.09	101.9	4.6	104.5	50.1	164.5	1246.4	**101.9**	**4.6**
8	1283	35295	1.3	21.1566	3.9	0.1034	4.4	0.0159	2.1	0.47	101.5	2.1	99.9	4.2	62.7	92.5	**101.5**	**2.1**
9	2311	169432	14.6	19.9853	3.1	0.1575	3.5	0.0228	1.8	0.50	145.6	2.6	148.6	4.9	196.7	70.9	**145.6**	**2.6**
10	454	20562	0.8	21.5022	9.0	0.1503	9.3	0.0234	2.6	0.28	149.4	3.9	142.2	12.4	24.0	215.4	**149.4**	**3.9**
11	2618	282418	0.6	20.3493	2.3	0.1606	3.5	0.0237	2.7	0.77	151.0	4.0	151.3	5.0	154.6	53.2	**151.0**	**4.0**
12	308	17503	0.7	21.2391	19.6	0.1201	20.2	0.0185	5.0	0.25	118.1	5.9	115.1	22.0	53.5	471.2	**118.1**	**5.9**
13	293	10973	1.0	26.2360	23.7	0.1223	24.0	0.0233	3.7	0.15	148.3	5.4	117.2	26.6	-477.2	635.2	**148.3**	**5.4**
14	957	63684	0.4	20.1568	5.1	0.1576	5.4	0.0230	1.7	0.32	146.8	2.5	148.6	7.4	176.8	119.0	**146.8**	**2.5**
15	430	24826	0.6	20.2033	9.8	0.1598	10.1	0.0234	2.7	0.26	149.2	3.9	150.5	14.2	171.4	228.6	**149.2**	**3.9**
16	323	27116	1.1	20.6078	11.0	0.1588	12.2	0.0237	5.2	0.43	151.2	7.8	149.7	17.0	124.9	259.6	**151.2**	**7.8**
17	471	28016	0.8	20.2655	11.4	0.1609	11.5	0.0236	1.9	0.17	150.7	2.9	151.5	16.2	164.2	266.2	**150.7**	**2.9**
18	205	8267	2.0	22.9482	27.5	0.0997	30.4	0.0166	12.8	0.42	106.1	13.5	96.5	28.0	-134.5	692.6	**106.1**	**13.5**
19	532	15149	0.8	21.0621	9.4	0.1555	9.5	0.0238	1.3	0.14	151.4	2.0	146.8	13.0	73.4	225.0	**151.4**	**2.0**

20	392	15405	1.0	22.3874	10.6	0.1521	11.3	0.0247	3.9	0.34	157.3	6.0	143.8	15.1	-73.7	259.4	**157.3**	**6.0**
21	156	5067	1.1	22.6718	29.3	0.0984	29.9	0.0162	6.1	0.21	103.5	6.3	95.3	27.2	-104.7	732.8	**103.5**	**6.3**
22	1034	5174	0.7	23.9844	37.8	0.0155	38.4	0.0027	6.4	0.17	17.3	1.1	15.6	5.9	-245.0	987.0	**17.3**	**1.1**
23	327	12483	1.4	18.4754	18.5	0.1168	19.0	0.0156	4.2	0.22	100.1	4.2	112.2	20.1	376.3	418.9	**100.1**	**4.2**
24	456	30221	0.7	20.1940	15.5	0.1068	15.6	0.0156	2.1	0.13	100.1	2.1	103.1	15.3	172.5	363.2	**100.1**	**2.1**
25	1695	99964	0.4	20.4109	1.7	0.1590	2.2	0.0235	1.5	0.66	150.0	2.2	149.9	3.1	147.5	39.6	**150.0**	**2.2**
26	4923	10356	0.7	20.6052	2.5	0.1016	14.7	0.0152	14.4	0.99	97.2	13.9	98.3	13.7	125.2	59.0	**97.2**	**13.9**
27	316	6692	0.9	22.9623	26.6	0.0938	27.1	0.0156	4.9	0.18	100.0	4.9	91.1	23.6	-136.1	669.0	**100.0**	**4.9**
28	332	4102	0.8	21.4277	12.8	0.1435	13.2	0.0223	2.8	0.21	142.1	4.0	136.1	16.8	32.3	308.9	**142.1**	**4.0**
29	573	21656	0.7	20.8544	8.3	0.1475	9.9	0.0223	5.3	0.54	142.3	7.5	139.7	12.9	96.9	197.6	**142.3**	**7.5**
30	483	19574	0.7	21.9442	7.9	0.1481	8.2	0.0236	2.4	0.29	150.2	3.6	140.3	10.8	-25.0	191.2	**150.2**	**3.6**
31	326	17126	1.2	19.9647	11.2	0.1668	12.0	0.0242	4.2	0.35	153.8	6.3	156.6	17.3	199.1	260.9	**153.8**	**6.3**
32	103	5397	1.3	14.1329	92.9	0.1516	93.6	0.0155	11.5	0.12	99.4	11.4	143.3	125.8	950.4	290.0	**99.4**	**11.4**
33	702	16962	0.9	18.6893	10.5	0.1929	14.1	0.0262	9.4	0.67	166.4	15.5	179.1	23.2	350.4	237.7	**166.4**	**15.5**
34	830	32119	3.7	20.4105	4.0	0.1592	4.7	0.0236	2.4	0.52	150.1	3.6	150.0	6.6	147.6	94.6	**150.1**	**3.6**
35	379	17804	1.0	20.6713	4.3	0.1624	5.9	0.0243	4.0	0.68	155.1	6.1	152.8	8.3	117.7	101.3	**155.1**	**6.1**
36	210	12608	0.8	22.1604	16.0	0.1534	17.6	0.0246	7.2	0.41	157.0	11.1	144.9	23.7	-48.9	391.9	**157.0**	**11.1**
37	908	4392	0.7	19.8816	6.7	0.1727	7.6	0.0249	3.5	0.46	158.5	5.4	161.7	11.3	208.8	156.4	**158.5**	**5.4**
38	994	27944	1.2	20.3438	4.3	0.1614	4.8	0.0238	2.0	0.42	151.7	3.0	152.0	6.7	155.3	101.6	**151.7**	**3.0**
39	502	19226	0.5	21.5410	9.4	0.1448	10.2	0.0226	4.0	0.39	144.2	5.6	137.3	13.1	19.6	226.4	**144.2**	**5.6**
40	167	5294	1.6	22.3440	44.2	0.1039	46.6	0.0168	14.8	0.32	107.7	15.8	100.4	44.5	-69.0	1127.7	**107.7**	**15.8**
41	191	14690	1.0	19.5798	25.1	0.1704	25.6	0.0242	5.0	0.20	154.1	7.7	159.8	37.8	244.1	585.6	**154.1**	**7.7**
42	370	16915	1.0	21.7661	11.3	0.1517	11.5	0.0239	2.0	0.17	152.6	3.0	143.4	15.3	-5.3	273.2	**152.6**	**3.0**
43	295	17562	1.5	20.2751	14.7	0.1091	17.1	0.0160	8.7	0.51	102.6	8.9	105.1	17.1	163.1	345.2	**102.6**	**8.9**
44	454	110990	4.6	16.7159	1.5	0.7785	2.5	0.0944	2.0	0.79	581.4	11.1	584.6	11.2	597.2	33.3	**581.4**	**11.1**
45	1019	51299	0.5	20.3258	5.9	0.1621	6.6	0.0239	3.0	0.45	152.3	4.5	152.6	9.4	157.3	138.3	**152.3**	**4.5**
46	294	9307	0.7	18.5920	22.1	0.1167	23.2	0.0157	6.9	0.30	100.7	6.9	112.1	24.6	362.1	504.9	**100.7**	**6.9**
47	2903	172497	0.6	20.4162	1.2	0.1560	2.1	0.0231	1.8	0.84	147.2	2.6	147.2	2.9	146.9	27.0	**147.2**	**2.6**
48	384	19231	0.5	21.4515	18.5	0.1511	19.0	0.0235	4.5	0.23	149.8	6.6	142.9	25.4	29.7	446.8	**149.8**	**6.6**
49	187	16560	1.5	18.8591	38.0	0.1174	41.5	0.0161	16.8	0.40	102.7	17.1	112.7	44.3	329.8	891.2	**102.7**	**17.1**
50	160	10266	1.2	22.2272	22.9	0.1490	23.0	0.0240	2.0	0.09	153.0	3.0	141.0	30.3	-56.2	565.2	**153.0**	**3.0**
51	340	42125	0.7	20.3513	11.0	0.1567	11.6	0.0231	3.5	0.30	147.4	5.0	147.8	15.9	154.3	259.0	**147.4**	**5.0**
52	838	27936	0.8	21.0545	8.7	0.1022	9.0	0.0156	1.9	0.22	99.8	1.9	98.8	8.4	74.2	208.1	**99.8**	**1.9**

53	661	36388	0.6	19.3864	6.9	0.1666	7.1	0.0234	1.8	0.25	149.3	2.6	156.5	10.3	267.0	158.2	**149.3**	**2.6**
54	438	7876	0.9	21.2296	9.9	0.1537	10.4	0.0237	3.2	0.31	150.8	4.7	145.2	14.0	54.5	235.5	**150.8**	**4.7**
55	481	1363	1.5	18.7169	17.7	0.1423	18.1	0.0193	3.4	0.19	123.3	4.1	135.1	22.9	347.0	404.1	**123.3**	**4.1**
56	884	12203	0.6	19.5235	9.6	0.1453	9.8	0.0206	1.9	0.19	131.3	2.5	137.7	12.6	250.7	221.3	**131.3**	**2.5**
57	1041	76312	0.7	20.1619	4.6	0.1607	4.9	0.0235	1.6	0.34	149.7	2.4	151.3	6.8	176.2	106.9	**149.7**	**2.4**
58	1162	7156	0.7	19.4303	4.0	0.1667	4.8	0.0235	2.5	0.53	149.7	3.7	156.5	6.9	261.8	93.0	**149.7**	**3.7**
59	106	3415	0.8	20.2224	103.5	0.1029	104.4	0.0151	13.2	0.13	96.5	12.7	99.4	99.2	169.2	930.7	**96.5**	**12.7**
60	388	21726	0.9	19.6673	5.6	0.1411	6.7	0.0201	3.7	0.56	128.4	4.8	134.0	8.4	233.9	128.9	**128.4**	**4.8**
61	162	7340	0.8	20.0883	34.6	0.1405	35.0	0.0205	5.2	0.15	130.6	6.7	133.5	43.8	184.7	828.5	**130.6**	**6.7**
62	948	24579	0.7	20.3184	8.5	0.1019	9.2	0.0150	3.7	0.40	96.0	3.5	98.5	8.6	158.2	198.1	**96.0**	**3.5**
63	371	22931	0.7	20.2844	9.4	0.1619	9.9	0.0238	3.2	0.33	151.7	4.9	152.3	14.1	162.1	220.4	**151.7**	**4.9**
64	334	16499	1.7	21.4784	21.6	0.1012	23.0	0.0158	7.9	0.34	100.8	7.9	97.8	21.5	26.6	524.1	**100.8**	**7.9**
65	431	127231	2.1	14.9181	1.9	1.1390	5.0	0.1232	4.6	0.92	749.2	32.6	772.0	27.0	838.8	39.6	**749.2**	**32.6**
66	158	776	1.4	20.1878	37.2	0.1032	37.6	0.0151	5.6	0.15	96.7	5.4	99.7	35.8	173.2	896.6	**96.7**	**5.4**
67	509	9715	0.7	20.4459	11.6	0.1538	11.9	0.0228	2.8	0.24	145.3	4.1	145.2	16.1	143.5	272.7	**145.3**	**4.1**
68	311	7211	1.5	22.3072	12.3	0.0980	13.8	0.0159	6.3	0.46	101.4	6.3	94.9	12.5	-64.9	300.3	**101.4**	**6.3**
69	823	25093	1.3	19.8743	3.3	0.1663	4.3	0.0240	2.8	0.64	152.7	4.2	156.2	6.2	209.6	77.0	**152.7**	**4.2**
70	757	102441	1.0	19.6970	5.7	0.1663	6.5	0.0238	3.0	0.47	151.4	4.5	156.2	9.4	230.3	132.2	**151.4**	**4.5**
71	461	17973	0.7	21.5478	16.1	0.1534	16.8	0.0240	4.6	0.27	152.7	6.9	144.9	22.6	18.9	389.4	**152.7**	**6.9**
72	194	11822	-0.9	21.2086	22.5	0.1260	23.8	0.0194	7.7	0.32	123.8	9.5	120.5	27.1	56.9	543.3	**123.8**	**9.5**
73	533	23204	0.7	21.0010	12.5	0.1577	12.8	0.0240	2.6	0.20	153.0	3.9	148.7	17.7	80.3	298.1	**153.0**	**3.9**
74	525	36488	2.1	22.6029	15.0	0.0975	15.7	0.0160	4.6	0.29	102.3	4.6	94.5	14.2	-97.2	370.8	**102.3**	**4.6**
75	857	13850	0.8	19.7246	7.6	0.1668	19.2	0.0239	17.7	0.92	152.0	26.5	156.6	27.9	227.1	175.6	**152.0**	**26.5**
76	438	36195	1.4	20.2670	16.5	0.1091	17.4	0.0160	5.5	0.32	102.5	5.6	105.1	17.4	164.1	387.8	**102.5**	**5.6**
77	406	70053	11.1	16.7307	2.9	0.3285	7.2	0.0399	6.6	0.92	252.0	16.3	288.4	18.0	595.3	62.2	**252.0**	**16.3**
78	271	8435	0.8	23.1108	21.8	0.1410	22.4	0.0236	5.3	0.24	150.5	7.9	133.9	28.2	-152.0	546.6	**150.5**	**7.9**
79	302	3262	1.0	19.4258	15.6	0.1750	16.6	0.0247	5.5	0.33	157.0	8.5	163.8	25.1	262.3	361.2	**157.0**	**8.5**
80	1030	89381	3.0	20.2439	4.1	0.1526	8.3	0.0224	7.2	0.87	142.8	10.2	144.2	11.2	166.7	96.8	**142.8**	**10.2**
81	315	20847	0.8	19.9265	13.5	0.1667	13.8	0.0241	2.8	0.20	153.5	4.3	156.6	20.1	203.6	315.7	**153.5**	**4.3**
82	401	28765	0.9	18.8260	15.8	0.1140	16.4	0.0156	4.6	0.28	99.6	4.6	109.7	17.1	333.8	359.2	**99.6**	**4.6**
83	568	2867	0.4	19.2946	14.5	0.1726	15.3	0.0242	4.8	0.31	153.9	7.3	161.7	22.9	277.9	334.2	**153.9**	**7.3**
84	499	24697	1.0	19.7885	6.9	0.1414	10.5	0.0203	7.9	0.75	129.5	10.1	134.3	13.2	219.7	160.2	**129.5**	**10.1**
85	132	6366	1.3	13.8675	30.4	0.1595	31.8	0.0160	9.3	0.29	102.6	9.4	150.3	44.5	989.1	633.3	**102.6**	**9.4**

86	1435	78326	0.8	20.2349	3.8	0.1668	5.2	0.0245	3.5	0.68	155.9	5.4	156.6	7.6	167.8	89.3	**155.9**	**5.4**
87	84	2285	1.3	11.0560	107.7	0.2028	108.7	0.0163	14.8	0.14	104.0	15.3	187.5	188.3	1435.0	68.1	**104.0**	**15.3**
88	341	27950	0.8	19.7714	12.1	0.1710	12.7	0.0245	3.9	0.31	156.1	6.0	160.3	18.9	221.6	281.5	**156.1**	**6.0**
89	153	5349	1.5	16.5228	43.3	0.1350	43.6	0.0162	5.3	0.12	103.5	5.4	128.6	52.7	622.3	978.4	**103.5**	**5.4**
						Isotope ratios					Apparent ages (Ma)							
Analysis	U	206Pb	U/Th	206Pb*	±	207Pb*	±	206Pb*	±	error	206Pb*	±	207Pb*	±	206Pb*	±	**Best age**	**±**
	(ppm)	204Pb		207Pb*	(%)	235U*	(%)	238U	(%)	corr.	238U*	(Ma)	235U	(Ma)	207Pb*	(Ma)	**(Ma)**	**(Ma)**
WW082309-01: Section C (4m), 31°36.885'N 83°33.737'E																		
1	904	36814	5.4	20.2746	4.9	0.1725	5.9	0.0254	3.3	0.56	161.5	5.3	161.6	8.8	163.2	114.7	**161.5**	**5.3**
2	315	14096	0.6	20.2816	6.8	0.1697	8.6	0.0250	5.4	0.62	158.9	8.4	159.1	12.7	162.4	158.8	**158.9**	**8.4**
3	947	27382	1.7	19.8833	2.9	0.2000	9.8	0.0288	9.3	0.96	183.3	16.9	185.1	16.5	208.6	66.5	**183.3**	**16.9**
4	537	22562	5.0	20.2977	8.0	0.1578	8.2	0.0232	2.0	0.25	148.0	3.0	148.7	11.4	160.5	186.8	**148.0**	**3.0**
5	851	20081	0.9	20.1615	3.5	0.1609	4.8	0.0235	3.2	0.67	149.9	4.8	151.5	6.7	176.2	82.6	**149.9**	**4.8**
6	2509	45605	1.5	20.3647	1.5	0.1096	2.8	0.0162	2.3	0.84	103.5	2.4	105.6	2.8	152.8	35.9	**103.5**	**2.4**
7	557	35351	1.1	20.2101	5.9	0.1907	6.3	0.0280	2.3	0.36	177.8	4.0	177.3	10.3	170.6	137.4	**177.8**	**4.0**
8	354	63467	1.1	19.9459	9.2	0.1805	10.4	0.0261	4.8	0.46	166.2	7.9	168.5	16.2	201.3	214.8	**166.2**	**7.9**
9	340	19276	1.4	19.4784	9.5	0.1731	10.5	0.0244	4.6	0.43	155.7	7.0	162.1	15.7	256.0	217.8	**155.7**	**7.0**
10	616	167429	1.1	20.3505	5.2	0.1669	6.1	0.0246	3.1	0.52	156.9	4.9	156.8	8.9	154.4	122.5	**156.9**	**4.9**
11	505	38743	1.2	19.8548	4.1	0.1656	4.7	0.0238	2.2	0.48	151.9	3.4	155.6	6.7	211.9	94.8	**151.9**	**3.4**
12	416	12184	1.2	19.0191	14.3	0.0564	15.0	0.0078	4.4	0.29	50.0	2.2	55.8	8.1	310.7	327.0	**50.0**	**2.2**
13	564	31664	2.6	21.4653	7.2	0.1003	7.5	0.0156	2.1	0.28	99.9	2.1	97.1	7.0	28.1	173.2	**99.9**	**2.1**
14	1690	149667	1.6	20.5066	2.8	0.1042	2.9	0.0155	0.9	0.30	99.2	0.8	100.7	2.8	136.5	64.8	**99.2**	**0.8**
15	740	23871	1.0	20.0294	6.2	0.1028	6.5	0.0149	2.0	0.31	95.6	1.9	99.4	6.2	191.6	143.8	**95.6**	**1.9**
16	606	37379	1.0	20.8588	3.0	0.1573	5.2	0.0238	4.2	0.81	151.6	6.4	148.3	7.2	96.4	72.0	**151.6**	**6.4**
17	964	224603	1.1	20.0994	3.6	0.1517	4.5	0.0221	2.7	0.59	141.0	3.7	143.4	6.0	183.4	84.7	**141.0**	**3.7**
18	1411	14053	0.7	19.9552	2.0	0.1527	10.2	0.0221	10.0	0.98	140.9	13.9	144.3	13.7	200.2	47.0	**140.9**	**13.9**
19	366	57884	1.9	20.8849	11.2	0.1057	11.7	0.0160	3.2	0.27	102.4	3.2	102.0	11.4	93.4	267.1	**102.4**	**3.2**
20	501	22769	0.9	18.7616	8.6	0.1718	10.2	0.0234	5.4	0.53	148.9	7.9	161.0	15.1	341.6	195.7	**148.9**	**7.9**
21	1379	18060	1.1	20.0721	2.2	0.1647	3.1	0.0240	2.1	0.69	152.7	3.2	154.8	4.4	186.6	51.2	**152.7**	**3.2**
22	511	27675	1.0	20.0985	3.9	0.1591	5.0	0.0232	3.2	0.64	147.8	4.6	149.9	7.0	183.5	89.8	**147.8**	**4.6**

23	285	9738	1.7	19.9368	10.1	0.1628	10.8	0.0235	4.0	0.37	150.0	5.9	153.2	15.4	202.3	234.5	**150.0**	**5.9**
24	1153	6069	1.6	19.6985	4.7	0.1796	7.9	0.0257	6.3	0.81	163.4	10.2	167.8	12.2	230.2	107.7	**163.4**	**10.2**
25	815	7621	0.7	20.1745	3.5	0.1621	4.6	0.0237	3.1	0.67	151.1	4.6	152.5	6.6	174.7	80.5	**151.1**	**4.6**
26	1276	27687	0.7	20.6886	2.5	0.1031	3.1	0.0155	1.9	0.61	99.0	1.9	99.6	3.0	115.8	58.3	**99.0**	**1.9**
27	1883	32808	1.1	20.8864	2.7	0.1383	5.2	0.0210	4.4	0.85	133.7	5.8	131.6	6.4	93.2	64.8	**133.7**	**5.8**
28	1117	23105	1.2	20.0656	2.5	0.1729	7.5	0.0252	7.0	0.94	160.2	11.1	161.9	11.2	187.3	58.8	**160.2**	**11.1**
29	732	39754	0.8	19.6757	3.5	0.1753	5.4	0.0250	4.1	0.75	159.3	6.4	164.0	8.1	232.8	81.5	**159.3**	**6.4**
30	494	15179	1.0	19.2133	5.3	0.1631	5.8	0.0227	2.3	0.39	144.9	3.3	153.4	8.3	287.5	122.1	**144.9**	**3.3**
31	450	6566	1.1	19.3371	7.2	0.1564	9.4	0.0219	6.0	0.64	139.9	8.3	147.5	12.9	272.8	164.6	**139.9**	**8.3**
32	1140	37688	0.7	19.9930	2.9	0.1637	4.8	0.0237	3.8	0.80	151.3	5.7	154.0	6.8	195.8	67.0	**151.3**	**5.7**
33	401	1537	1.0	19.9967	9.4	0.1590	10.0	0.0231	3.2	0.32	146.9	4.6	149.8	13.9	195.4	219.9	**146.9**	**4.6**
34	350	16520	1.5	18.4382	8.0	0.1776	9.1	0.0238	4.1	0.46	151.3	6.2	166.0	13.9	380.8	181.1	**151.3**	**6.2**
35	422	6533	1.6	18.2877	12.6	0.1775	13.2	0.0235	4.0	0.30	150.0	6.0	165.9	20.2	399.2	282.3	**150.0**	**6.0**
36	1194	19387	1.5	20.5399	6.4	0.1052	7.0	0.0157	2.7	0.39	100.2	2.7	101.6	6.8	132.7	151.4	**100.2**	**2.7**
37	485	3730	1.0	19.8869	9.0	0.1687	9.3	0.0243	2.4	0.26	155.0	3.7	158.3	13.7	208.1	209.4	**155.0**	**3.7**
38	1167	9207	0.6	20.5587	2.6	0.1590	4.0	0.0237	3.0	0.75	151.0	4.4	149.8	5.5	130.6	62.0	**151.0**	**4.4**
39	1716	68731	1.4	20.3582	1.1	0.1568	2.5	0.0232	2.3	0.91	147.6	3.4	147.9	3.5	153.6	24.6	**147.6**	**3.4**
40	341	15245	0.8	20.1063	5.5	0.1627	5.6	0.0237	1.0	0.18	151.2	1.5	153.1	7.9	182.6	127.5	**151.2**	**1.5**
41	582	4854	1.1	19.4066	4.6	0.1666	5.7	0.0235	3.4	0.59	149.4	5.0	156.5	8.3	264.6	106.3	**149.4**	**5.0**
42	380	17705	1.0	20.3887	13.7	0.1146	14.2	0.0169	3.4	0.24	108.3	3.7	110.2	14.8	150.1	323.5	**108.3**	**3.7**
43	696	88991	1.0	19.2574	3.3	0.2093	4.4	0.0292	2.9	0.67	185.7	5.3	192.9	7.7	282.3	74.5	**185.7**	**5.3**
44	280	12474	1.0	20.7457	13.3	0.1587	14.1	0.0239	4.7	0.34	152.2	7.1	149.6	19.6	109.2	314.9	**152.2**	**7.1**
45	885	22813	1.5	19.0127	9.8	0.1214	10.6	0.0167	3.9	0.37	107.0	4.2	116.3	11.6	311.4	224.2	**107.0**	**4.2**
46	487	820	2.5	18.6132	17.7	0.1660	17.9	0.0224	2.6	0.14	142.9	3.6	156.0	25.9	359.5	402.4	**142.9**	**3.6**
47	645	38894	1.0	19.9746	5.9	0.1619	6.1	0.0235	1.6	0.26	149.5	2.3	152.4	8.6	197.9	136.3	**149.5**	**2.3**
48	429	20851	1.4	19.3986	6.7	0.1701	7.0	0.0239	2.1	0.30	152.5	3.2	159.5	10.4	265.5	154.0	**152.5**	**3.2**
49	323	18546	1.3	20.9945	7.8	0.1714	10.0	0.0261	6.2	0.62	166.1	10.2	160.7	14.9	81.0	185.8	**166.1**	**10.2**
50	798	52848	2.3	20.1961	8.9	0.1139	9.6	0.0167	3.6	0.37	106.6	3.8	109.5	10.0	172.2	209.0	**106.6**	**3.8**
51	1208	7087	1.0	20.4569	4.1	0.1345	6.4	0.0200	5.0	0.77	127.4	6.3	128.1	7.7	142.2	95.4	**127.4**	**6.3**
52	661	22474	0.6	20.2949	5.4	0.1628	6.1	0.0240	2.8	0.46	152.7	4.2	153.2	8.7	160.9	127.5	**152.7**	**4.2**
53	1085	20244	0.7	20.1564	2.9	0.1558	8.0	0.0228	7.4	0.93	145.1	10.7	147.0	10.9	176.8	66.7	**145.1**	**10.7**
54	787	36687	1.3	20.6737	12.6	0.1075	13.5	0.0161	5.0	0.37	103.1	5.1	103.7	13.3	117.5	297.7	**103.1**	**5.1**
55	719	41848	0.8	20.3939	2.9	0.1465	7.9	0.0217	7.4	0.93	138.2	10.1	138.8	10.3	149.5	67.0	**138.2**	**10.1**

56	594	5147	0.9	17.1397	18.3	0.2038	19.0	0.0253	5.1	0.27	161.3	8.1	188.3	32.7	542.7	403.0	**161.3**	**8.1**
57	717	71276	1.1	20.4621	2.6	0.1606	3.5	0.0238	2.5	0.69	151.9	3.7	151.3	5.0	141.7	60.0	**151.9**	**3.7**
58	447	4880	1.1	19.8988	12.4	0.1050	13.0	0.0152	4.1	0.32	97.0	4.0	101.4	12.6	206.8	287.5	**97.0**	**4.0**
59	728	23641	1.1	19.5254	5.0	0.1701	5.8	0.0241	2.9	0.50	153.5	4.4	159.5	8.6	250.5	116.2	**153.5**	**4.4**
60	237	39273	0.6	20.1743	6.5	0.1627	7.0	0.0238	2.5	0.37	151.7	3.8	153.1	9.9	174.8	151.0	**151.7**	**3.8**
61	393	21534	1.1	20.2419	9.7	0.1676	10.0	0.0246	2.3	0.23	156.7	3.5	157.3	14.6	167.0	228.1	**156.7**	**3.5**
62	588	83445	1.1	19.8074	5.5	0.1684	5.7	0.0242	1.4	0.24	154.1	2.1	158.0	8.3	217.4	127.6	**154.1**	**2.1**
63	1545	109553	3.0	20.3404	1.2	0.1556	5.3	0.0230	5.2	0.98	146.3	7.5	146.8	7.2	155.6	27.5	**146.3**	**7.5**
64	327	6925	1.1	19.5297	10.7	0.1642	10.9	0.0233	2.1	0.19	148.2	3.1	154.4	15.7	250.0	247.4	**148.2**	**3.1**
65	380	39245	1.5	19.6658	9.1	0.1596	9.5	0.0228	2.5	0.26	145.1	3.6	150.3	13.3	234.0	211.5	**145.1**	**3.6**
66	276	18390	0.9	19.8681	9.8	0.1665	10.2	0.0240	2.8	0.28	152.9	4.3	156.4	14.8	210.3	227.9	**152.9**	**4.3**
67	385	16492	0.7	20.2019	5.6	0.1714	5.8	0.0251	1.5	0.26	159.9	2.4	160.6	8.7	171.6	131.8	**159.9**	**2.4**
68	631	16124	0.6	20.0662	5.0	0.1571	5.9	0.0229	3.2	0.54	145.7	4.6	148.2	8.2	187.3	116.0	**145.7**	**4.6**
69	502	11999	0.8	20.2698	7.7	0.1592	8.2	0.0234	2.9	0.35	149.2	4.3	150.0	11.4	163.7	179.3	**149.2**	**4.3**
70	370	39594	0.9	19.8482	7.3	0.1611	7.9	0.0232	3.2	0.40	147.8	4.7	151.7	11.2	212.7	168.4	**147.8**	**4.7**
71	600	18729	0.9	20.6363	3.1	0.1606	4.3	0.0240	3.0	0.69	153.1	4.5	151.2	6.1	121.7	74.0	**153.1**	**4.5**
72	824	15389	1.5	19.8232	4.1	0.1107	4.9	0.0159	2.6	0.53	101.7	2.6	106.6	4.9	215.6	95.8	**101.7**	**2.6**
73	260	19859	1.5	19.7774	14.7	0.1136	15.3	0.0163	4.0	0.26	104.2	4.2	109.2	15.8	220.9	342.8	**104.2**	**4.2**
74	264	12073	1.2	24.8621	21.7	0.0905	22.1	0.0163	4.4	0.20	104.4	4.6	88.0	18.7	-336.7	564.3	**104.4**	**4.6**
75	801	8488	0.6	19.2865	6.6	0.1748	8.0	0.0244	4.4	0.56	155.7	6.8	163.6	12.0	278.8	151.8	**155.7**	**6.8**
76	920	32683	1.6	20.1159	3.2	0.1816	7.1	0.0265	6.3	0.89	168.5	10.5	169.4	11.0	181.5	75.6	**168.5**	**10.5**
77	498	8558	0.9	20.4407	6.0	0.1687	6.1	0.0250	1.3	0.21	159.3	2.0	158.3	9.0	144.1	140.5	**159.3**	**2.0**
78	803	46779	1.1	20.7507	3.5	0.1083	4.3	0.0163	2.5	0.57	104.2	2.6	104.4	4.3	108.7	83.8	**104.2**	**2.6**
79	1790	113795	1.1	20.0783	1.6	0.1706	2.4	0.0248	1.8	0.75	158.2	2.8	159.9	3.6	185.9	37.2	**158.2**	**2.8**
80	789	6283	2.8	20.8693	7.7	0.1097	9.9	0.0166	6.2	0.62	106.1	6.5	105.7	9.9	95.2	183.4	**106.1**	**6.5**
81	259	7209	0.9	20.7994	5.1	0.1610	5.5	0.0243	2.0	0.37	154.7	3.1	151.6	7.8	103.1	121.7	**154.7**	**3.1**
82	995	65598	0.7	19.9173	2.1	0.1629	3.4	0.0235	2.7	0.79	149.9	4.0	153.2	4.9	204.6	48.4	**149.9**	**4.0**
83	541	11924	1.0	20.8126	10.0	0.1195	10.3	0.0180	2.5	0.24	115.3	2.8	114.6	11.2	101.6	236.9	**115.3**	**2.8**
84	1125	32290	0.7	20.3533	3.1	0.1745	3.8	0.0258	2.3	0.61	164.0	3.8	163.4	5.8	154.1	71.5	**164.0**	**3.8**
85	833	37156	1.2	21.1238	4.1	0.1188	4.5	0.0182	1.8	0.41	116.3	2.1	114.0	4.8	66.4	97.2	**116.3**	**2.1**
86	470	28495	0.7	20.6242	4.3	0.1566	4.6	0.0234	1.5	0.32	149.2	2.2	147.7	6.3	123.1	102.1	**149.2**	**2.2**
87	619	4732	1.1	19.3883	4.1	0.1833	5.9	0.0258	4.2	0.71	164.1	6.8	170.9	9.3	266.7	94.6	**164.1**	**6.8**
88	597	63268	1.1	19.9310	3.6	0.1681	4.6	0.0243	2.9	0.63	154.8	4.4	157.8	6.7	203.0	83.1	**154.8**	**4.4**

89	977	33563	0.8	20.1950	1.8	0.1677	3.4	0.0246	2.9	0.84	156.4	4.5	157.4	5.0	172.4	42.8	**156.4**	**4.5**
						Isotope ratios					Apparent ages (Ma)							
Analysis	U	206Pb	U/Th	206Pb*	±	207Pb*	±	206Pb*	±	error	206Pb*	±	207Pb*	±	206Pb*	±	**Best age**	**±**
	(ppm)	204Pb		207Pb*	(%)	235U*	(%)	238U	(%)	corr.	238U*	(Ma)	235U	(Ma)	207Pb*	(Ma)	**(Ma)**	**(Ma)**
BH082509-07: Section N2 (380m), 31°44.264'N 83°35.774'E																		
1	1055	55513	2.0	21.2695	7.0	0.0682	8.1	0.0105	4.0	0.50	67.4	2.7	67.0	5.2	50.0	167.2	**67.4**	**2.7**
2	108	90413	0.8	12.3227	3.3	2.3079	4.2	0.2063	2.7	0.63	1208.9	29.2	1214.7	30.0	1225.1	65.0	**1225.1**	**65.0**
3	238	11454	2.3	23.0847	14.6	0.1455	15.3	0.0244	4.5	0.29	155.1	6.9	137.9	19.7	-149.2	364.2	**155.1**	**6.9**
4	669	13239	2.0	21.0093	16.0	0.0503	16.8	0.0077	5.0	0.30	49.2	2.5	49.9	8.2	79.3	381.4	**49.2**	**2.5**
5	602	58432	2.1	19.9989	7.3	0.1699	7.7	0.0246	2.7	0.34	156.9	4.1	159.3	11.4	195.1	168.8	**156.9**	**4.1**
6	301	2069	1.6	20.0149	10.3	0.1651	11.1	0.0240	4.2	0.38	152.7	6.4	155.1	16.0	193.3	240.3	**152.7**	**6.4**
7	146	192853	3.1	5.5254	0.7	12.7712	2.5	0.5118	2.4	0.96	2664.3	52.3	2662.9	23.4	2661.9	11.2	**2661.9**	**11.2**
8	1050	40818	3.9	20.3754	2.9	0.1633	4.0	0.0241	2.7	0.68	153.7	4.1	153.6	5.7	151.6	68.8	**153.7**	**4.1**
9	309	29773	2.2	19.1611	15.6	0.1717	15.9	0.0239	3.1	0.20	152.0	4.7	160.9	23.7	293.7	358.1	**152.0**	**4.7**
10	1154	37972	1.9	20.0406	11.8	0.0518	12.4	0.0075	3.8	0.31	48.4	1.8	51.3	6.2	190.3	275.0	**48.4**	**1.8**
11	335	110406	2.7	17.2964	2.2	0.6996	5.2	0.0878	4.8	0.91	542.3	24.8	538.6	21.9	522.8	47.9	**542.3**	**24.8**
12	718	29271	0.9	18.7700	5.2	0.1685	5.8	0.0229	2.5	0.43	146.2	3.6	158.1	8.5	340.6	118.7	**146.2**	**3.6**
13	1382	288850	12.5	16.4527	0.8	0.8336	2.0	0.0995	1.8	0.90	611.3	10.4	615.6	9.1	631.5	18.3	**611.3**	**10.4**
14	302	12431	1.6	23.3605	11.8	0.1342	13.0	0.0227	5.6	0.43	144.9	8.0	127.9	15.6	-178.8	294.3	**144.9**	**8.0**
15	252	12815	1.6	18.6190	5.3	0.1754	11.2	0.0237	9.9	0.88	150.9	14.8	164.1	17.0	358.8	120.2	**150.9**	**14.8**
16	35	21263	0.7	9.8972	6.1	2.8946	8.7	0.2078	6.1	0.71	1217.0	68.1	1380.5	65.6	1643.3	113.9	**1643.3**	**113.9**
17	168	8371	1.6	18.6036	19.6	0.1471	20.0	0.0199	3.9	0.20	126.7	4.9	139.4	26.1	360.7	447.0	**126.7**	**4.9**
18	291	21255	1.6	21.7441	11.9	0.1516	12.3	0.0239	3.3	0.27	152.3	4.9	143.4	16.5	-2.9	287.2	**152.3**	**4.9**
19	241	19092	1.8	22.1384	8.8	0.1458	9.9	0.0234	4.5	0.45	149.2	6.6	138.2	12.8	-46.4	214.8	**149.2**	**6.6**
20	74	39579	1.6	12.9956	4.8	1.9745	6.7	0.1861	4.7	0.70	1100.2	47.7	1106.9	45.4	1119.9	95.9	**1119.9**	**95.9**
21	680	14437	1.5	19.1651	4.8	0.1710	5.6	0.0238	2.9	0.52	151.4	4.4	160.3	8.3	293.2	109.7	**151.4**	**4.4**
22	161	17896	1.4	18.5680	14.2	0.1867	15.7	0.0251	6.6	0.42	160.1	10.4	173.8	25.0	365.0	322.0	**160.1**	**10.4**
23	422	185470	3.9	12.6045	0.8	2.1891	2.9	0.2001	2.8	0.96	1176.0	29.9	1177.6	20.2	1180.6	15.5	**1180.6**	**15.5**
24	1207	41631	2.1	20.6677	4.0	0.1670	6.5	0.0250	5.1	0.79	159.4	8.0	156.8	9.4	118.1	94.4	**159.4**	**8.0**
25	569	141911	19.1	14.9970	2.7	1.1521	5.2	0.1253	4.5	0.86	761.0	32.0	778.2	28.2	827.8	55.5	**761.0**	**32.0**

26	129	5504	1.0	29.1572	62.7	0.0828	63.3	0.0175	8.7	0.14	111.9	9.6	80.7	49.2	-765.4	1938.9	**111.9**	**9.6**
27	679	37409	2.7	20.3408	3.5	0.1613	3.8	0.0238	1.4	0.37	151.6	2.1	151.9	5.3	155.6	82.2	**151.6**	**2.1**
28	670	216145	15.1	16.8725	0.9	0.7736	3.4	0.0947	3.3	0.96	583.1	18.2	581.8	15.0	577.0	19.4	**583.1**	**18.2**
29	187	9051	2.0	20.2621	16.6	0.1669	17.5	0.0245	5.6	0.32	156.2	8.6	156.8	25.4	164.6	389.9	**156.2**	**8.6**
30	439	16858	1.7	20.0485	7.8	0.1639	8.3	0.0238	3.0	0.36	151.9	4.5	154.2	11.9	189.3	180.9	**151.9**	**4.5**
31	664	33378	2.0	20.2689	4.6	0.1644	5.7	0.0242	3.4	0.60	153.9	5.2	154.6	8.2	163.8	106.4	**153.9**	**5.2**
32	367	17118	1.4	20.7967	12.6	0.1731	13.6	0.0261	5.1	0.38	166.2	8.4	162.1	20.4	103.5	299.6	**166.2**	**8.4**
33	303	8956	1.7	17.4331	16.8	0.1936	19.4	0.0245	9.7	0.50	155.9	14.9	179.7	32.0	505.5	372.9	**155.9**	**14.9**
34	676	41914	79.0	20.2331	4.3	0.1679	6.2	0.0246	4.4	0.72	156.9	6.9	157.6	9.0	168.0	100.2	**156.9**	**6.9**
35	208	64146	2.6	12.4223	1.7	2.2630	3.7	0.2039	3.3	0.89	1196.1	36.2	1200.8	26.1	1209.3	32.5	**1209.3**	**32.5**
36	1587	79109	1.4	20.2611	2.9	0.1667	3.4	0.0245	1.8	0.53	156.0	2.8	156.6	5.0	164.7	67.8	**156.0**	**2.8**
37	328	8230	2.4	21.7904	8.7	0.1516	10.5	0.0240	5.8	0.56	152.7	8.8	143.3	14.0	-8.0	210.7	**152.7**	**8.8**
38	323	113168	175.5	12.4840	1.3	2.1897	2.0	0.1983	1.6	0.78	1166.0	17.1	1177.8	14.3	1199.5	25.2	**1199.5**	**25.2**
39	1345	894189	11.1	13.4190	2.9	1.6028	7.3	0.1560	6.7	0.92	934.5	58.2	971.3	45.5	1055.6	57.7	**1055.6**	**57.7**
40	243	22343	1.6	21.0138	12.1	0.1582	14.9	0.0241	8.7	0.58	153.5	13.1	149.1	20.7	78.8	288.9	**153.5**	**13.1**
41	962	192498	1.2	17.0892	1.0	0.7323	3.2	0.0908	3.0	0.95	560.0	16.3	557.9	13.7	549.2	21.5	**560.0**	**16.3**
42	1049	7721	2.0	24.2730	33.2	0.0148	33.4	0.0026	3.3	0.10	16.8	0.6	14.9	4.9	-275.3	865.6	**16.8**	**0.6**
43	313	49830	1.9	20.9251	11.6	0.1544	12.3	0.0234	3.9	0.32	149.3	5.7	145.8	16.7	88.9	276.6	**149.3**	**5.7**
44	420	101192	1.6	17.6247	2.5	0.6642	3.3	0.0849	2.2	0.65	525.3	10.9	517.2	13.4	481.4	55.3	**525.3**	**10.9**
45	642	6314	7.2	19.7503	16.4	0.0315	18.8	0.0045	9.3	0.49	29.0	2.7	31.5	5.8	224.1	381.2	**29.0**	**2.7**
46	147	208640	1.7	5.0632	0.5	14.3965	2.6	0.5287	2.6	0.98	2735.8	57.9	2776.2	25.1	2805.7	7.7	**2805.7**	**7.7**
47	397	6660	1.4	25.2750	23.3	0.0420	26.0	0.0077	11.6	0.45	49.4	5.7	41.8	10.6	-379.3	610.6	**49.4**	**5.7**
48	501	11490	1.6	19.8456	6.8	0.1738	8.1	0.0250	4.4	0.54	159.3	7.0	162.7	12.2	213.0	158.0	**159.3**	**7.0**
49	969	376242	12.9	13.2434	0.6	1.7976	1.9	0.1727	1.8	0.94	1026.8	17.0	1044.6	12.4	1082.1	12.8	**1082.1**	**12.8**
50	176	11497	1.7	21.1712	17.7	0.1591	18.3	0.0244	4.6	0.25	155.6	7.0	149.9	25.5	61.1	424.0	**155.6**	**7.0**
51	192	27228	1.7	22.8966	25.0	0.1497	25.3	0.0249	4.0	0.16	158.3	6.3	141.6	33.4	-129.0	624.7	**158.3**	**6.3**
52	447	14232	1.3	20.7539	6.7	0.1538	8.3	0.0232	5.0	0.60	147.6	7.2	145.3	11.3	108.3	157.7	**147.6**	**7.2**
53	206	22530	1.6	18.7455	18.9	0.1806	19.3	0.0246	4.1	0.21	156.4	6.4	168.6	30.0	343.5	430.7	**156.4**	**6.4**
54	173	159535	3.1	12.6454	1.1	2.2701	2.2	0.2082	1.9	0.86	1219.2	20.8	1203.1	15.3	1174.2	21.7	**1174.2**	**21.7**
55	2376	24036	1.9	19.6865	12.2	0.0188	12.5	0.0027	2.9	0.23	17.3	0.5	19.0	2.3	231.6	281.9	**17.3**	**0.5**
56	49	14056	1.0	12.3186	5.6	2.1730	8.0	0.1941	5.7	0.71	1143.8	59.3	1172.4	55.6	1225.7	110.9	**1225.7**	**110.9**
57	549	15013	1.9	22.8110	26.5	0.0477	27.0	0.0079	4.9	0.18	50.6	2.5	47.3	12.5	-119.7	664.6	**50.6**	**2.5**
58	387	3546	1.8	17.0797	22.0	0.1899	23.5	0.0235	8.3	0.35	149.9	12.3	176.5	38.1	550.4	485.2	**149.9**	**12.3**

59	532	10090	1.3	20.0095	8.3	0.1630	9.7	0.0237	5.0	0.52	150.7	7.5	153.4	13.8	193.9	192.3	**150.7**	**7.5**
60	151	128400	5.1	9.0966	0.8	4.9360	4.0	0.3256	3.9	0.98	1817.3	61.7	1808.4	33.6	1798.3	15.1	**1798.3**	**15.1**
61	756	21824	1.0	20.6674	6.5	0.1583	10.4	0.0237	8.1	0.78	151.2	12.1	149.2	14.4	118.1	153.3	**151.2**	**12.1**
62	188	7012	1.3	19.7469	28.4	0.0918	30.4	0.0132	10.7	0.35	84.2	9.0	89.2	25.9	224.5	669.0	**84.2**	**9.0**
63	441	28357	1.9	20.2992	11.5	0.1593	11.8	0.0235	2.5	0.22	149.4	3.7	150.1	16.5	160.4	270.1	**149.4**	**3.7**
64	210	11540	1.9	17.7486	19.2	0.1878	19.7	0.0242	4.4	0.23	154.0	6.7	174.7	31.6	465.9	428.0	**154.0**	**6.7**
65	209	57901	0.8	16.6748	3.4	0.8217	3.9	0.0994	2.0	0.51	610.7	11.5	609.0	17.8	602.5	72.6	**610.7**	**11.5**
66	672	36633	1.9	19.8023	4.2	0.1722	6.8	0.0247	5.4	0.79	157.5	8.3	161.4	10.1	218.1	96.8	**157.5**	**8.3**
67	401	3100	2.2	7.0060	458.4	0.0478	458.6	0.0024	13.6	0.03	15.7	2.1	47.5	215.8	2260.6	840.5	**2260.6**	**840.5**
68	103	78298	2.9	12.8064	3.2	2.1578	4.1	0.2004	2.5	0.60	1177.6	26.5	1167.6	28.3	1149.1	64.4	**1149.1**	**64.4**
69	187	128488	1.8	9.2561	0.8	4.6078	2.6	0.3093	2.4	0.95	1737.4	37.1	1750.7	21.5	1766.6	15.1	**1766.6**	**15.1**
70	464	33958	1.1	19.7233	7.3	0.1659	8.8	0.0237	4.8	0.55	151.2	7.2	155.9	12.7	227.3	169.8	**151.2**	**7.2**
71	881	15655	2.4	23.4450	13.8	0.0447	14.7	0.0076	5.1	0.35	48.8	2.5	44.4	6.4	-187.8	345.9	**48.8**	**2.5**
72	406	39740	1.5	19.0670	9.3	0.1798	9.6	0.0249	2.4	0.26	158.3	3.8	167.9	14.8	304.9	211.7	**158.3**	**3.8**
73	237	12229	1.7	22.8790	14.4	0.1461	15.4	0.0242	5.5	0.36	154.4	8.4	138.4	19.9	-127.1	356.2	**154.4**	**8.4**
74	507	140868	3.0	13.2021	1.0	1.8181	2.1	0.1741	1.9	0.89	1034.6	18.0	1052.0	13.9	1088.3	19.1	**1088.3**	**19.1**
75	541	2957	1.8	23.9864	44.0	0.0146	45.4	0.0025	11.0	0.24	16.3	1.8	14.7	6.6	-245.2	1162.0	**16.3**	**1.8**
76	130	885	1.8	24.7211	29.8	0.0992	31.8	0.0178	11.1	0.35	113.6	12.5	96.0	29.1	-322.0	778.7	**113.6**	**12.5**
77	313	19415	1.4	20.5058	12.7	0.1547	12.8	0.0230	1.9	0.15	146.6	2.8	146.0	17.5	136.6	299.2	**146.6**	**2.8**
78	242	14042	1.9	20.7445	10.5	0.1593	11.4	0.0240	4.5	0.40	152.7	6.8	150.1	15.9	109.3	247.9	**152.7**	**6.8**
79	202	20697	1.8	20.9275	19.5	0.1595	20.3	0.0242	5.5	0.27	154.2	8.4	150.3	28.3	88.6	466.0	**154.2**	**8.4**
80	649	24136	1.7	19.4236	6.0	0.1682	14.1	0.0237	12.8	0.90	151.0	19.1	157.9	20.6	262.5	138.2	**151.0**	**19.1**
81	868	1113517	36.3	9.1936	0.2	4.3879	4.9	0.2926	4.9	1.00	1654.4	72.0	1710.1	40.9	1778.9	4.2	**1778.9**	**4.2**
82	955	37950	1.5	21.6323	8.1	0.0686	8.4	0.0108	2.0	0.23	69.0	1.3	67.3	5.5	9.5	196.3	**69.0**	**1.3**
83	40	19109	1.9	12.5343	6.9	2.0345	7.4	0.1850	2.5	0.35	1094.0	25.7	1127.1	50.1	1191.6	136.3	**1191.6**	**136.3**
84	261	26648	1.7	20.9422	14.0	0.1508	16.4	0.0229	8.6	0.52	145.9	12.4	142.6	21.8	86.9	332.2	**145.9**	**12.4**
85	373	19585	1.7	20.2020	10.5	0.1578	11.5	0.0231	4.5	0.40	147.4	6.6	148.8	15.9	171.6	246.5	**147.4**	**6.6**
86	333	22436	1.5	18.8482	6.9	0.1782	10.0	0.0244	7.2	0.72	155.1	11.0	166.5	15.3	331.2	157.5	**155.1**	**11.0**
87	686	20497	1.2	21.9595	21.2	0.0510	21.8	0.0081	5.2	0.24	52.1	2.7	50.5	10.8	-26.7	519.2	**52.1**	**2.7**
88	326	23660	2.1	21.0242	10.1	0.1569	10.5	0.0239	2.8	0.27	152.4	4.2	148.0	14.5	77.6	241.0	**152.4**	**4.2**
89	275	23829	2.1	21.6658	18.4	0.1567	19.0	0.0246	4.4	0.23	156.8	6.8	147.8	26.1	5.7	447.2	**156.8**	**6.8**
90	195	134252	1.0	12.7473	1.9	2.1236	5.8	0.1963	5.4	0.94	1155.6	57.5	1156.5	39.7	1158.2	37.3	**1158.2**	**37.3**
91	571	4508	3.7	29.5663	69.3	0.0130	69.6	0.0028	6.3	0.09	18.0	1.1	13.1	9.1	-804.8	2221.3	**18.0**	**1.1**

						Isotope ratios					Apparent ages (Ma)							
Analysis	U	206Pb	U/Th	206Pb*	±	207Pb*	±	206Pb*	±	error	206Pb*	±	207Pb*	±	206Pb*	±	**Best age**	**±**
	(ppm)	204Pb		207Pb*	(%)	235U*	(%)	238U	(%)	corr.	238U*	(Ma)	235U	(Ma)	207Pb*	(Ma)	**(Ma)**	**(Ma)**
BH082509-04: Section N2 (90m), 31°44.026'N 83°35.908'E																		
1	319	13084	0.8	21.0091	10.2	0.1578	10.4	0.0240	1.9	0.19	153.1	2.9	148.7	14.4	79.3	243.1	**153.1**	**2.9**
2	222	24265	1.1	21.3965	12.7	0.1518	13.7	0.0236	4.9	0.36	150.1	7.3	143.5	18.3	35.8	306.0	**150.1**	**7.3**
3	187	16782	1.3	21.3517	20.6	0.1560	20.9	0.0242	3.9	0.19	153.8	6.0	147.2	28.7	40.8	496.5	**153.8**	**6.0**
4	266	14737	1.2	21.7160	10.4	0.1533	11.7	0.0241	5.5	0.46	153.8	8.3	144.8	15.9	0.2	251.4	**153.8**	**8.3**
5	358	34553	0.9	21.1402	7.3	0.1650	8.0	0.0253	3.2	0.40	161.0	5.1	155.0	11.5	64.6	174.3	**161.0**	**5.1**
6	223	13139	1.2	23.8793	21.9	0.1415	22.3	0.0245	4.1	0.18	156.0	6.3	134.4	28.1	-233.9	558.9	**156.0**	**6.3**
7	450	40989	1.1	21.2830	5.8	0.1597	6.3	0.0246	2.4	0.38	157.0	3.7	150.4	8.8	48.5	138.1	**157.0**	**3.7**
8	462	26574	1.2	21.0004	9.1	0.1647	10.8	0.0251	5.8	0.54	159.8	9.1	154.8	15.5	80.3	216.6	**159.8**	**9.1**
9	772	29864	1.1	19.9914	7.4	0.1652	7.6	0.0239	1.9	0.24	152.5	2.8	155.2	11.0	196.0	172.2	**152.5**	**2.8**
10	186	14214	1.2	26.2292	30.1	0.1344	30.5	0.0256	5.3	0.17	162.8	8.5	128.1	36.8	-476.5	812.0	**162.8**	**8.5**
11	239	21243	1.2	19.9491	9.8	0.1731	10.0	0.0250	2.0	0.20	159.5	3.2	162.1	15.0	200.9	228.8	**159.5**	**3.2**
12	349	15621	0.8	19.9168	7.6	0.1654	9.2	0.0239	5.2	0.56	152.2	7.8	155.4	13.3	204.7	176.9	**152.2**	**7.8**
13	705	124544	0.9	19.5208	7.6	0.1750	10.3	0.0248	6.9	0.67	157.8	10.8	163.8	15.6	251.1	175.4	**157.8**	**10.8**
14	183	2804	2.4	26.6998	72.1	0.0396	74.3	0.0077	18.0	0.24	49.2	8.8	39.4	28.7	-523.8	2218.0	**49.2**	**8.8**
15	230	9458	1.3	20.8396	15.2	0.1574	15.7	0.0238	4.1	0.26	151.6	6.1	148.5	21.7	98.6	361.7	**151.6**	**6.1**
16	510	391031	2.4	12.2489	0.5	2.3610	3.8	0.2097	3.7	0.99	1227.4	41.8	1230.9	26.9	1236.9	8.9	**1236.9**	**8.9**
17	43	25834	1.1	14.3491	6.7	1.3540	8.0	0.1409	4.4	0.55	849.8	35.1	869.3	46.8	919.3	137.3	**849.8**	**35.1**
18	354	41056	1.2	20.8545	11.4	0.1653	11.8	0.0250	2.9	0.25	159.2	4.6	155.4	17.0	96.9	271.4	**159.2**	**4.6**
19	470	173428	5.5	8.0677	0.3	6.2920	2.9	0.3682	2.9	1.00	2020.7	50.9	2017.3	25.8	2013.9	4.9	**2013.9**	**4.9**
20	222	25579	1.4	21.0767	18.5	0.1619	19.1	0.0247	4.9	0.25	157.6	7.6	152.4	27.0	71.7	442.1	**157.6**	**7.6**
21	373	24100	1.3	21.7969	7.9	0.1539	8.2	0.0243	2.1	0.26	154.9	3.2	145.3	11.1	-8.8	191.9	**154.9**	**3.2**
22	300	10885	0.8	21.6706	9.3	0.1581	10.4	0.0248	4.7	0.45	158.2	7.3	149.0	14.5	5.2	225.4	**158.2**	**7.3**
23	625	6050	1.7	16.7232	23.5	0.0249	26.4	0.0030	12.0	0.45	19.4	2.3	25.0	6.5	596.2	515.7	**19.4**	**2.3**
24	158	194200	1.6	12.5677	1.7	2.2491	2.9	0.2050	2.3	0.81	1202.1	25.4	1196.5	20.1	1186.3	33.0	**1186.3**	**33.0**
25	281	7320	0.9	18.6931	18.5	0.1921	23.0	0.0260	13.7	0.59	165.8	22.4	178.4	37.7	349.9	421.9	**165.8**	**22.4**
26	245	9916	1.2	21.3474	30.0	0.1602	30.3	0.0248	4.1	0.13	158.0	6.4	150.9	42.5	41.3	732.0	**158.0**	**6.4**

27	216	8779	1.2	19.4863	16.4	0.1740	16.9	0.0246	4.0	0.24	156.6	6.2	162.9	25.4	255.1	378.9	**156.6**	**6.2**
28	124	6630	1.5	21.2583	24.4	0.1627	25.7	0.0251	8.3	0.32	159.7	13.1	153.1	36.6	51.3	588.9	**159.7**	**13.1**
29	272	16130	1.2	21.4504	13.0	0.1576	13.2	0.0245	2.4	0.18	156.2	3.8	148.6	18.2	29.8	311.9	**156.2**	**3.8**
30	150	7819	1.1	25.1160	25.9	0.1346	26.5	0.0245	5.7	0.22	156.2	8.8	128.2	31.9	-362.9	679.0	**156.2**	**8.8**
31	2886	207300	1.3	20.1160	1.1	0.1711	2.9	0.0250	2.6	0.92	158.9	4.1	160.3	4.2	181.5	25.4	**158.9**	**4.1**
32	264	13622	1.3	21.7457	17.9	0.1575	18.2	0.0248	3.1	0.17	158.2	4.8	148.5	25.1	-3.1	435.2	**158.2**	**4.8**
33	230	5663	1.0	22.0922	45.2	0.0596	45.5	0.0096	4.7	0.10	61.3	2.9	58.8	26.0	-41.4	1152.2	**61.3**	**2.9**
34	225	9816	1.3	19.8288	21.6	0.1669	21.9	0.0240	3.9	0.18	152.9	5.9	156.7	31.8	215.0	504.7	**152.9**	**5.9**
35	279	11124	0.8	22.4338	13.6	0.1231	14.9	0.0200	6.1	0.41	127.9	7.7	117.9	16.6	-78.8	333.3	**127.9**	**7.7**
36	185	13151	0.8	22.1511	17.1	0.1557	17.6	0.0250	4.2	0.24	159.2	6.6	146.9	24.1	-47.8	418.3	**159.2**	**6.6**
37	172	14435	1.2	27.3251	36.6	0.1232	36.9	0.0244	4.9	0.13	155.5	7.5	117.9	41.1	-586.2	1019.5	**155.5**	**7.5**
38	208	19640	1.3	18.8802	17.2	0.1766	17.5	0.0242	3.3	0.19	154.0	5.0	165.1	26.7	327.3	393.7	**154.0**	**5.0**
39	248	20874	0.9	23.3955	17.4	0.1469	18.0	0.0249	4.7	0.26	158.8	7.3	139.2	23.4	-182.5	436.5	**158.8**	**7.3**
40	1048	12881	1.7	21.3479	33.2	0.0171	34.1	0.0026	7.8	0.23	17.0	1.3	17.2	5.8	41.3	813.4	**17.0**	**1.3**
41	180	6959	1.2	19.3455	9.2	0.1761	9.5	0.0247	2.5	0.26	157.4	3.9	164.7	14.5	271.8	211.2	**157.4**	**3.9**
42	199	10278	1.3	23.6339	20.3	0.1351	20.9	0.0232	5.1	0.24	147.6	7.4	128.7	25.2	-207.9	512.7	**147.6**	**7.4**
43	304	10070	1.0	20.9393	37.2	0.0570	39.0	0.0087	11.8	0.30	55.5	6.5	56.3	21.4	87.3	910.7	**55.5**	**6.5**
44	246	15794	1.1	21.1008	15.1	0.1522	16.2	0.0233	5.9	0.36	148.5	8.6	143.9	21.7	69.0	359.8	**148.5**	**8.6**
45	252	23353	1.2	19.2226	14.8	0.1780	15.6	0.0248	5.0	0.32	158.1	7.8	166.4	24.0	286.4	340.0	**158.1**	**7.8**
46	281	25983	1.3	22.4780	14.2	0.1545	14.8	0.0252	3.9	0.27	160.4	6.2	145.9	20.1	-83.6	350.4	**160.4**	**6.2**
47	191	12477	1.0	20.9898	14.9	0.1596	15.0	0.0243	2.3	0.15	154.7	3.5	150.3	21.0	81.5	354.7	**154.7**	**3.5**
48	260	20267	1.0	24.0146	19.3	0.1452	20.1	0.0253	5.6	0.28	161.0	8.9	137.7	25.8	-248.2	491.0	**161.0**	**8.9**
49	262	18219	1.2	21.8568	24.1	0.1579	24.3	0.0250	2.3	0.10	159.4	3.7	148.9	33.6	-15.4	591.0	**159.4**	**3.7**
50	310	22518	1.2	20.6592	14.5	0.1618	14.7	0.0242	2.6	0.18	154.4	4.0	152.3	20.9	119.1	343.4	**154.4**	**4.0**
51	184	21014	1.1	21.6086	16.6	0.1560	18.4	0.0244	8.0	0.43	155.7	12.3	147.2	25.2	12.1	401.2	**155.7**	**12.3**
52	146	5365	1.2	18.9094	26.8	0.1818	27.0	0.0249	3.8	0.14	158.7	6.0	169.6	42.3	323.8	617.9	**158.7**	**6.0**
53	341	361106	2.1	11.7257	1.1	2.5867	3.3	0.2200	3.1	0.95	1281.7	36.3	1296.9	24.2	1322.0	20.6	**1322.0**	**20.6**
54	145	11502	1.2	24.4327	46.3	0.1416	46.8	0.0251	6.7	0.14	159.8	10.6	134.5	59.0	-292.0	1239.7	**159.8**	**10.6**
55	496	36904	0.9	19.6631	8.0	0.1699	8.7	0.0242	3.4	0.40	154.3	5.2	159.3	12.8	234.4	184.2	**154.3**	**5.2**
56	538	185650	2.4	12.3869	2.6	1.8332	4.3	0.1647	3.4	0.79	982.8	30.8	1057.4	27.9	1214.9	50.9	**1214.9**	**50.9**
57	293	12670	1.4	23.4631	25.0	0.0759	25.5	0.0129	5.1	0.20	82.7	4.2	74.3	18.3	-189.7	633.5	**82.7**	**4.2**
58	358	10759	2.0	20.7567	16.2	0.1061	16.8	0.0160	4.5	0.27	102.1	4.5	102.4	16.4	108.0	384.6	**102.1**	**4.5**
59	670	22855	1.4	18.6768	10.7	0.1777	11.8	0.0241	4.9	0.42	153.4	7.5	166.1	18.1	351.9	242.5	**153.4**	**7.5**

60	257	21024	1.4	19.7037	10.5	0.1738	11.7	0.0248	5.1	0.43	158.2	7.9	162.7	17.6	229.6	244.0	**158.2**	**7.9**
61	194	19522	1.4	20.2559	22.3	0.1685	22.5	0.0247	3.1	0.14	157.6	4.9	158.1	32.9	165.3	525.7	**157.6**	**4.9**
62	218	17937	1.2	23.5758	25.9	0.1390	26.4	0.0238	4.7	0.18	151.4	7.1	132.1	32.7	-201.7	659.7	**151.4**	**7.1**
63	265	11658	1.2	18.5259	7.0	0.1813	7.6	0.0244	2.9	0.38	155.2	4.4	169.2	11.9	370.1	158.6	**155.2**	**4.4**
64	105	4547	2.1	2.0335	1409.6	1.0450	1409.6	0.0154	12.8	0.01	98.6	12.5	726.4		4216.7	456.3	**4216.7**	**456.3**
65	485	112152	1.3	20.5409	6.7	0.1586	9.0	0.0236	6.0	0.67	150.6	8.9	149.5	12.5	132.6	158.0	**150.6**	**8.9**
66	304	47892	1.3	20.9915	5.9	0.1571	7.8	0.0239	5.1	0.66	152.4	7.7	148.2	10.8	81.3	140.2	**152.4**	**7.7**
67	213	11256	1.4	19.4773	16.7	0.1703	17.0	0.0241	3.3	0.20	153.3	5.0	159.7	25.2	256.2	386.6	**153.3**	**5.0**
68	233	14574	1.0	20.4975	20.9	0.1656	21.1	0.0246	3.1	0.15	156.8	4.8	155.6	30.4	137.6	494.5	**156.8**	**4.8**
69	408	38079	1.2	21.3185	8.7	0.1571	9.1	0.0243	2.5	0.28	154.8	3.9	148.2	12.5	44.5	208.1	**154.8**	**3.9**
70	289	11967	1.4	21.5773	10.3	0.1520	10.5	0.0238	1.8	0.18	151.6	2.8	143.7	14.0	15.6	248.1	**151.6**	**2.8**
71	210	10787	1.4	21.5552	20.5	0.1039	20.9	0.0162	4.2	0.20	103.8	4.3	100.4	19.9	18.0	495.8	**103.8**	**4.3**
72	199	9993	1.1	24.1259	16.1	0.1371	17.1	0.0240	5.7	0.33	152.8	8.6	130.4	20.9	-259.9	411.0	**152.8**	**8.6**
73	297	31061	0.9	20.7238	19.0	0.1577	19.0	0.0237	1.9	0.10	151.0	2.9	148.7	26.3	111.7	450.8	**151.0**	**2.9**
74	151	11627	1.1	22.9734	26.0	0.1446	26.3	0.0241	3.9	0.15	153.4	5.9	137.1	33.8	-137.3	653.3	**153.4**	**5.9**
75	305	13979	1.0	23.8995	21.0	0.1367	21.2	0.0237	2.4	0.12	151.0	3.6	130.1	25.9	-236.0	536.0	**151.0**	**3.6**
76	197	8718	1.2	20.2808	20.2	0.1627	20.6	0.0239	3.7	0.18	152.5	5.6	153.1	29.2	162.5	477.4	**152.5**	**5.6**
77	46	8899	1.9	6.2531	1.4	8.8793	3.7	0.4027	3.5	0.93	2181.4	64.1	2325.7	34.0	2454.8	23.2	**2454.8**	**23.2**
78	480	19429	1.4	19.9657	7.3	0.1602	7.7	0.0232	2.3	0.30	147.9	3.4	150.9	10.7	199.0	169.7	**147.9**	**3.4**
79	241	15251	1.3	21.9325	17.5	0.1489	17.8	0.0237	3.0	0.17	150.9	4.5	141.0	23.4	-23.8	427.6	**150.9**	**4.5**
80	239	6892	1.0	22.5377	14.8	0.1475	14.9	0.0241	2.2	0.15	153.5	3.4	139.7	19.5	-90.1	363.4	**153.5**	**3.4**
81	339	13799	1.4	20.4966	6.6	0.1593	7.5	0.0237	3.4	0.46	150.9	5.1	150.1	10.4	137.7	156.2	**150.9**	**5.1**
82	106	4150	1.7	22.3674	63.2	0.0916	65.7	0.0149	17.9	0.27	95.1	16.9	89.0	56.0	-71.5	1713.5	**95.1**	**16.9**
83	252	21184	1.1	20.8196	14.4	0.1557	15.2	0.0235	4.8	0.32	149.8	7.1	146.9	20.8	100.8	343.0	**149.8**	**7.1**
84	1707	94985	0.6	19.2819	5.0	0.1596	5.9	0.0223	3.1	0.52	142.3	4.4	150.4	8.3	279.4	115.2	**142.3**	**4.4**
85	188	7782	1.1	22.5038	17.7	0.1464	18.0	0.0239	3.4	0.19	152.2	5.1	138.7	23.3	-86.4	435.5	**152.2**	**5.1**
86	196	12025	1.3	20.6338	17.6	0.1575	17.8	0.0236	2.7	0.15	150.2	4.0	148.5	24.6	122.0	417.6	**150.2**	**4.0**
87	197	11075	1.0	20.8109	13.1	0.1659	14.6	0.0250	6.5	0.44	159.4	10.2	155.9	21.1	101.8	311.0	**159.4**	**10.2**
88	198	16036	1.3	25.6502	19.3	0.1270	19.7	0.0236	4.1	0.21	150.6	6.1	121.4	22.6	-417.7	508.8	**150.6**	**6.1**
89	207	13898	1.3	21.5689	24.8	0.1565	25.6	0.0245	6.3	0.25	155.9	9.8	147.6	35.1	16.5	603.1	**155.9**	**9.8**
90	425	13337	1.6	19.0868	17.2	0.0945	18.3	0.0131	6.3	0.35	83.8	5.3	91.7	16.1	302.5	394.3	**83.8**	**5.3**
91	645	228895	37.5	16.5482	1.6	0.6595	4.5	0.0792	4.2	0.94	491.1	20.0	514.3	18.2	619.0	34.4	**491.1**	**20.0**
92	311	30158	1.1	18.4541	9.1	0.1782	9.8	0.0238	3.8	0.38	151.9	5.6	166.5	15.1	378.9	204.6	**151.9**	**5.6**

93	345	23993	1.3	20.1536	4.5	0.1640	5.7	0.0240	3.5	0.62	152.7	5.3	154.2	8.2	177.2	104.7	**152.7**	**5.3**
94	264	18063	1.3	18.7032	8.8	0.1718	9.0	0.0233	1.9	0.21	148.5	2.8	160.9	13.4	348.7	199.7	**148.5**	**2.8**
95	1119	75561	53.2	16.4502	0.9	0.6531	4.3	0.0779	4.2	0.98	483.7	19.8	510.4	17.4	631.8	19.2	**483.7**	**19.8**
96	344	16304	1.0	20.3467	6.6	0.1600	7.2	0.0236	2.7	0.37	150.4	4.0	150.7	10.0	154.9	155.7	**150.4**	**4.0**

Appendix 2: Section C Detrital and Conglomerate Clast Zircon (U-Th)/He results

Sample locations (see Fig. 2): 31°36.885'N 83°33.737'E (base), 31°36.727'N 83°32.864'E (top)

Sample	level (m)	sample type	Age, Ma	err., Ma	U (ppm)	Th (ppm)	Sm (ppm)	Th/U	He (nmol/g)	mass (ug)	Ft	comment
zWW082309-01-1	4	sandstone	9.6	0.8	330.0	225.8	0.6	0.68	16.6	21.47	0.83	
zWW082309-01-2	4	sandstone	7.8	0.6	699.2	207.3	0.3	0.30	25.8	11.77	0.82	
zWW082309-01-3	4	sandstone	9.8	0.8	655.4	253.7	0.5	0.39	29.5	6.46	0.78	
zWW082309-01-4	4	sandstone	46.5	3.7	127.7	64.8	0.1	0.51	27.7	6.51	0.77	outlier,omitted from mean
zWW082309-01-5	4	sandstone	8.9	0.7	557.8	174.6	0.2	0.31	23.4	11.16	0.81	
zWW082309-01-6	4	sandstone	8.5	0.7	179.0	138.6	0.5	0.77	7.6	7.28	0.78	
zWW082309-02-1	25	conglomerate clast	11.2	0.9	723.2	210.0	0.2	0.29	37.9	10.35	0.81	
zWW082309-02-2	25	conglomerate clast	-4.2	-0.3	0.4	0.4	0.0	1.05	0.0	6.16	0.77	lost grain
zWW082309-02-3	25	conglomerate clast	8.5	0.7	867.1	208.3	0.3	0.24	33.3	7.33	0.79	
zWW082309-02-4	25	conglomerate clast	8.7	0.5	966.2	368.3	0.5	0.38	39.2	8.23	0.80	
zWW082309-06-1	250	conglomerate clast	9.7	0.8	1321.2	830.7	0.8	0.63	62.8	7.92	0.79	
zWW082309-06-2	250	conglomerate clast	-0.4	0.0	0.2	0.4	0.0	1.87	0.0	11.75	0.81	lost grain
zWW082309-06-3	250	conglomerate clast	8.1	0.6	1054.3	419.6	0.6	0.40	39.7	7.59	0.79	
zWW082309-06-4	250	conglomerate clast	9.4	0.6	536.6	250.7	0.4	0.47	24.9	12.34	0.82	
zWW082309-07-1	273	sandstone	7.5	0.6	694.6	247.4	0.9	0.36	24.6	9.87	0.81	
zWW082309-07-2	273	sandstone	8.2	0.7	497.9	218.2	1.2	0.44	19.0	7.66	0.79	
zWW082309-07-3	273	sandstone	9.4	0.8	235.9	157.8	0.5	0.67	10.9	7.90	0.79	
zWW082309-07-4	273	sandstone	8.2	0.7	1367.2	361.9	0.4	0.26	50.1	6.11	0.78	
zWW082309-07-5	273	sandstone	8.5	0.7	345.1	105.0	0.2	0.30	13.6	8.62	0.80	
zWW082309-07-6	273	sandstone	8.9	0.7	251.9	171.7	0.6	0.68	10.7	5.43	0.76	
zWW082609-01-1	424	sandstone	7.8	0.6	265.0	168.5	0.9	0.64	10.1	9.41	0.79	
zWW082609-01-2	424	sandstone	7.8	0.6	316.2	118.2	0.2	0.37	11.5	7.71	0.79	
zWW082609-01-3	424	sandstone	9.5	0.6	577.6	382.3	0.8	0.66	28.2	13.52	0.82	
zWW082609-01-4	424	sandstone	7.6	0.5	383.9	158.1	0.5	0.41	13.9	12.06	0.81	
zWW082609-01-5	424	sandstone	8.1	0.5	882.0	317.0	0.6	0.36	33.0	8.37	0.79	
zWW082609-01-6	424	sandstone	7.8	0.5	283.6	185.5	0.5	0.65	11.2	11.90	0.81	

zWW082609-02-1	425	conglomerate clast	7.7	0.6	505.2	173.3	0.3	0.34	19.0	16.37	0.84
zWW082609-02-2	425	conglomerate clast	7.5	0.6	780.2	281.2	0.5	0.36	27.2	9.10	0.79
zWW082609-02-3	425	conglomerate clast	8.2	0.7	747.6	226.8	0.4	0.30	28.2	9.33	0.80
zWW082609-05-1	635	sandstone	7.2	0.4	424.8	193.2	0.3	0.45	14.0	5.52	0.77
zWW082609-05-2	635	sandstone	7.9	0.5	459.2	261.1	1.0	0.57	17.0	6.11	0.77
zWW082609-05-3	635	sandstone	7.2	0.4	1169.8	262.1	0.5	0.22	35.8	4.26	0.75
zWW082609-05-4	635	sandstone	8.8	0.5	1000.9	403.4	0.4	0.40	42.7	13.38	0.82
zWW082609-05-5	635	sandstone	6.8	0.4	849.7	143.5	0.3	0.17	25.4	6.14	0.79
zWW082609-05-6	635	sandstone	7.2	0.4	291.2	135.3	0.3	0.46	9.3	3.82	0.74
zWW082609-06-1	647	conglomerate clast	7.5	0.6	227.6	119.4	0.2	0.52	8.2	8.93	0.79
zWW082609-06-2	647	conglomerate clast	9.1	0.7	122.0	79.3	0.3	0.65	5.3	5.84	0.77
zWW082609-06-3	647	conglomerate clast	7.8	0.6	113.9	81.1	0.4	0.71	4.4	8.04	0.79

Appendix 3: Conglomerate Clast Apatite (U-Th)/He results

Sample	Section	level (m)	Age [Ma]	± [Ma]	U [ppm]	Th [ppm]	Sm [ppm]	Th/U	He [nmol/g]	mass [µg]	Ft	comment
BH082509-09: Range-front section N2, 31°44.432'N 83°35.651'E												
BH082509-09-1	N2	555	7.5	0.4	20.1	62.0	64.9	3.1	0.97	2.8	0.68	
BH082509-09-2	N2	555	13.4	0.8	21.1	80.1	74.8	3.8	1.92	4.3	0.65	
BH082509-09-3	N2	555	7.3	0.4	22.3	69.9	67.5	3.1	0.98	3.8	0.63	
BH082809-01: Range-front section N1, 31°42.935'N 83°35.428'E												
BH082809-01-1	N1	230	16.4	1.0	10.9	46.0	92.4	4.2	1.31	4.6	0.66	
BH082809-01-2	N1	230	25.9	1.6	17.9	47.0	75.8	2.6	2.60	3.4	0.63	
BH082809-01-3	N1	230	40.0	2.4	19.2	47.8	86.5	2.5	4.58	5.5	0.68	
BH082809-05: Range-front section N1, 31°43.453'N 83°34.961'E												
BH082809-05-1	N1	650	13.2	0.8	10.5	10.1	30.2	1.0	0.66	3.2	0.71	
BH082809-05-2	N1	650	9.3	0.6	22.8	24.6	42.3	1.1	0.91	3.0	0.63	
BH082809-05-3	N1	650	8.7	0.5	22.6	68.3	66.1	3.0	1.16	3.8	0.63	
WW082309-02: Range-front section C, 31°36.842'N 83°33.681'E												
WW082309-02-1	C	25	7.1	0.4	50.6	54.4	71.9	1.1	1.90	8.6	0.78	
WW082309-02-2	C	25	4.3	0.3	111.2	125.0	92.5	1.1	2.40	10.1	0.74	
WW082309-02-3	C	25	3.1	0.2	107.4	85.7	63.9	0.8	1.54	9.3	0.73	
WW082309-06: Range-front section C, 31°36.768'N 83°33.448'E												
WW082309-06-1	C	250	25.9	0.17	52.9	67.9	41.8	1.28	6.9	8.58	0.71	probable inclusion, omitted
WW082309-06-2	C	250	8.6	0.06	60.1	65.1	43.4	1.08	2.3	4.83	0.67	
WW082609-02: Range-front section C, 31°36.763'N 83°33.219'E												
WW082609-02-1	C	425	29.3	0.19	51.5	138.3	52.2	2.68	8.6	4.16	0.64	probable inclusion, omitted
WW082609-02-2	C	425	2.8	0.02	55.9	94.4	59.5	1.69	0.8	3.70	0.70	
WW082609-06: Range-front section C, 31°36.727'N 83°32.864'E												
WW082609-06-1	C	647	2.9	0.2	72.2	111.2	13.3	1.5	1.15	6.0	0.75	
WW082609-06-2	C	647	2.1	0.1	76.4	105.0	12.9	1.4	0.76	5.7	0.68	
WW082609-06-3	C	647	2.5	0.1	73.5	93.5	14.5	1.3	0.88	5.5	0.69	

12. References

Anders, M.H., and Schlische, R.W., 1994, Overlapping Faults, Intrabasin Highs, and the Growth of Normal Faults: The Journal of Geology , v. 102, p. 165-179

Armijo, R., Tapponnier, P., Mercier, J.L., and Han, T.L., 1986, Quaternary extension in southern Tibet: Field observations and tectonic implications: Journal of Geophysical Research, v. 91, p. 13,803-13,872.

Adhikari, B.R., and Wagreich, M., 2011, Provenance evolution of collapse graben fill in the Himalaya-The Miocene to Quaternary Thakkhola-Mustang Graben (Nepal): Sedimentary Geology, v. 233, p. 1-14.

Bird, P., 1991, Lateral extrusion of lower crust from under high topography, in the isostatic limit: Journal of Geophysical Research, v. 96, p. 10,275–10,286.

Blisniuk, P.M., Hacker, B.R., Glodny, J., Ratschbacher, L., Bi, S.W., Wu, Z.H., McWilliams, M.O., and Calvert, A., 2001, Normal faulting in central Tibet since at least 13.5 Myr ago: Nature, v. 412 (6847), p. 628–632.

Buck, W. R., 1988, Flexural rotation of normal faults: Tectonics, v. 7, p. 959-973.

Buck, W.R., 1991, Modes of continental lithospheric extension: Journal of Geophysical Research, v. 96, p. 20,161-10,178.

Clark, M.K., and Royden, L.H., 2000, Topographic ooze: Building the eastern margin of Tibet by lower crustal flow: Geology, v. 28, p. 703–706.

Coleman, M.E., and Hodges, K.V., 1995, Evidence for Tibetan plateau uplift before 14 m.y. ago from a new minimum estimate for east-west extension: Nature, v. 374, p. 49-52.

Colombo, F., 1994, Normal and reverse unroofing sequences in syntectonic conglomerates as evidence of progressive basinward deformation: Geology, v. 22, p. 235–238.

Dart, C., Cohen, H.A., Akyüz, H.S., Barka, A., 1995, Basinward migration of rift-border faults: Implications for facies distributions and preservation potential: Geology, v. 23, p. 69–72.

Davis, G.A., and Lister, G.A., 1988, Detachment faulting in continental extension: Perspectives from the southwestern U.S. Cordillera, *in* Clark, S.P., Jr., Burchfiel, B.C., and Suppe, J., eds., Processes in continental lithospheric deformation: Geological Society of America Special Paper 218, p. 133–159.

Dewey, J.F., Shackleton, R.M., Chang, C., and Sun, Y., 1988, The tectonic evolution of the Tibetan Plateau: Philosophical Transactions of Royal Society of London, v. A327, p. 379–413.

Dickinson, W.R., 1970, Interpreting detrital modes of graywacke and arkose: Journal of Sedimentary Petrology, v. 40, p. 695–707.

Dickinson, W.R., 1985, Interpreting provenance relation from detrital modes of sandstones, *in* Zuffa, G.G., ed., Provenance of Arenites, p. 333–363, Reidel Publishing Company, Dordrecht.

Dickinson, W.R., and Suczek, C.A., 1979, Plate tectonics and sandstone compositions: American Association of Petroleum Geologists Bulletin, v. 63, p. 2164-2182.

Dickinson, W.R., Beard, L.S., Brakenridge, G.R., Erjavec, J.L., Ferguson, R.C., Inman, K.F., Knepp, R.A., Lindberg, F.A., and Ryberg, P.T., 1983, Provenance of North American Phanerozoic sandstones in relation to tectonic setting: Geological Society of America
Bulletin, v. 94, p. 222–235.

Dupont-Nivet, G., Lippert, P.C., van Hinsbergen, D.J.J., Meijers, M.J.M., Kapp, P., 2010, Palaeolatitude and age of the Indo-Asia collision: Palaeomagnetic constraints: Geophysical Journal International, v. 182, p. 1189-1198.

Edwards, M.A., and Harrison, T.M., 1997, When did the roof collapse? Late Miocene north-south extension in the high Himalaya revealed by Th-Pb monazite dating of the Khula Kangri granite: Geology, v. 25, p. 543-546.

Ehlers T.A., and Farley, K.A., 2003, Apatite (U-Th)/He thermochronometry: Methods and applications to problems in tectonics and surface processes: Earth and Planetary Science Letters, v. 206, p. 1–14.

Ellis, P. G. and McClay, K. R., 1988, Listric extensional fault systems - results of analogue model experiments: Basin Research, v. 1, p. 55–70

England, P., and Houseman, G., 1989, Extension during continental convergence, with application to the Tibetan plateau: Journal of Geophysical Research, v. 94, p. 17,561-17,579.

England, P., and Searle, M., 1986, The Cretaceous-Tertiary deformation of the Lhasa block and its implications for crustal thickening in Tibet: Tectonics, v. 5, p. 1–14.

Folk, R.L., 1980, Petrology of Sedimentary Rocks, Austin, Texas, Hemphill Publishing Company, 184 p.

Friedmann, S.J. and Burbank, D.W., 1995, Rift basins and supradetachment basins: intracontinental extensional end-members: Basin Research, v. 7, p. 109–127

Garzione, C.N., DeCelles, P.G., Hodkinson, D.G., Ojha, T.P., and Upreti, B.N., 2003, East-west extension and Miocene environmental change in the southern Tibetan plateau: Thakkhola graben, central Nepal: Geological Society of America Bulletin, v. 115, p. 3-20.

Gawthorpe, R. L. and Leeder, M. R., 2000, Tectono-sedimentary evolution of active extensional basins: Basin Research, v. 12, p. 195–218

Gazzi, P., 1966, I minerali pesanti nei flysch arenacei fra Monte Ramaceto e Monte Molinatico (Appennino settentrionale), Mineralogica et Petrographica Acta, v. 11, p. 197–212.

Gehrels, G., 2000, Introduction to detrital zircons studies of Paleozoic and Triassic strata in western Nevada and northern California, *in* Soreghan, M.J., and Gehrels, G., eds., Paleozoic and Triassic paleogeography and tectonics of western Nevada and northern California, Geological Society of America Special Paper, v. 347, p. 1-17.

Gehrels, G.E., Valencia, V.A., and Ruiz, J., 2008, Enhanced precision, accuracy, efficiency, and spatial resolution of U-Pb ages by laser ablation-multicollector-inductively coupled plasma-mass spectrometry: Geochemistry Geophysics Geosystems, v. 9, Q12001, doi:10.1029/2009GC002749.

Gibbs, A., 1987, Development of extension and mixed-mode sedimentary basins, *in* Coward, M.P., Dewey, J.F., and Hancock, P.L., eds., Continental extensional tectonics: Geological Society of London Special Publication, v. 28, p. 19-33.

Hamblin, A.P., 1992, Half-graben lacustrine sedimentary rocks of the lower Carboniferous Strathlorne Formation, Horton Group, Cape Breton Island, Nova Scotia, Canada: Sedimentology, v. 39, p. 263-284.

Hampton, B.A., and Horton, B.K., 2007, Sheetflow fluvial processes in a rapidly subsiding basin, Altiplano plateau, Bolivia: Sedimentology, v. 54, p. 1121-1147.

Harrison, T.M., Copeland, P., Kidd, W.S.F., and Lovera, O.M., 1995, Activation of the Nyainqentanghla shear zone: Implications for uplift of the southern Tibetan Plateau: Tectonics, v. 14, p. 658–676.

Harrison, T.M., and Zeitler, P.K., 2005, Fundamentals of noble gas thermochronometry, *in* Reiners, P.W., and Ehlers, T.A., eds., Low-Temperature Thermochronology: Techniques, Interpretations, and Applications: Reviews in Mineralogy and Geochemistry, v. 58, p. 123–149, Mineralogical Society of America, Washington, DC.

Horton, B.K., 2012, Cenozoic evolution of hinterland basins in the Andes and Tibet, in Busby, C., and Azor, A., editors, Tectonics of Sedimentary Basins: Recent Advances: Wiley-Blackwell, Oxford, UK, p. 427-444.

Horton, B.K., and Schmitt, J.G., 1996, Sedimentology of a lacustrine fan-delta system, Miocene Horse Camp Formation, Nevada, USA: Sedimentology, v. 43, p. 133–155.

Horton, B.K, and Schmitt, J.G., 1998, Development and exhumation of a Neogene sedimentary basin during extension, Nevada: Geological Society of America Bulletin, v. 110, p. 163-172.

Ingersoll, R.V., Bullard, T.F., Ford, R.L., Grimm, J.P., Pickle, J.D., and Sares, S.W., 1984, The effect of grain size on detrital modes: A test of the Gazzi-Dickinson point-counting method: Journal of Sedimentary Petrology, v. 54, p. 103–116.

Kapp, J.L.D., Harrison, T.M., Kapp, P., Grove, M., Lovera, O.M., and Lin, D., 2005, Nyainqentanglha Shan: A window into the tectonic, thermal, and geochemical evolution of the Lhasa block, southern Tibet: Journal of Geophysical Research, v. 110, B08413, doi:10.1029/2004JB003330.

Kapp, P., and Guynn, J.H., 2004, Indian punch rifts Tibet: Geology, v. 32, p. 993-996.

Kapp, P., Taylor, M., Stockli, D., and Ding, L., 2008, Development of active low-angle normal fault systems during orogenic collapse: Insight from Tibet: Geology, v. 36, p. 7-10.

Kapp, P., Yin, A., Harrison, T.M., and Ding, L., 2005, Cretaceous-Tertiary shortening, basin development, and volcanism in central Tibet: Geological Society of America Bulletin, v. 117, p. 865-878.

Kempf, O., Blisniuk, P.M., Wang, S.F., Fang, X.M., Wrozyna, C., and Schwalb, A., 2009, Sedimentology, sedimentary petrology, and paleoecology of the monsoon-driven, fluvio-lacustrine Zhada Basin, SW-Tibet: Sedimentary Geology, v. 222, p. 27-41.

Leeder, M.R. and Gawthorpe, R.L., 1987, Sedimentary models for extensional tilt-block/half-graben basins: Geological Society, London, Special Publications, v. 28, p. 139-152

Leier, A.L., DeCelles, P.G., Kapp, P., and Ding, L., 2007, The Takena Formation of the Lhasa terrane, southern Tibet: the record of a Late Cretaceous retroarc foreland basin: Geological Society of America Bulletin, v. 119, p. 31–48.

Link, M.H., and Osborne, R.H., 1978, Lacustrine facies in the Pliocene Ridge Basin Group: Ridge Basin, California, *in* Matter, A., and Tucker, M.E., eds., Modern and ancient lake sediments: International Association of Sedimentologists Special Publication 2, p. 169-187.

Lister, G. S., and Davis, G. A., 1989, The origin of metamorphic core complexes and detachment faults formed during Tertiary continental extension in the northern Colorado River region, U.S.A.: Journal of Structural Geology, v. 11, p. 65-94.

Masek, J.G., Isacks, B.L., and Fielding, E.J., 1994, Rift flank uplift in Tibet: Evidence for a viscous lower crust: Tectonics, v. 13, p. 659-667.

Miall, A.D., 1996, The geology of fluvial deposits: New York, Springer-Verlag, 582 p.

Miller, C., Schuster, R., Klotzli, U., Frank, W., and Grasemann, B., 2000, Late Cretaceous-Tertiary magmatic and tectonic events in the Transhimalaya batholith (Kailas area, SW Tibet): Schweiz. Mineral. Petrogr. Mitt., v.80, p. 1–20

Molnar, P. and Tapponnier, P., 1975, Cenozoic tectonics of Asia: Effects of a continental collision: Science, v. 189, p. 419–426.

Molnar, P., and Tapponnier, P., 1978, Active tectonics of Tibet: Journal of Geophysical Research, v. 83, p. 5361-5375.

Molnar, P., England, P., and Martinod, J., 1993, Mantle dynamics, the uplift of the Tibetan Plateau, and the Indian monsoon: Reviews of Geophysics, v. 31, p. 357–396.

Murphy, M.A., Yin, A., Harrison, T.M., Duerr, S.B., Chen, Z., Ryerson, F.J., Kidd, W.S.F., Wang, X., and Zhou, X., 1997, Did the Indo-Asian collision alone create the Tibetan plateau? Geology, v. 25, p. 719-722.

Ni, J., and York, J., 1978, Late Cenozoic tectonics of the Tibetan plateau: Journal of Geophysical Research, v. 83, p. 5377–5384.

Northrup, C.J., Royden, L.H., and Burchfiel, B.C., 1995, Motion of the Pacific plate relative to Eurasia and its potential relation to Cenozoic extension along the eastern margin of Eurasia: Geology, v. 23, p. 719-722.

Pan, G., Ding, J., Yao, D., and Wang, L., 2004, Geological map of the Qinghai-Xizang (Tibet) Plateau and adjacent areas: Chengdu, Chengdu Cartographic Publishing House, scale 1:1,000,000.

Patriat, P., and Achache, J., 1984, India-Eurasia collision chronology has implications for crustal shortening and driving mechanism of plates: Nature, v. 311 (5987), p. 615–621.

Reiners P.W., Spell T.L., Nicolescu S., and Zanetti K.A., 2004, Zircon (U-Th)/He thermochronometry: He diffusion and comparisons with $^{40}Ar/^{39}Ar$ dating. Geochim Cosmochim Acta, v. 68, p. 1857–1887.

Ridgway, K. D., and DeCelles, P. G., 1993, Stream-dominated alluvial fan and lacustrine depositional systems in Cenozoic strike-slip basins, Denali fault system, Yukon Territory, Canada: Sedimentology, v. 40, p. 645-666.

Royden, L.H., Burchfiel, B.C., King, R.W., Wang, E., Chen, Z., Shen, F., and Liu, Y., 1997, Surface deformation and lower crustal flow in eastern Tibet: Science, v. 276, p. 788–790.

Royden, L.H., Burchfiel, B.C., and van der Hilst, R., 2008, The geologic evolution of the Tibetan Plateau: Science, 321, 1054-1058.

Ruppel, C., 1995, Extensional processes in continental lithosphere: Journal of Geophysical Research, v. 100, p. 24,187-24,215.

Saylor, J., DeCelles, P., Gehrels, G., Murphy, M., Zhang, R., and Kapp, P., 2010, Basin formation in the High Himalaya by arc-parallel extension and tectonic damming: Zhada basin, southwestern Tibet: Tectonics, v. 29, TC1004, doi:10.1029/2008TC002390.

Searle, M.P., Windley, B.F., Coward, M.P., Cooper, D.J.W., Rex, A.J., Li, T., Xiao, X., Jan, M.Q., Thakur, V.C., and Kumar, S., 1987, The closing of the Tethys and the tectonics of the Himalaya: Geological Society of America Bulletin, v. 98, p. 678–701.

Slingerland, R., and Smith, N.D., 2004, River avulsions and their deposits: Annual Review of Earth and Planetary Sciences, v. 32, p. 257-285.

Smith, G. A., 2000, Recognition and significance of streamflow-dominated piedmont facies in extensional basins: Basin Research, v. 12, p. 399-411.

Spiegel, C., Kohn, B., Belton, D., Berner, Z., and Gleadow, A., 2009, Apatite (U–Th–Sm)/He thermochronology of rapidly cooled samples: The effect of He implantation: Earth and Planetary Science Letters, v. 285, p. 105-114

Steel, R. J., and Aasheim, S., 1978, Alluvial sand deposition in a rapidly subsiding basin (Devonian, Norway), in Miall, A. D., ed., Fluvial sedimentology: Canadian Society of Petroleum Geologists Memoir 5, p. 385-412.

Stockli, D.F., Farley, K.A. and Dumitru, T.A., 2000, Calibration of the (U-Th)/He thermochronometer on an exhumed normal fault block in the White Mountains, eastern California and western Nevada: Geology, v. 28, p. 983–986.

Stockli, D.F, Taylor, M., Yin, A., Harrison, T.M., D'Andrea, J., Kapp, P., and Ding, L., 2002, Late Miocene-Pliocene inception of E-W extension in Tibet as evidenced by apatite (U-Th)/He data: Geological Society of America Abstracts with Programs, v. 34, p. 411.

Stockli, D., 2005, Application of low-temperature thermochronometry to extensional tectonic settings, *in* Reiners, P.W., and Ehlers, T.A., eds., Low-Temperature Thermochronology: Techniques, Interpretations, and Applications: Reviews in Mineralogy and Geochemistry, v. 58, p. 420-461, Mineralogical Society of America, Washington, DC.

Tapponnier, P., and Molnar, P., 1977, Active faulting and tectonics in China: Journal of Geophysical Research, v. 82(20), p. 2905–2930

Tapponnier, P., Peltzer, G., Le Dain, A.Y., Armijo, R., and Cobbold, P., 1982, Propagating extrusion tectonics in Asia: New insights from simple experiments with plasticine: Geology, v. 10, p. 611–616.

Tapponnier, P., Xu, Z., Roger, F., Meyer, B., Arnaud, N., Wittlinger, G., and Yang, J., 2001, Oblique stepwise rise and growth of the Tibet Plateau: Science, v. 294, p. 1671–1677.

Taylor, M.T., Kapp, P.A., and Horton, B.K., 2012, Basin response to active extension and strike-slip deformation in the hinterland of the Tibetan plateau, in Busby, C., and Azor, A., editors, Tectonics of Sedimentary Basins: Recent Advances: Wiley-Blackwell, Oxford, UK, p. 445-460.

Taylor, M., Yin, A., Ryerson, F.J., Kapp, P., and Ding, L., 2003, Conjugate strike-slip faulting along the Bangong-Nujiang suture zone accommodates coeval east-west extension and north-south shortening in the interior of the Tibetan Plateau: Tectonics, v. 22, 1044, doi:10.1029/2002TC001361.

Volkmer, J.E., 2010, The Cretaceous-Tertiary tectonic evolution of the Lhasa Terrane, Tibet [Ph.D. dissertation]: University of Arizona, Tucson, 213 p.

Volkmer, J.E., Kapp, P., Guynn, J.H., and Lai, Q.Z., 2007, Cretaceous-Tertiary structural evolution of the north central Lhasa terrane, Tibet: Tectonics, v. 26, TC6007, doi:10.1029/2005TC001832.

Wang, Q., Wyman, D.A., Li, Z.X., Sun, W.D., Chung, S.L., Vasconcelos, P.M., Zhang, Q.Y., Dong, H., Yu, Y.S., Pearson, N., Qiu, H.N., Zhu, T.X., and Feng, X.T., 2010, Eocene north-south trending dikes in central Tibet: New constraints on the timing of east-west extension with implications for early plateau uplift? Earth and Planetary Science Letters, v. 298, p. 205-216.

Wang, Q., Zhang, P.-Z., Freymueller, J.T., Bilham, R., Larson, K.M., Lai, X., You, X., Niu, Z., Wu, J., Li, Y., Liu, J., Yang, Z., and Chen, Q., 2001, Present-day crustal deformation in China constrained by global positioning system measurements: Science, v. 294, p. 574–577.

Wernicke, B., 1981, Low-angle normal faults in the Basin and Range Province: nappe tectonics in an extending orogen: Nature, v. 291, p. 645-648.

Wernicke, B., 1985, Uniform-sense normal simple shear of the continental lithosphere: Canadian Journal of Earth Sciences, v. 22, p. 108–125.

Wernicke, B. P., and Axen, G. J., 1988, On the role of isotasy in the evolution of normal fault systems: Geology, v.16, p. 848-851.

Whipple, K. X., and Dunne, T., 1992, The influence of debris-flow rheology on fan morphology, Owens Valley, California: Geological Society of America Bulletin, v. 104, p. 887-900.

Yarnold, J.C., 1993, Rock-avalanche characteristics in dry climates and the effect of flow into lakes: Insights from mid-Tertiary sedimentary breccias near Artillery Peak, Arizona: Geological Society of America Bulletin, v. 105, p. 345-360.

Yin, A., 2000, Mode of Cenozoic east-west extension in Tibet suggesting a common origin of rifts in Asia during the Indo-Asian collision: Journal of Geophysical Research, v. 105, p. 21,745-21,759.

Yin, A., 2010, Cenozoic tectonic evolution of Asia: A preliminary synthesis: Tectonophysics, v. 488, p. 293-325.

Yin, A., and Harrison, T.M., 2000, Geologic evolution of the Himalayan-Tibetan orogen: Annual Review of Earth and Planetary Sciences, v. 28, p. 211–280.

Yin, A., Kapp, P.A., Murphy, M.A., Manning, C.E., Harrison, T.M., Grove, M., Ding, L., Deng, X.-G., Wu, C.-M., 1999, Significant late Neogene east-west extension in northern Tibet: Geology, v. 27, p. 787–790.

Zhang, K.J., Xia, B.D., Wang, G.M., Li, Y.T., and Ye, H.F., 2004, Early Cretaceous stratigraphy, depositional environments, sandstone provenance, and tectonic setting of central Tibet, western China: Geological Society of America Bulletin, v. 116, p. 1202–1222.

Zhang, P.Z., Shen, Z., Wang, M., Gan, W.J., Burgmann, R., and Molnar, P., 2004, Continuous deformation of the Tibetan Plateau from global positioning system data, Geology, v. 32, p. 809–812.